2016

Validation Of Integrated Coast-Ocean Model Cche2D-Coast And Development Of Wind Model

Afshin Gazerzadeh
University of Mississippi

VALIDATION OF INTEGRATED COAST-OCEAN MODEL CCHE2D-COAST AND DEVELOPMENT OF WIND MODEL

A Thesis
presented in partial fulfillment of requirements
for the degree of Master of Science
in the School of Engineering
in the Department of National Center for Computational Hydro-Science and Engineering
The University of Mississippi

by

AFSHIN GAZERAZDEH

AUGUST 2016

ABSTRACT

The eastern and southern coastlines of the United States are two of the most cyclone-prone areas of the world. The effects of tropical cyclones vary mainly depending on wind intensity and geological features of the coast that it is crossing. Higher winds potentially generate higher storm surges and consequently larger floods occur along the coastlines. Therefore, it is critical to accurately predict winds, storm surge, and waves associated with a hurricane.

In the present study, an integrated coastal and ocean process model, CCHE2D-Coast, is validated by assessing the model's capabilities in simulating coast-ocean circulations driven by the astronomical tides on the U.S. East Coast. Through the skill assessment, discrepancies between numerically simulated water surface elevations and observed tidal elevations at NOAA tide gages are quantified. On the other hand, statistical errors of the tidal constituents parameters, amplitude and phase, are also determined. In this study, the tidal harmonic constants are identified by using a newly-developed parameter identification approach.

CCHE2D-Coast is also further examined under meteorological forces driven by a hurricane. CCHE2D-Coast is applied to simulate meteorological and hydrodynamic processes during Hurricane Bob (1991) on the US Atlantic coast. Hindcasting storm surges and waves induced by Bob's winds and tides were performed before and after the landfall of this hurricane. The results showed that the model performed well in reproducing the dynamic process driven by astronomical and meteorological forces.

To improve the model's accuracy in reproducing hurricane wind fields during a real-time hurricane forecast, a hurricane wind model is developed in order to incorporate asymmetric effects into the Holland parametric wind model. The method is validated using the National Oceanic and Atmospheric Administration (NOAA)/ National Hurricane Center (NHC)/ Automated Tropical Cyclone Forecast's (ATCF) guidelines. The best track date, which contains six-hourly information on the location, maximum winds, radii of 3 wind isotach, and central pressure of Hurricane Gustave (2008) is used to compute the wind field in the Gulf of Mexico. The simulation result suggests that the wind model performed well in reconstructing wind field. The asymmetric model captured the directional change of hurricane wind velocity around the storm center.

LIST OF ABBREVIATIONS AND SYMBOLS

Long	Longitude
M2	Principal lunar semidiurnal constituent
M4	Shallow water overtides of principal lunar constituent
M6	Shallow water overtides of principal lunar constituent
N2	Larger lunar elliptic semidiurnal constituent
NB	Normalized Bias
NDBC	National Data Buoy Center
NHC	National Hurricane Center
nmi	Nautical Miles
NOAA	National Oceanic and Atmospheric Administrations
NRMSD	Normalized Root-Mean Square Deviation
Pc	Central Pressure
Pn	Ambient Pressure
Q1	Larger lunar elliptic diurnal constituent
R2	Coefficient of Determination
Rmax	Maximum Radius
S2	Principal solar semidiurnal constituent
SI	Scatter Index
Vgmax	Maximum sustained wind speed
Vt	Translational Speed

ACKNOWLEDMENTS

I would like to thank my supervisor, Dr. Yan Ding for his help through the completion this study. I also wish to thank my committee members, Dr. Mustafa Altinakar and Dr. Yafei Jia for their helpful involvement in my work. I have been fortunate to have such a notable group of scientists in my corner.

Special thanks must go to Luc Rébillout for his help with chapter 4 of this study.

I am grateful to Paul Smith, Dr. Yavuz Ozeren, Dr. Sara Wellman, Nuttita Pophet, and Saeed Arab for their support in a variety of ways.

I would also like to thank my lovely family and supportive relatives for their love, laughter and music that have kept me smiling and inspired.

DEDICATION

My thesis is dedicated to the memory of my grandfather, Ali Habibi.

His words of love and encouragement in pursuit

of education and excellence

still inspire.

TABLE OF CONTENTS

LIST OF TABLES

LIST OF FIGURES

CHAPTER I:

A BRIEF INTRODUCTION OF INTEGRATED COAST-OCEAN MODEL CCHE2D-COAST

In this chapter, a brief description of the integrated coast-ocean processes model, CCHE2D-Coast, is presented. CCHE2D-Coast is an integrated coastal and ocean processes modeling system developed in the National Center for Computational Hydro-science and Engineering (NCCHE) at the University of Mississippi (e.g. Ding and Wang, 2008; Ding et al., 2013; Ding et al. 2014). It is applicable for simulating multi-scale hydrodynamics and morphodynamics of free-surface water flows such as river flows, tidal currents, waves, storm surges induced by tropical cyclonic wind, sediment transport, and morphological changes over large-scale coastal regions.

Schematic layout of the model flow chart is depicted in Figure 1. This modularized application software is developed by using the state-of-art numerical simulation techniques and innovative physical knowledge in river, coastal, and ocean engineering.

CCHE2D-Coast has been applied to solve engineering problems for flooding and inundation management, erosion protection, and infrastructure planning and design in coasts and estuaries. The integrated model is embodied into a user-friendly interface, CCHE2D-GUI, which supports this integrated model for generating computational grids, monitoring computational progress during computations, and visualizing numerical results during and after simulations. CCHE2D-Coast is able to simulate large-scale and long-term problems on a standard PC. The low cost and accurate simulations make this tool specifically attractive to engineers and researchers in the areas.

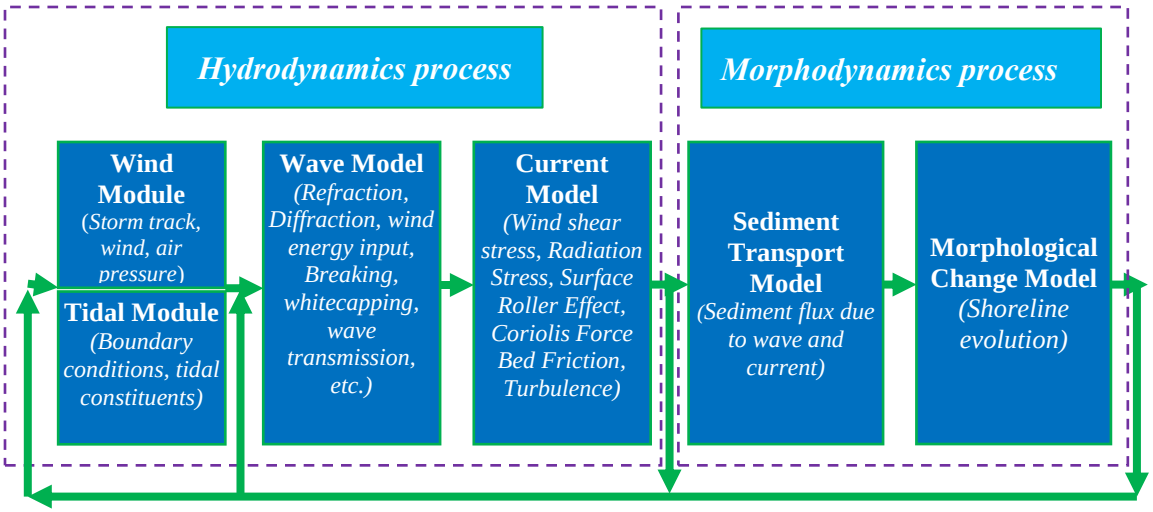

Figure 1. Flowchart of CCHE2D-Coast

CCHE2D-Coast has integrated systematically four major submodels for simulating deformations and transformations of irregular/multidirectional waves, tropical cyclonic barometric pressure and wind fields along storm tracks, tidal and wave-induced currents, and coastal morphological changes. For computing irregular waves, a multi-directional spectral wave action equation is adopted in the wave spectral module. The following wave deformation/transformation processes are included in the CCHE2D-Coast wave model.

- Refraction
- Diffraction
- Shoaling effect
- Wave breaking
- Wave transmission through coastal structures
- Bottom friction
- Wave-current interaction

- Vegetation attenuation effect
- Wind-induced wave
- Whitecapping

CCHE2D-Coast provides two options for modeling wave actions: a half-plane wave model and a full-plane wave model (Ding et al. 2013b). The former is to compute wave fields only from the upwinding direction to the downwind direction, for example, to simulate deformation and transformation processes of swelling waves from deepwater to shallow waters at shore. The latter is the simulation option by which the computations of wave fields are performed by scanning the domain back and forth in wind directions. The full-plane wave simulation can be used for computing waves induced by cyclonic wind fields.

The wave spectra are discretized into a number of frequency bins, based on the equal energy dividend, by which each frequency bin represents an individual wave. The bins for wave directions are also discretized to cover a half-plane wave direction (θ) domain from $+\pi/2$ to $-\pi/2$.

In this model, the wave-action equation and the shallow water equations were discretized in a same non-orthogonal quadrilateral grid system. Because non-orthogonal meshes have less restrictions for grid shapes than curvilinear grids (orthogonal grids), CCHE2D-Coast has more flexibility to simulate coastal and ocean processes in complex coastal zones with irregular coastlines.

In this model, a nonlinear parametric hurricane cyclonic wind module is integrated to model cyclonic barometric pressure and wind fields along storm tracks by considering the decay effect of landfall and the earth surface resistance.

The hydrodynamic model contains the depth−averaged 2−D continuity and momentum equations to simulate flows driven by hydrological forcing such as tides, waves, river inflows, surface winds, and turbulence flows in a large-scale coastal and estuarine region. For detail and description regarding the different model's module, please see the CCHE2D-Coast quick start guide.

A time-marching algorithm was used to compute tidal and wave-induced currents (Jia et al. 2002). A validated algorithm in CCHE2D for the treatment of wetting and drying processes was directly used for predicting the tidal flat variations and coastal inundations.

CCHE2D-Coast provides two kinds of geographical coordinate systems (GCS): the Cartesian coordinates and the spherical coordinates. For the regional scale simulations, the model in the Cartesian coordinates requires geographically projected x- and y-coordinates; the spherical grid of CCHE2D then is based on geographic coordinate systems which commonly have units in decimal degrees measuring degrees of longitude and degrees of latitude.

The CCHE2D-Coast in the Cartesian coordinate system has been extensively validated by simulating waves, wave-induced currents, and morphological changes in coastal applications in various laboratories and field scales (e.g. Ding et al. 2006; Ding and Wang 2008; Ding et al. 2013). The purpose of this study is to validate the hydrodynamic model of CCHE2D-Coast in the spherical coordinates, in which the computational grid is generated on the GCS.

As a summary, CCHE2D-Coast has the following principal features for simulating hydrodynamic and morphodynamic processes driven by tropical cyclones:

- Deformation and transformation of multidirectional and irregular waves,
- Tidal currents and River flows,

- Coriolis force,
- Tropical cyclonic wind and atmospheric pressure
- Bottom friction,
- Storm surges and wave setup induced by cyclonic wind and wave fields
- Nearshore currents induced by short-period waves
- Sediment transport due to waves and currents,
- Coastal/estuarine morphodynamic processes
- Morphological changes around coastal structures, e.g., groins, offshore breakwaters, artificial headlands, jetties, artificial reefs, etc.

In the presented study, validation of CCHE2D-Coast model is presented in section two, which considers simulation cases and quality measures and corresponding skill assessment metric's results under astronomical tide-only driving forces. The Third chapter of this study presents a simulation result of wind, wave, and storm surge under Hurricane Bob (1991) forces. The fourth chapter presents the detail of newly-developed asymmetric hurricane parametric wind model. The final conclusion and remarks are presented in chapter five.

CHAPTER II:

SKILL ASSESSMENT OF A COAST-OCEAN CIRCULATION MODEL FOR THE U.S. EAST COAST

In this chapter, coastal circulation driven by astronomical tide is simulated for U.S. East coast. The major objective of this part is to evaluate the quality of the integrated modeling system in simulating flow dynamics and capturing different features of water circulation in coastal and shallow estuaries. The aim was to objectively assess the ability of the hydrodynamic model to hindcast conditions driven by tidal forces across the U.S. East Coast. In order to determine whether the numerical model is reliable and accurate in simulating coastal hydrodynamic process, a number of statistical measures are employed to quantify the errors.

As tidal forces are dominant dynamics in coastal regions, the ability to simulate coastal and ocean flow circulations driven by astronomical tides is essential for maritime navigation strategic management, coastal projects, and the study of marine systems and estuarine biology. Knowledge of tide hydrodynamics is an inseparable part of any marine biology study, as tidal currents greatly influence aquatic life in shallow coastal regions. Spatial and temporal variation of tidal water levels and velocities is important information required for recreational and commercial activities along the coastline.

If the rise in water level as a result of tropical storm forces coincides with high tide, it can cause more severe flooding in coastal zones. Thus, accurate prediction of storm tide, the water level rise due to the combination of storm surge and the astronomical tide is required for coastal flooding management and resilience development.

Early research on tidal flow dynamics was largely focused on analytical studies using linearized versions of the complete equations of motion. With the advancement in computing machines, analytical based studies were no longer pursued and eventually replaced by numerical models. As result of such technological advancement, finite difference methods were first employed to

solve the complete equations of motion (Leendertse, 1967). Therefore, the finite difference method was developed that could contain the transport equations, which allowed specific applications to shallow estuarine systems (Reid and Bodine, 1968; Leendertse, 1970; Leendertse and Gritton, 1971; Hess, 1976).

Tide modeling has been discussed in numerous studies, as the common application, due to observability of water level, in Coast-Ocean hydrodynamic models validation, testing their capability, and skill assessment, as well as hindcasting and forecasting sea (Blumberg et al, 1999; Zhang et al, 2006;). In most cases, the ability of integrated model systems to reproduce tidal current was successfully tested. However, the accuracy of simulated tide is heavily reliant on geometry and other hydrographic data. Capturing tide variation as a scenario of model validation is important since coastal circulation under tidal currents controls the main processes in shallow estuaries.

Accurate tide prediction is essential for coastal infrastructure planning and construction activities in inlet, coastal and offshore areas. In the past decades, a considerable amount of research has been conducted to study the tidal flow circulation patterns existent across coastal, shallow estuaries, and other small water bodies (e.g. Lynch, 1983; Westerink and Gray, 1991).

Modern technology in parallel with advancement in numerical models and data assimilation has made it possible to generate realistic and accurate global tidal models. Over the past decades, several models have been developed; from the early empirical solution which was provided by Schwiderski (1980) to the advanced and sophisticated finite element global models which have been used in recent years. For instance, the FES12 model, the latest version of the FES series of global finite element tide, was initiated by Le Provost et al. (1998). The model is able to generate

ocean tide elevations and currents computed by up-to-date finite elements modelling and data assimilation. DTU10, a global ocean tide model, was developed by Cheng and Andersen (2011) using the latest seventeen years multi Mission measurements from TOPEX/Poseidon (T/P) satellite altimetry for sea level residuals analysis. The model resolution is 0.125^{o} x 0.125^{o}, including the 12 major tidal constituents. TPXO8 model is the most recent in a series of tidal solutions produced using the representer-based variational scheme described by Egbert et al. (1994) and Egbert and Erofeeva (2002).

Although dramatic progress has been achieved in improving the accuracy of global tide models, there are still limits and numerous complications associated with their applications. Some issues such as the necessity for approximate parameterizations of dissipation in the tidal equations, ocean bed topography, accurate open ocean boundary condition, and the effects of ocean stratification on the barotropic tides, which requires full 3D models, have not been effectively resolved (Egbert 2004).

The accuracy of global ocean models has been discussed in several papers (Andersen et al. 1995; Ray 1996, 1997, and 2009; King and Padman 2005, Timko et al. 2012). For instance, Shum (1997) made a comprehensive study on ten global ocean tide models. The degree to which the global tide models were improved, investigated through a variety of assessments and metrics with regard to tide gauges and some other recorded data (Shum et al. 1997). Stammer (2014) also evaluated the accuracy of several global tide models against in-situ measured data. Ten tidal harmonic constituents in the diurnal, semidiurnal, and quarter-diurnal bands were employed to assess the accuracy of the models (Stammer et al. 2014).

Advances in scientific computing, utilizing robust numerical methods, accelerated the development of integrated model systems which has greatly enhanced the ocean circulation models over the last decades.

Technological improvements have allowed for higher resolution that conforms to shallow estuary geometry and have produced models capable of simulating flow dynamics more accurately at both small and large scales. As a result, several coastal ocean hydrodynamic models have been developed and successfully implemented in many studies over the past years (Pain et al. 2005 and Piggott et al. 2008); For instance, ADCIRC (Advanced Circulation), which is a 2D, depth-integrated, and baratropic time-dependent long-wave hydrodynamic circulation model developed by Luettich and Westerink (Luettich et al. 1992). FVCOM is a prognostic, finite-volume, free-surface, and unstructured-grid coastal ocean circulation model (Chen et al. (2003). Several other 2D-3D ocean circulation models also exist which have a wide range of capabilities; DHI MIKE package (MIKE 21 & MIKE 3 Flow Model FM (http://www.mikebydhi.com)), CH3D which is curvilinear hydrodynamics (Sheng 1986), ELCIRC which is an unstructured-grid model designed for the simulation of 3D baroclinic circulation (Zhang et at. 2004), NCOM is a hydrostatic, baroclinic, with Boussinesq approximation, free-surface, data assimilated ocean circulation model (Barron et al., 2005), HYCOM (Halliwell et al., 1998), The Princeton Ocean Model (POM) which is able to simulate flow circulation and mixing processes in regional shallow water, and global ocean (Blumberg, Mellor, 1987), SELFE (Zhang and Baptista, 2008), DELFT3D developed by Delft Hydraulics((www.deltares.nl) has a capability to simulate Coast-Ocean hydrodynamics in 2D-3D configuration under several driving forces such as wind, waves, and tide.

Theoretical aspects of model skill assessment and its application have been broadly referenced in literatures. Dee (1995) presented a pragmatic view of model validation; standard validation documents and processes are outlined as well as useful framework for organizing and presenting available information about model validation (Dee 1995). Lynch 2009 constitutes an effort to develop the theoretical basis for the underlying problem of skill assessment in all of its relevant senses (Lynch 2009).

Several skill assessment procedures have been developed to quantify model's performance quality. Different statistical approaches have been employed in different studies, with regard to specific applications, to measure corresponding misfit (which measures discrepancies between modeled and observation variables); Stow et al 2009 reviewed a number of skill assessment approaches and metrics; including univariate comparison of predictions and observations such as r or R (the correlation coefficient), RMSE (the root-mean-square error), AE (the average error or Bias), AAE (the average absolute error), and RI (the reliability index), and MEF (the modelling efficiency).

Similarly, studies such as Wilmott 1981; Wilmott et al 1985; Vested et al (1995); Warner et al (2005); Dingman et al (1986); Robinson et al (2002); Wallhead et al (2009); Stumpf et al (2009); Fitzpatrick (2009); Sheng and Kim (2009); Williams et al 1989; presented a set of standard analysis and quantitative metrics to assess performance of global/regional, biological/physical hydrodynamic models.

In tidal regions, a comparison of identified tidal harmonic constants with known values can help to further assess the quality of the model in simulating water level. To this end, an optimization algorithm is employed to identify harmonic tidal components. The Limited memory Broyden–

Fletcher–Goldfarb–Shanno approach (Liu and Nocedal, 1989), known as LBFGS, is employed as parameter identification algorithm.

LBFGS, from a family of quasi-Newton methods, is a popular algorithm for parameter identification problems (Ding. et al, 2004). The newly-developed parameter identification approach is used to identify the amplitudes and phases of the tidal constituents corresponding to the particular measurement sites. The results demonstrated that the model can identify the tidal harmonic constituents with relatively small error. On the other hand, the hydrodynamic model accurately simulated the U.S East coast circulation under tidal forces.

Computational domain

A typical CCHE2D/CCHE2D-Coast computational mesh is formed by constructing non-orthogonal quadrilateral grids using bathymetrical and topographic data. Figure 2 is the computational mesh was created using the CCHE-MESH program (Zhang and Jia 2009).

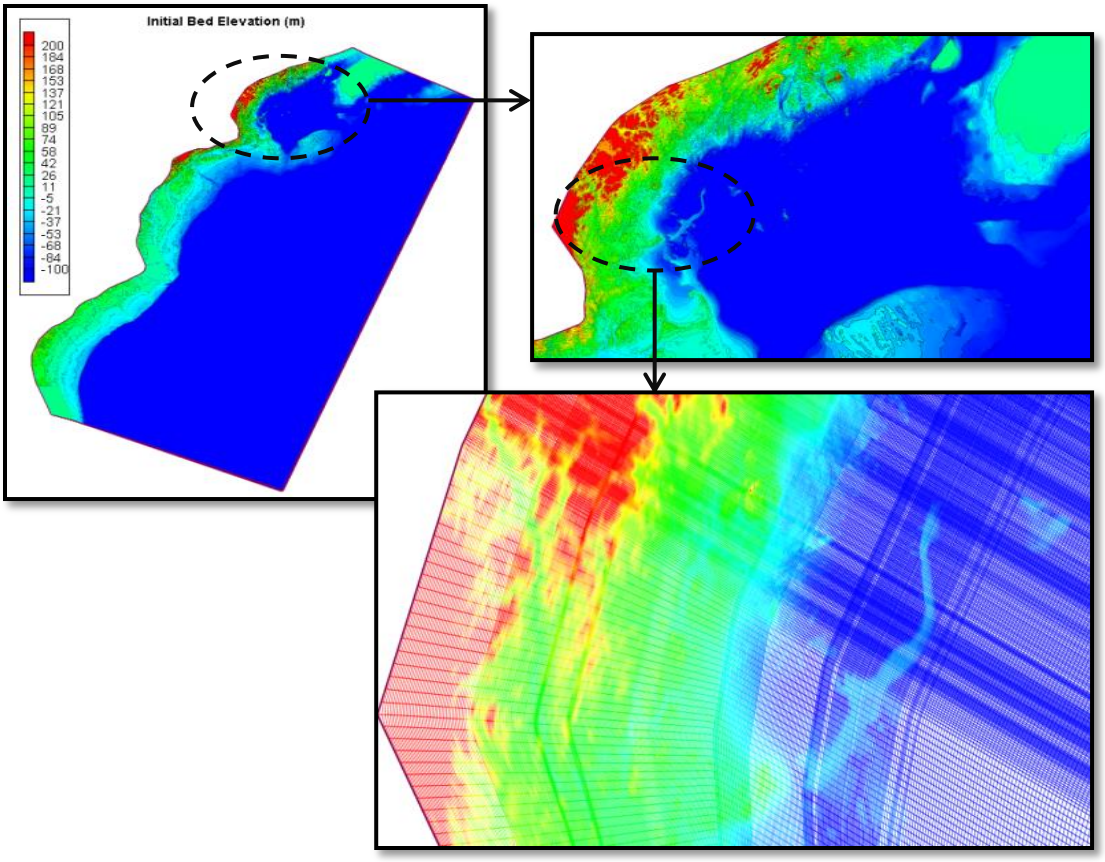

Figure 2. Computational domain in East Coast and Bathymetry and topography data

The multi-block methodology was employed to decompose the computational domain into several subdomains, which were meshed separately. This was necessary in order to be able to accurately represent various features at various scales. The final mesh to cover the computational domain shown in Figure 2 has a total of 1,777,426 nodes (2,591 grid points in the longitudinal direction and 686 grid points in the latitudinal direction). Horizontal coordinate of nodes in computational domain is in longitude and latitude and values of the bed elevations is based on the in the geodetic North American Vertical Datum of 1988 (NAVD88).

BOUNDARY CONDITION

It is imperative for a reliable and accurate tide circulation model to be able to include the main astronomical forces influencing tide. Tide is composed of harmonic constituents that are induced by wide range of gravitational forces; however, not all of these known forces significantly influence the tide and tide currents. A few tidal constituent components can impose large enough forces on water bodies across the earth that they can considerably affect the flow circulation pattern. Consequently, in this study, a small number of tidal constituents are used to generate tide water level as open ocean boundaries.

The tidal potential and constituents, phase and amplitude, were obtained from the ADCIRC tidal table (Mukai et al. 2002). The primary harmonic components are O1, K1, Q1, M2, S2, N2, and K2 astronomical tidal constituents as well as the steady, M4 and M6 overtides.

OBSERVATION

The NOAA operates several monitoring gauge stations to record and publicly provide observation data at the U.S. Coastline. In this study, the observed water level that is collected from several stations is illustrated in Figure 3. The supporting information including a list of monitoring stations, ID, and location is also summarized in Table 1. The time series of observation is employed for the purpose of skill assessment. Moreover, harmonic constituent values published by NOAA at the same monitoring stations are collected to further evaluate model performance through harmonic analysis.

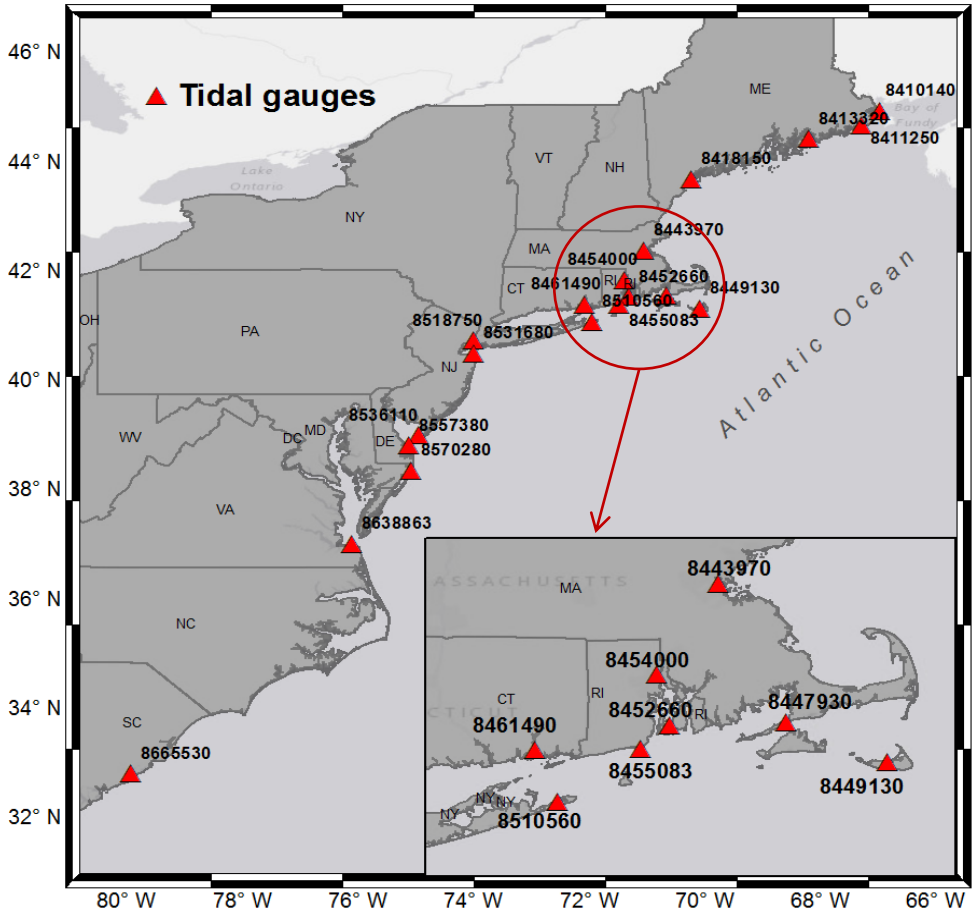

Figure 3. Map of observational measuring gauges operated by NOAA.

SKILL ASSESSMENT OF CCHE2D-COAST MODEL

As shown in Figure 4, the study domain is vast, composed of the Northeast and Mid-Atlantic of the U.S. coast. It is a complicated system as a variety of different features exist in different spatial scales; spatial and temporal variation in topography, bathymetry, meteorology, and tidal forces has made tide dynamics significantly differ from north to south of the domain. Tidal water level range can vary from a couple of meters in Fundy Bay, which is the home of the highest tide along the U.S. East Coast, to the small tides in the Mid-Atlantic.

Table 1. List of NOAA observation stations used in skill assessment.

No.	Station Name, State	Station ID	Longitude	Latitude
1	East Port, ME	8410140	-66.9817	44.9033
2	Culter Naval Base, ME	8411250	-67.2967	44.6417
3	BarHarbor, ME	8413320	-68.2050	44.3917
4	Portland, ME	8418150	-70.2467	43.6567
5	Boston, MA	8443970	-71.0533	42.3533
6	Providence, RI	8454000	-71.4000	41.8067
7	Woods Hole, MA	8447930	-70.6717	41.5233
8	Nantucket island, MA	8449130	-70.0967	41.2850
9	Newport, RI	8452660	-71.3300	41.5050
10	Point Judith, RI	8455083	-71.4900	41.3633
11	New London, CT	8461490	-72.0889	41.3583
12	Montauk, NY	8510560	-71.9583	41.0483
13	The Battery, NY	8518750	-74.0133	40.7000
14	Sandy Hook, NJ	8531680	-74.0100	40.4667
15	Cape May, NJ	8536110	-74.9583	38.9683
16	Lewese, DE	8557380	-75.1200	38.7817
17	Ocean City, MD	8570280	-75.0833	38.3233
18	Chesapeake Bay Bridge Tunnel, VA	8638863	-76.1133	36.9817
19	Charleston, SC	8665530	-79.9250	32.7817

For the comparison between simulated and observed water level, the hydrodynamic model is driven by only harmonically-predicted astronomical tides for the ocean boundary water levels; there are no surface forces such as pressure or, wind and no river input discharges included in the computational domain. To quantitatively measure the quality of simulation, modeled variables are compared with their corresponding observed (accepted) values using number of statistical indices.

Criteria Definition

Number of statistical indices such Normalized Root-Mean Square Deviation (NRMSD), Coefficient of Determination (R2), Scatter Index (SI), and Normalized Bias (NB) are used to

quantify the misfit between model simulated variables and corresponding observation data; Denoting N= number of observations, a set of model simulation values as m, a set of observation values or known values as O, overbar is mean of the data. They are defined as:

$$\text{NRMSD} = \frac{\sqrt{\frac{1}{\text{N}}\sum_{i=1}^{N}(O_i - m_i)^2}}{Max(O_i)} \quad (1)$$

The normalized root-mean square deviation (Equation 1) is a frequently-used measure for discrepancies between the model prediction and the values actually observed. A close agreement can be achieved if a NRMSD is near zero. The maximum value of the observation set was chosen to normalize the root-mean square deviation. This index can indicate the model prediction accuracy in reproducing observation.

$$\text{R}^2 = 1 - \frac{SS_{\text{res}}}{SS_{\text{tot}}} \quad (2)$$

In Coefficient of Determination (R2) where variance of observation data $SS_{tot} = \sum_i (O_i - \bar{O})^2$, the sum of residual square $SS_{res} = \sum_i (O_i - m_i)^2$, and average of observation values is $\bar{O} = \frac{1}{N}\sum_{i=1}^{N} O_i$. Coefficient of determination, which is the square of the correlation coefficient, is a measure of the goodness-of-fit between two time series i.e. a measure that how many of data points are on the regression line. On the other hand, the more data on the regression line, the higher value of R2. If the prediction varies together with the observed data, a value near 1 (or 100%) can be achieved. However, a value near 1 indicates that all the modeled and observed data may not match each other. R2 of 0 indicates that the modeled data does not represent observed values. If prediction inversely varies with observation, a negative value of R2 will result.

$$\text{Averaged Bias (AB)} = \frac{\frac{1}{\mathrm{N}}\sum_{i=1}^{N} E_i}{\frac{1}{\mathrm{N}}\sum_{i=1}^{N}|O_i|} \quad (3)$$

Where $E_i = m_i - O_i$ denotes the error between the model and measurement.

$$\text{Scatterd Index (SI)} = \frac{\sqrt{\frac{1}{\mathrm{N}}\sum_{i=1}^{N}\left(E_i - \bar{E}\right)^2}}{\frac{1}{\mathrm{N}}\sum_{i=1}^{N}|O_i|} \quad (4)$$

Where the average error is $\bar{\mathrm{E}} = (1/\mathrm{N})\sum_{\mathrm{i}=1}^{\mathrm{N}}|\mathrm{O_i} - \mathrm{m_i}|$ .The Scatter Index (SI) is the ratio of the standard deviation of the observation-to-prediction discrepancies to the average observation values (Hanson et al. 2009).

Model validation

Spurious oscillation in water level frequently occurs once the simulation begins in a cold start. This part of the time series has to be eliminated from the main data set as it represents unrealistic flow behavior. Thus, a test was carried out to determine which part of the data set should be removed. A number of days from where the simulation had been started, need to be skipped. Root Mean Square Error (RMSE), Scatter Index (SI), Coefficient of Determination (R2), and Averaged Bias, as measures of discrepancy between simulation and observation, were computed. A range of zero skipped days, i.e. the entire data set was included, to fourteen days considered to measure the error in the test. The result showed that RMSE values were relatively unchanged after a period of seven days. This result suggests that for any quantitative comparison between modeled and simulation data, it is necessary to skip 7 days of the modeled time series because the model needs to reach an equilibrium state (Figure 4).

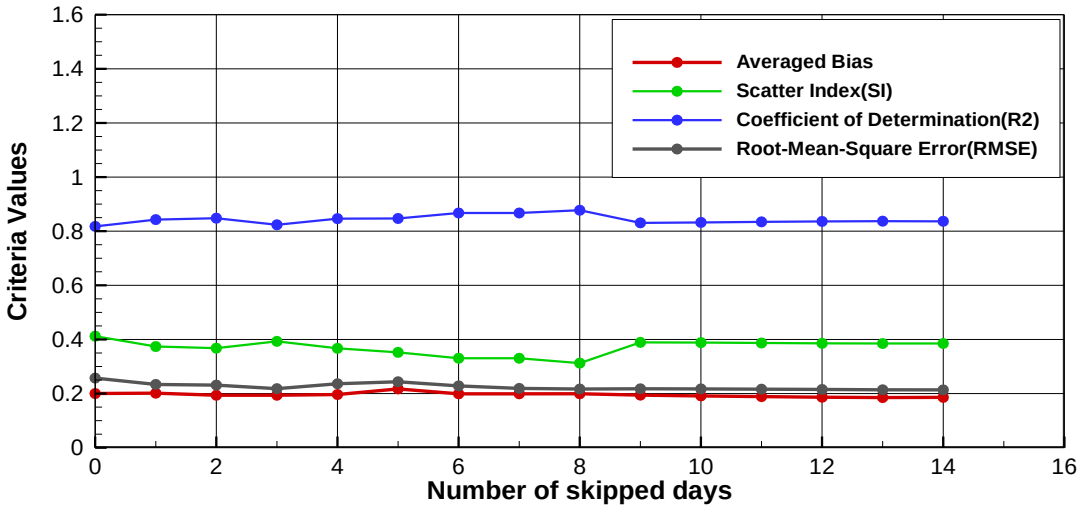

Figure 4. This figure illustrates that the model reached an equilibrium state after 7 days of simulation run.

To test the model performance, a number of phases were defined for model validation quality assurance. The model skill assessment procedure is divided into two parts. In the first phase, the model's capability to reproduce water level is tested against the observation data. In the second phase, the model skill is evaluated by performing harmonic analysis. Since the model is set up under astronomical tides-only simulation, where meteorological and other driving forces are not available, it cannot capture the effect of other existing forces on the modeled water level (non-tidal signals at the sea).

In the mesh configuration, efforts have been made to make monitoring points as close as possible to the real physical location of NOAA stations. However, in a few cases, lack of fine mesh made the monitoring points fall hundreds of meters away from NOAA observation gauges which can cause some error in simulated water level.

Model skill metrics

The most conventional way to compare simulated model variables with measurements is visual comparison. A graphical comparing of time series is widely used in model's performance assessment. Graphical plot reveals if the model fails or succeeds in reproducing the observed values. In addition, it can visually depict a bias in the model, or how well the model was able to capture variabilities and certain features.

However, with advancement in measurement technologies, a dense observational data set is available to be used in model validation or skill assessment. Thus, it is necessary to provide an objective means to quantitatively assess the quality of the model's performance. Therefore, a set of statistical measures and procedures are needed to conduct a comprehensive analysis of differences between model and measured data in a way that is suitable to a specific application.

There are a number of statistical measures that are useful to assess the model's behavior. There is no consensus on which statistical metric is the best in revealing the quality of a model's performance. On the other hand, there is no unique measure that can perfectly reveal the entire aspect of the model's behavior. Therefore, it is useful to employ several statistical tests to quantify misfit among the same set of data. Thus, the model's performance should be evaluated using several metrics. (Stow et al. 2009).

Fitzpatrick (2009) presented a summary of many of the skill metrics and procedures for model quality evaluation. Several statistical criteria have been employed in different studies and applications to quantify model accuracy as listed (Ganju et al. 2009; Jolliff et al. 2009; Brown and Davis 2006; Haefner 2005; Mason and Graham 1999; Parrish and Smith 1990; Reckhow et al. 1990; Reckhow and Chapra 1983; Thomann 1982):

- Basic discrepancy criteria such as absolute, relative, and root-mean-square error
- Correlation of observations and predictions such as coefficient of determination
- Parametric and nonparametric tests such as student's t test and Wilcoxin, respectively
- Plots of cumulative error, cumulative density functions, and model bias
- Receiver operator characteristic (ROC) curves
- Target and Taylor diagrams, useful visual methods for displaying multiple error criteria on a single plot

A number of the skill assessment metrics were selected to quantify the model's performance. In this study, the computation of metrics was focused on two sets of variables; the water level time series and harmonic constituents.

RESULT AND ANALYSIS

Comparing time series of tidal levels with observation (in time domain)

In this section, the model result was computed at monitoring points that were defined over the computational domain. The simulation result was compared with the observation data collected from measurements at 19 stations along U.S. Northeast and Mid-Atlantic coast. In Figure 5 and Figure 6, a visual comparison between the NOAA observed and modeled water level is displayed for several stations listed in Table 1. The figures start date is from 0:00 UTC July 30, 1991 to 0:00 UTC Aug 9, 1991. As the comparison shows, there is an obvious spurious oscillation of water level at 12:00 UTC Aug 1, 1991 where the short simulation run began (green line).

This unrealistic water surface variation originates from a cold start run. Therefore, as discussed in the previous section, the first 7 days of short and long simulation run were removed from the

skill assessment metric's measurements. There is a good agreement between model result and observation data set observed in visual illustration. The figures suggest that the model accurately captured sea water surface elevation variations. However, there are some misfits between the observed and modeled water level's amplitude.

It is worth noting that there are some other sources of error in tide modeling that can possibly lower the model's quality in simulating tide currents. Limits within the integrated model systems are comprised of many different aspects; a finer mesh size can considerably increase hydrodynamic model's accuracy in simulating flow circulation in shallow estuaries where the shape of the coastline and variability in near-shore bathymetry becomes very important.

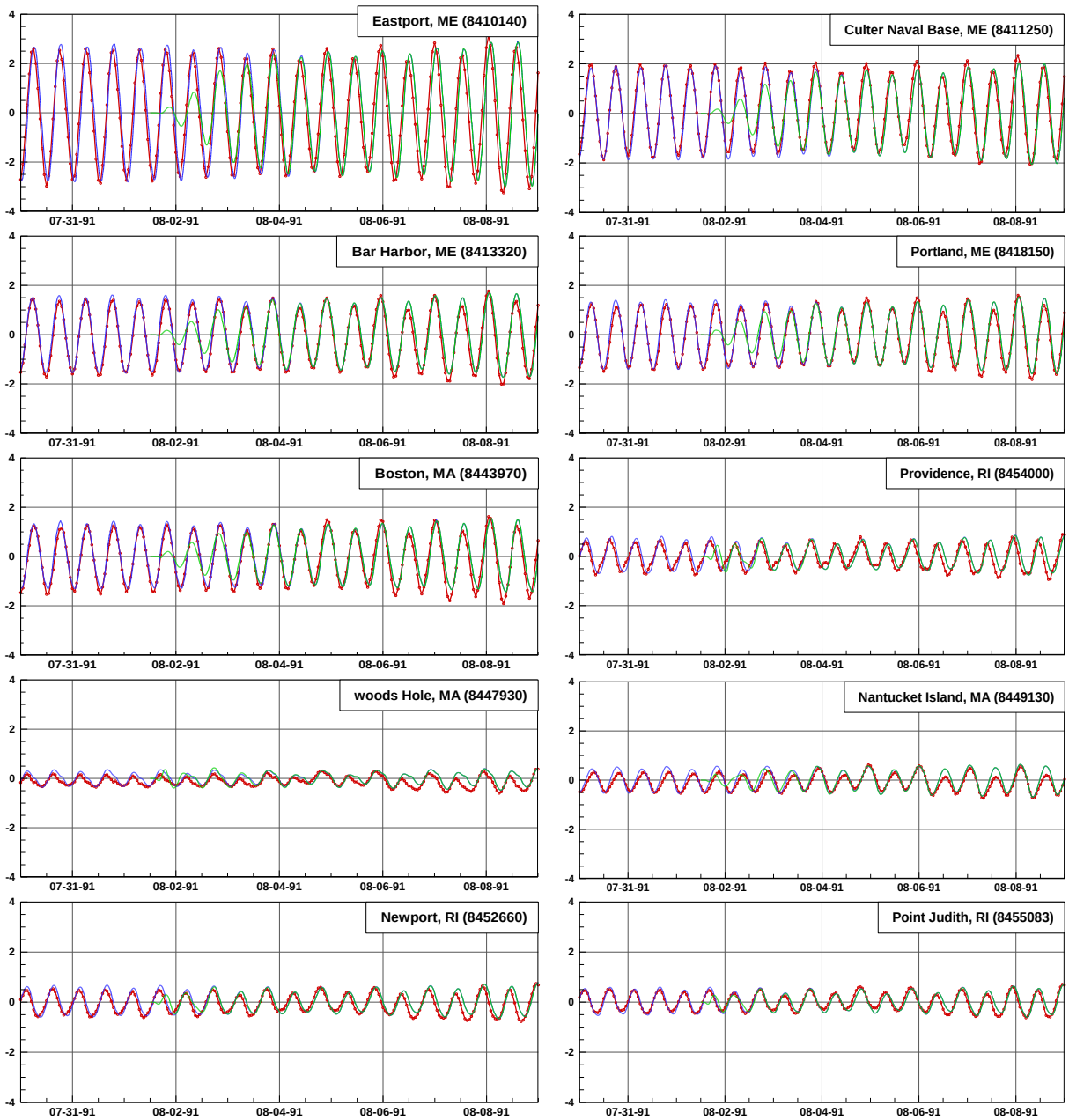

Figure 5. Time series of water level at 10 NOAA gauge stations listed in Table 1 (No. 1-10). Observed values are shown as a red line with red circles attached to it. Modeled results are shown as blue and green lines for the long and short simulation run, respectively.

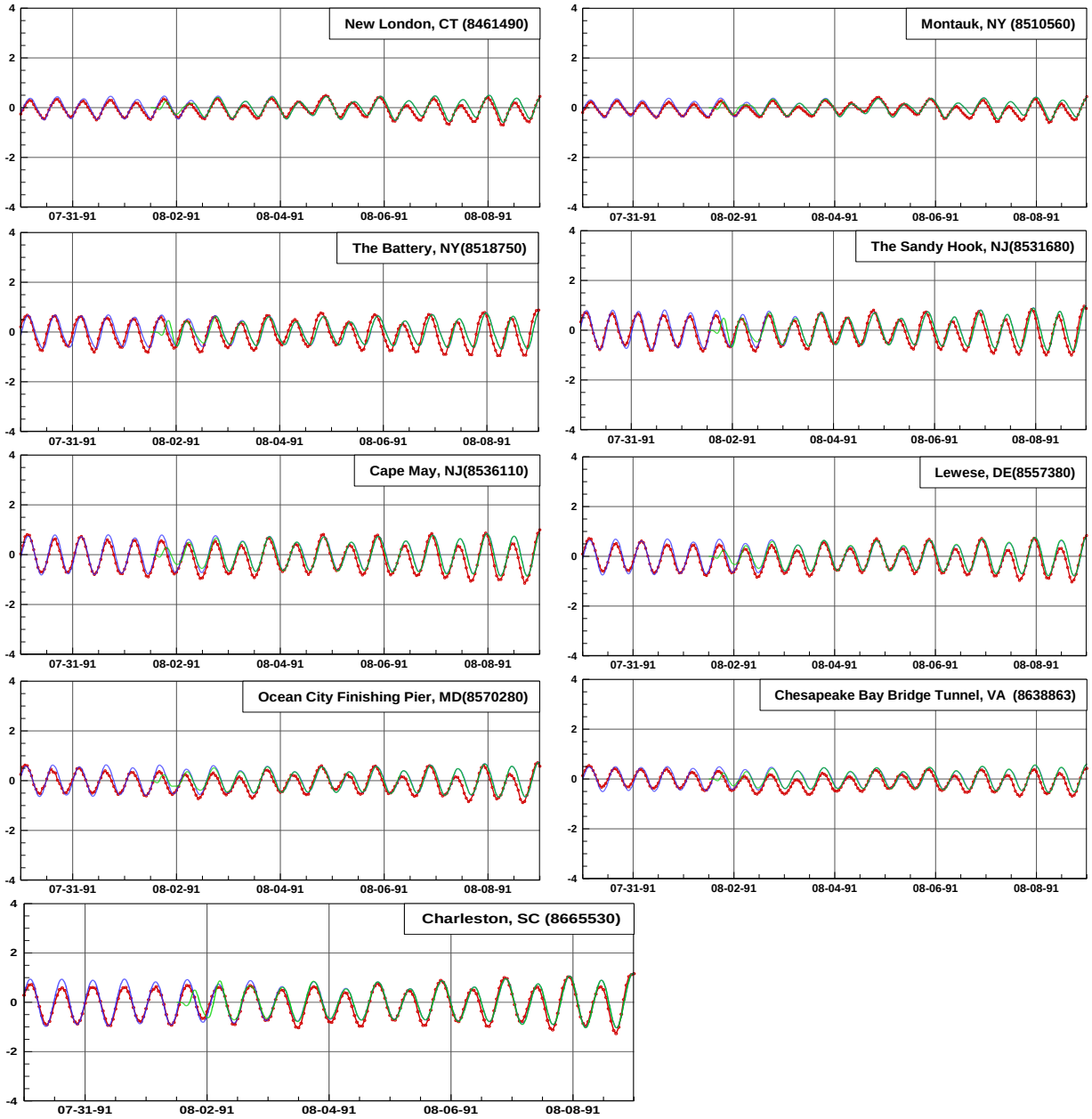

Figure 6. Time series of water level at 9 NOAA gauge stations listed in Table 1 (No. 11-19). Observed values are shown as a red line with red circles attached to it. Modeled results are shown as blue and green lines for the long and short simulation run, respectively.

Lack of background weather forces such as offshore wind in the model, and other inputs to the model such as freshwater discharges are among those sources of inaccuracy in modeled time

series. Therefore, a model that is capable of incorporating all these complex forces and features may be able to improve the accuracy of tide modeling in coastal regions.

The ideal observation data set that can be used in either visual comparison or skill assessment criteria is NOAA's prediction data, not actual measurements. This is because NOAA's predicted sea water level data does not include any effect from non-tidal signals such as wind and pressure forces. Thus, using an actual observation data set may increase the discrepancies associated within data comparison. However, to understand how accurately the model performed in reproducing tide in the both cases, a set of statistical criteria were computed.

Comparing tidal constituents with the known values (provided by NOAA)

Tidal harmonic constituents were derived from the time series using a harmonic analysis procedure. Newly-developed parameter identification was used to identify harmonic constants using modeled time series under astronomical tide-only simulation. Skill assessment criteria were computed based on the identified amplitudes and phases at several stations. The modeled time series, obtained from the long simulation run (108 days), is used for the harmonic analysis procedure.

Results from CCHE2D-Coast simulation run are shown in blue and green for the long and short simulation run, respectively. The Normalized Root-Mean-Square Deviation (NRMSD) criteria were used to quantify how well the optimization was performed. The skill assessment result is displayed in Figure 10 and Figure 11 for each of the stations. The result of skill assessment is presented in a radar layout indicating the value of the criteria for each parameter.

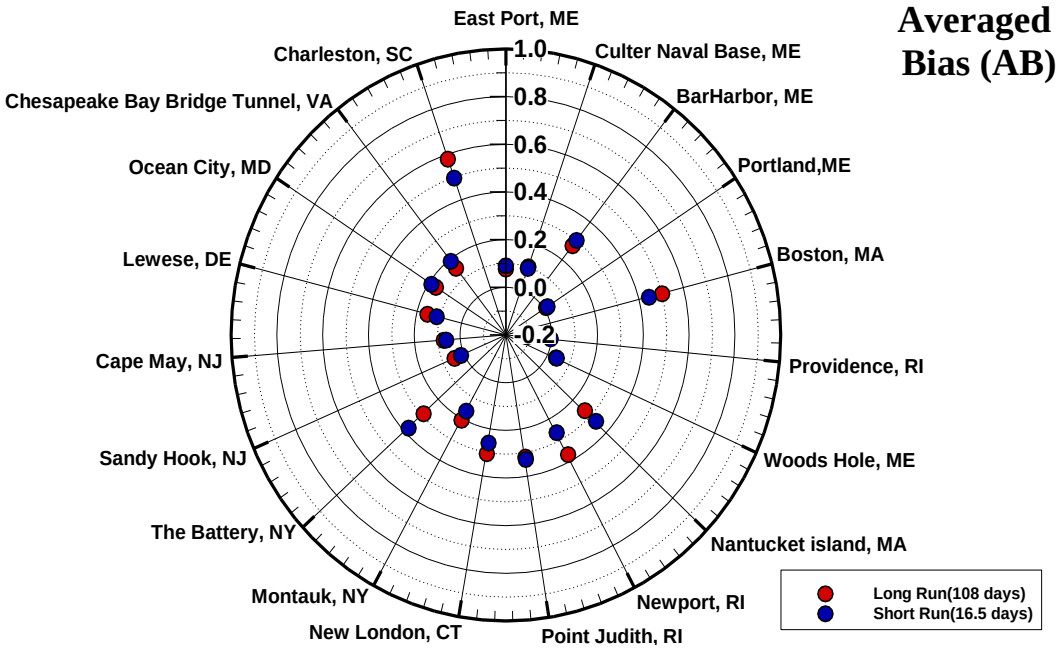

Figure 7. Calculated values of Averaged Bias in a radar layout; the points in red represent measured values from long simulation run (108 days) and points in blue represent values from short simulation run (16.5 days).

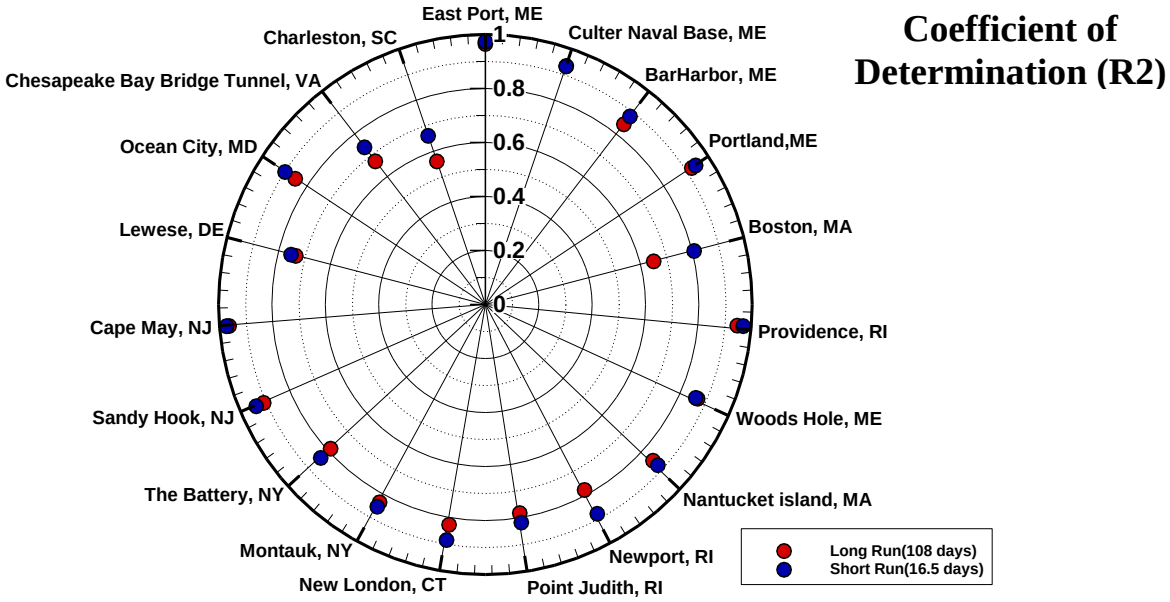

Figure 8. Calculated values of Coefficient of Determination(R2) in a radar layout; red points represent measured values from long simulation run (108 days) and blue points represent values from short simulation run (16.5 days).

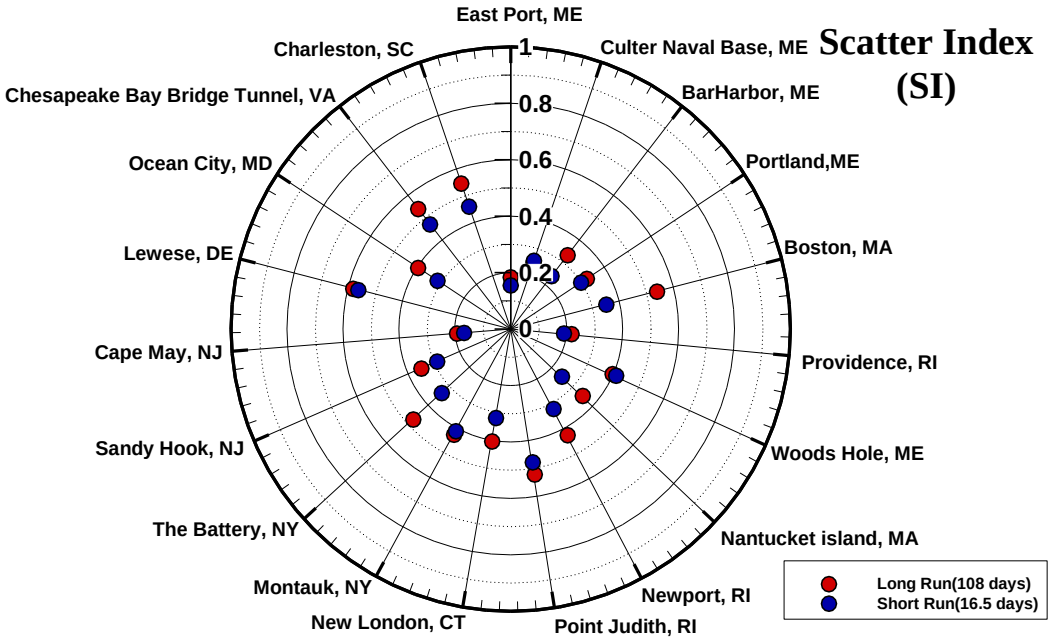

Figure 9. Calculated values of Scatter Index (SI) in a radar layout; red points represent measured values from long simulation run (108 days) and blue points represent values from short simulation run (16.5 days).

Analysis of assessment results in time domain

As shown in Figure 5 and Figure 6, simulated water level time series were compared to observed water levels. Moreover, statistical analyses were performed to measure the model skill with respect to reproduced tide in several stations. The agreement between model and observed data suggests that the model's accuracy is good in modeling tide currents and capturing variation of water elevation.

All three statistical indices employed as metrics are shown in Figure 6,

Figure 8, and Figure 9. The values of computed indices are in a very good range that indicates the model performed well in reproducing water level. The value of R2 in Eastport, Culter Naval Base, Providence, Cape May, Portland, providence, Woods Hole, Sandy Hook, and Cape May

are greater than 0.90, which represents a good closeness to a line of the best fit between the modeled and observed data. On the other hand, the regression line passes through 90% and greater of points on the scatter plot.

The highest linearity between observation and simulation exists in East port and Cape May with 96%, while R2 at Charleston is the lowest. The Average Bias (AB) value illustrates that the model overestimates the tide in most of the stations, whereas it only underestimates water level in Providence.

In a majority of the stations, R2 is greater than 0.85. However, deviation of the error from average error in some stations is not small. At Charleston, Averaged Bias (AB) and Scatter Index (SI) are large. This may be attributed to many factors, as partly explained in previous sections, such as the location of NOAA water level measuring gauges which may possibly be located in the bay or behind a barrier in embayment.

Similarly, a relatively large Averaged Bias (AB) in Chesapeake Bay Bridge, Lewese, the Battery, Newport, and Boston can arise from many sources such as a poor mesh in computational domain near these stations. Around these stations, a finer mesh may help to better capture small variabilities that affect modeled water level.

Analysis of assessment results of identified constituents

The tide harmonic constituents obtained from the parameter identification were compared to accepted values published for the NOAA stations. Statistical index was computed to measure the model skill with respect to the seven main tidal harmonic constituents; semi-diurnal constants, including M2, S2, N2, and K2 as well as O1, Q1, and K1 as diurnal tide components.

Model skill was evaluated based on the identified components, amplitude and phase, using the statistical index NRMSD. The result suggests that, regardless of physical geographic location and accuracy of reproduced time series, the parameter identification approach performed much better in identifying amplitude (Figure 10) than phase (Figure 11).

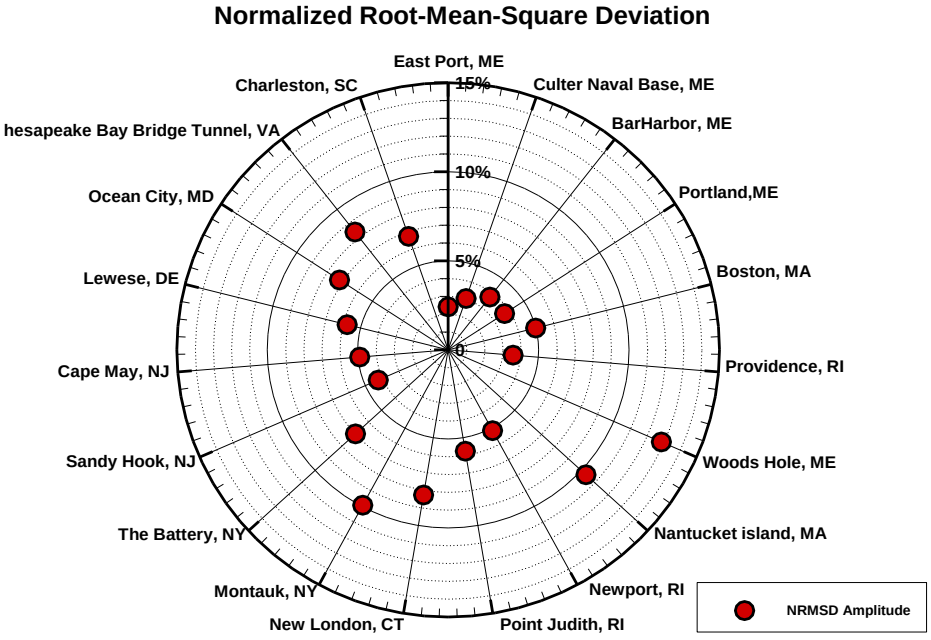

Figure 10. Skill assessment metric, Normalized Root-Mean-Square Deviation in identifying Amplitude.

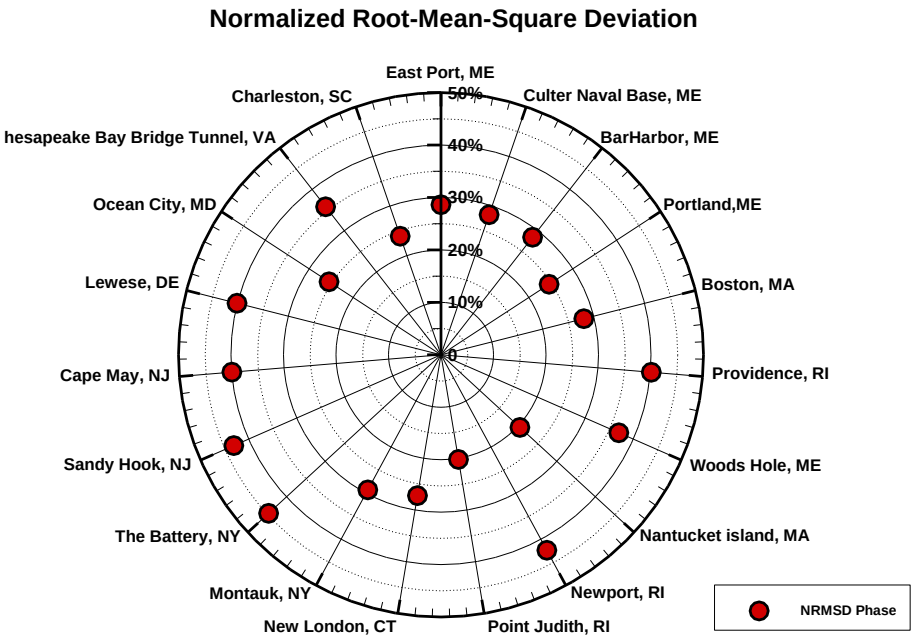

Figure 11. Skill assessment result, Normalized Root-Mean-Square Deviation in identifying phase.

The result indicated that the accuracy in identifying semi-diurnal tide constituents is greater than diurnal tide (Figure 10). This can be attributed to the stronger semi-diurnal tide signals as well as the larger range of semi-diurnal amplitude in the Atlantic Ocean.

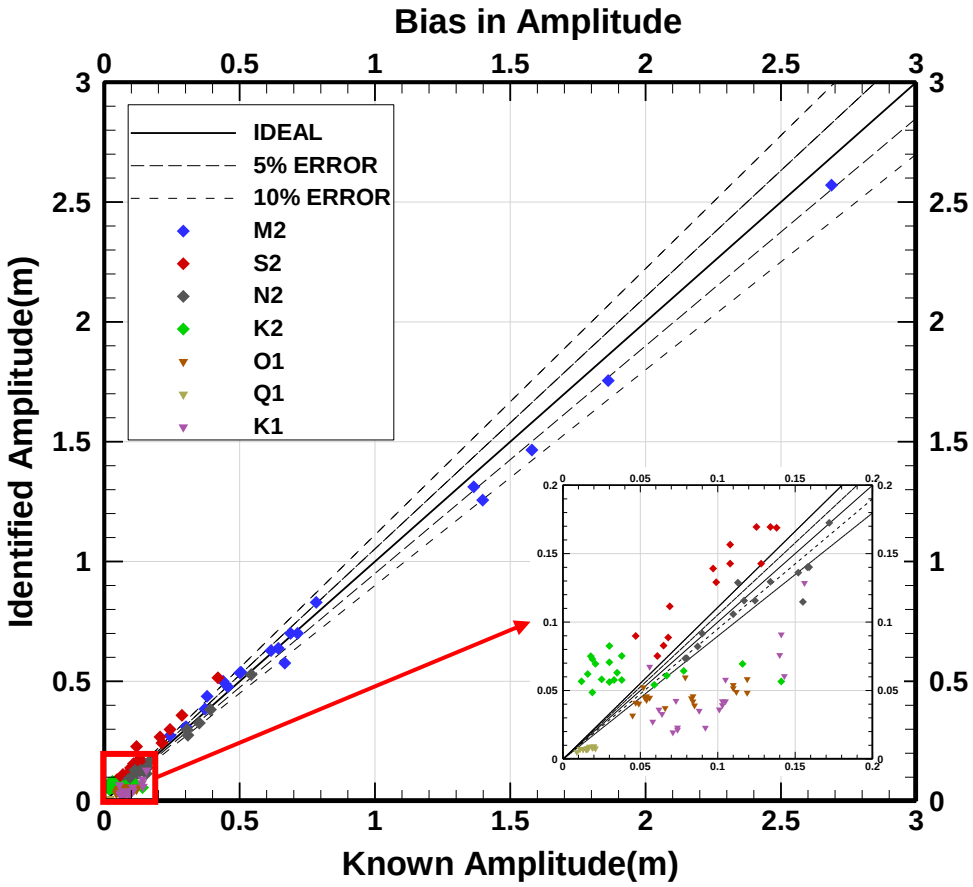

Figure 12. Scatter plot of the identified Amplitude versus know values.

However, comparing the values of NRMSD, from all 7 combined constituents, implies that all sets of identified amplitudes of the major tide constants are obtained well with an average of 6.2% in NRMSD; the criterion values fall within 2.4% for the lowest value at Eastport to 12.8% for the maximum value at Woods Hole with respect to the identified amplitude. The model identified M2 as the dominant constituent in the computational domain, and showed the least bias among all the other identified values, while K1 had the highest bias (Figure 13).

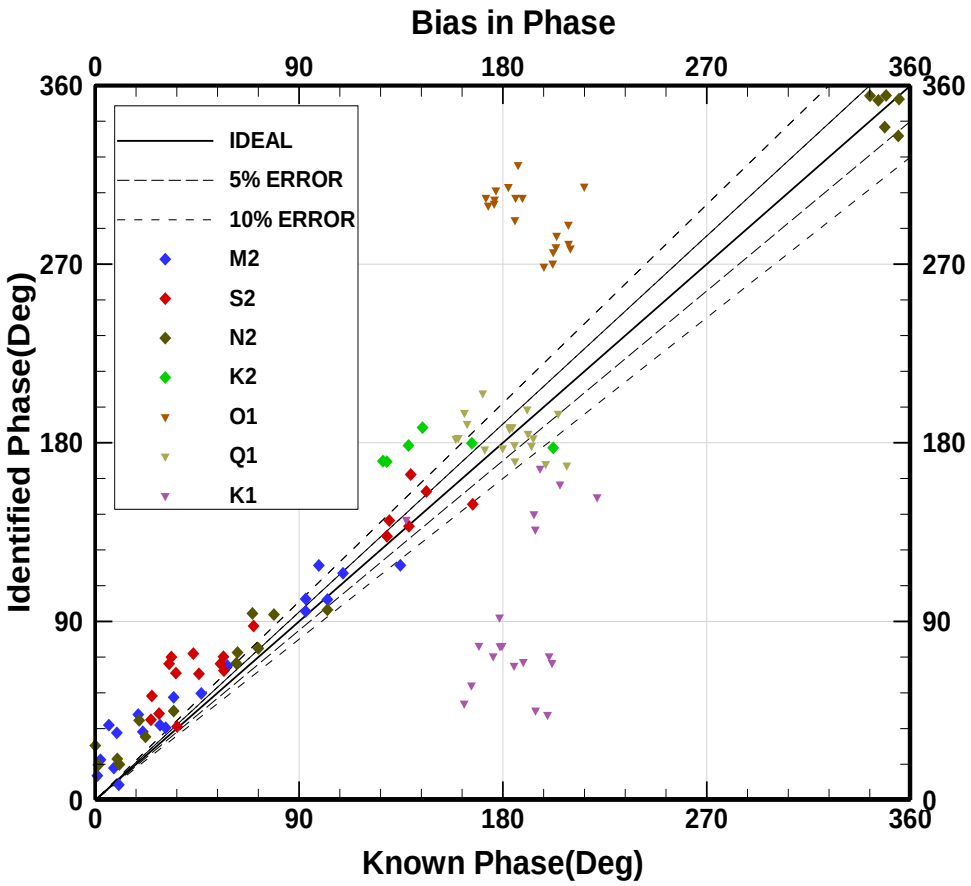

Figure 13. Scatter plot of identified Phase versus known values.

Accuracy of identified phase with regard to known values is slightly different from accuracy obtained in identified amplitudes. Bias in identified phase constituents is depicted in Figure 13. As it is shown in Figure 13, the bias in identified phase of K1, and O1 constituents is the largest, while identified phase of M2, and S2 has the lowest deviation from known values. Also, the average value of NRMSD is 31%. As mentioned earlier, the accuracy of identified harmonic constituents depends not only on modeled time series. Strength of parameter identification in identifying parameters is also dependent on many factors which will be explained in the next sections.

Harmonic Analysis

The routine prediction of tides at selected coastal stations is based on a simple principle. This principle asserts that the forces of any linear system can be decomposed into a sum of harmonics having the same frequencies but with different amplitudes and phases from the forces. For the open coastal stations, the prediction capability requires only that one have prior observation of the tides at that station over a suitable period of time from which the amplitudes and phases of the major tidal constituents can be ascertained. Thus, the problem is reduced to an analysis of the prior observations for the amplitudes and phases of the important periods. Once these values are known, the prediction for subsequent times is straight forward (Herbich 1999). Water elevation variation, for the tidal decomposition, can be written as:

$$X(t) = X_0 + \sum_{1}^{N} f_i A_i \cos\left(\omega_i t + V_i + u_i - \psi_i\right) \quad (5)$$

Where N is number of tidal components, X0 is initial water level, A_i is constant amplitudes, and ψ_i is constant phase (epochs). Nodal factor is given by f_i and the equilibrium argument by $V_i + u_i$. Among these terms, only the frequencies are an absolute constant for given constituents. The amplitudes and phases are spatially variable, but temporally constant values. The nodal factors and equilibrium arguments are spatially constant while they are temporally variable.

Parameter Identification Procedures

An efficient method of parameter identification is to take advantage of optimal control theories to minimize overall discrepancies between water level time series (calculated by traditional harmonic tide equation (Equation 5.) and in-situ measurements collected from NOAA tide and

current website. The discrepancies can be generally defined as a performance function in the form of:

$$J(X) = \sum_{j=1}^{M} \left(X_j^{cal} - X_j^{obs} \right)^2 \quad (6)$$

Where J is performance function that computes square error between water level calculated by harmonic tide equation (Eq 5) and observation data collected at each NOAA station. An iterative procedure is employed to minimize the performance function.

The L-BFGS algorithm, which is established on the basis of the LMQN (Limited-memory quasi-Newton) method, is capable of optimizing unconstrained problems, executed in parameter identification procedure (Ding et al, 2004). In L-BFGS algorithm is is capable of optimizations in large-scale problems because of the modest storage requirements using an approximation to the inverse Hessian matrix ΔJ. A software package of the L-BFGS algorithm is available in the Harwell Library under the name VA15 (More´ et al., 1993). For the details of mathematical theory about the algorithm, see Liu et al. 1989.

In L-BFGS algorithm, the norm of gradient of the objective function was computed (at each iteration), as well the value of objective function, in order to check if the optimal solution had been reached. In this study, the gradient of the performance function with regard to the two parameters were calculated. An instance of performance of objective and gradient function is illustrated in Figure 14. Gradients of performance function with regard to amplitude and phase are presented in Equation 7 and 8.

$$\frac{\partial J}{\partial A_i} = 2 \sum_{j=1}^{M} \left(X_j^{cal} - X_j^{obs} \right) \sum_{1}^{N} f_i \cos\left(\omega_i t + V_i + u_i - \psi_i \right) \quad (7)$$

$$\frac{\partial J}{\partial \psi_i} = 2\sum_{j=1}^{M}\left(X_j^{cal} - X_j^{obs}\right)\sum_{1}^{N} f_i \, \mathrm{A}_i \sin\left(\omega_i t + V_i + u_i - \psi_i\right) \tag{8}$$

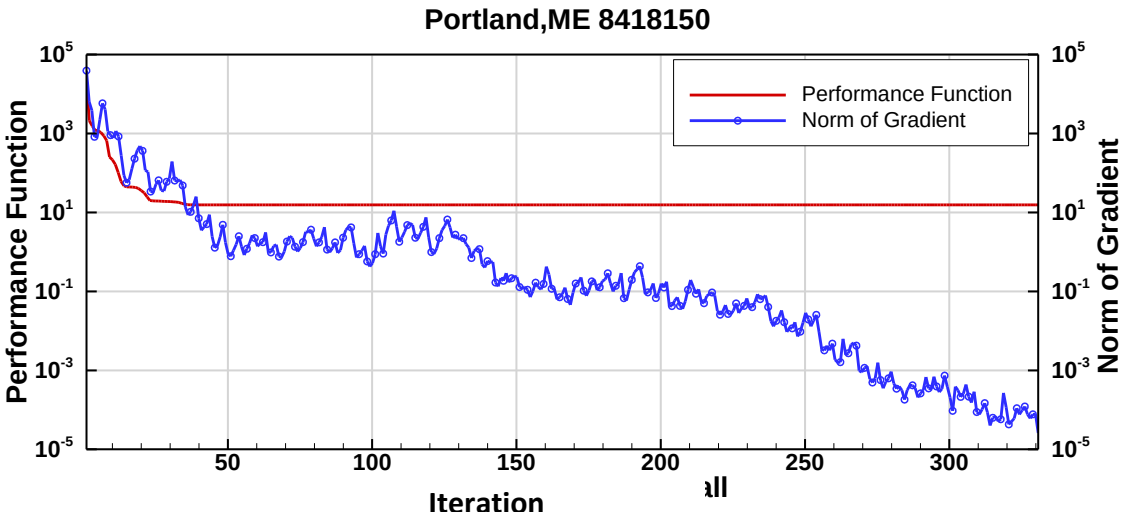

Figure 14. Convergence of norm of Gradient and performance function.

Hereafter, the L-BFGS algorithm is briefly introduced which can be found in most monographs about numerical optimization (e.g., Nocedal et al, 1999). Each iteration for updating the parameters has the form$\Psi_{k+1} = \Psi_k + \alpha_k d_k$, where H_k = approximate of inverse Hessian matrix which is update at every iteration through formula

$$H_{k+1} = V_k^T H_k V_k + \gamma_k p_k p_k^T \tag{9}$$

Where $p_k = \Psi_{k+1} - \Psi_k$; $q_k = \nabla J(\Psi_{k+1}) - \nabla J(\Psi_k)$; $\gamma_k = 1/(q_k^T q_k)$; $V_k = I - \gamma_k q_k p_k^T$; and I=identity matrix. However, the approximated inverse Hessian H_k is generally dense. Each iteration for updating the matrix can be performed a cost of $O(L^2)$ arithmetic operations, so that the cost of storage and manipulating it is prohibitive due to the large number L of the parameter n. Instead of using Eq $H_{k+1} = V_k^T H_k V_k + \gamma_k p_k p_k^T$), the H_k can be obtained implicitly by storing a certain number (e.g., m) of the vector pairs$\{p_k, q_k\}$.

The L-BFGS update formulas generate the matrix by using the vector pairs from the last m iterations (generally, $3 \leq m \leq 7$). The update matrix H_{k+1} is obtained by the following formula. Let $\hat{m} = \min\{k, m-1\}$. Then update H_0 $\hat{m}+1$ times by using the vector pairs $\{p_j, q_j\}$ where $j = k-\hat{m}, k-\hat{m}-1, \ldots, k-1$, and

$$H_{k+1} = \left(V_k^T \ldots V_{k-\hat{m}}^T\right) H_{k+1}^0 \left(V_{k-\hat{m}} \ldots V_k\right)$$
$$+ \gamma_{k-\hat{m}} \left(V_k^T \ldots V_{k-\hat{m}+1}^T\right) p_{k-\hat{m}} p_{k-\hat{m}}^T \left(V_{k-\hat{m}+1} \ldots V_k\right)$$
$$+ \gamma_{k-\hat{m}+1} \left(V_k^T \ldots V_{k-\hat{m}+2}^T\right) p_{k-\hat{m}+1} p_{k-\hat{m}+1}^T \left(V_{k-\hat{m}+2} \ldots V_k\right) + \ldots + \gamma_k p_k p_k^T \quad (10)$$

From this formula, one can derive a recursive procedure to compute the product $H_{k+1}\nabla J(\Psi_{k+1})$ efficiently. A two-loop recursion scheme which can obtain the product only using inner product of vectors requires totally $(4m+1)L$ arithmetic operations (Nocedal et al, 1999). This calculation for searching direction is advantageous when the number of parameters becomes large. Moreover, this recursive iteration allows the initial matrix H_{k+1}^0 to be chosen freely and to vary between iterations (Liu et al, 1989; Nocedal et al, 1999).

CHAPTER III:

HINDCASTING STORM SURGE AND WAVES IN HURRICANE BOB IN THE GULF OF MAINE USING CCHE2D-COAST

In this chapter, CCHE2D-Coast is applied to simulate meteorological and hydrodynamic processes during Hurricane Bob (1991) on the US Atlantic coast. Simulated physical parameters, i.e. wind speed, pressure, water surface elevations, significant wave heights, and peak wave periods in several monitoring points across the computational domain were carefully compared with the recorded data at corresponding NOAA CO-OPS and NDBC buoy stations. The model was validated by comparing hindcasting results with the observed data. The error in simulated parameters was small and comparison was found to be in a good agreement with corresponding observed data.

On 19-20 August 1991, the Category 3 Hurricane Bob touched down on the East Coast and brought significant flooding into the New England Coast and the Gulf of Maine area. Hurricane Bob originally appeared as a low-pressure area in the Atlantic Ocean near the Bahamas (74.3° W, 25.6° N) at 00:00 GMT on August 16, 1991. The depression steadily intensified and became a tropical storm 18 hours later. The storm continued to strengthen as it moved northwestward and became ‘‘Hurricane Bob’’ at 77.10° W, 29.00° N at 18:00 GMT on August 17th, 1991.

Hurricane Bob initially moved northeastward and brushed the North Carolina shelf between 18:00 GMT on August 18, 1991 through 00:00 GMT on August 19, 1991 during which it reached to the hurricane category 3 with maximum sustained winds of 51.4 m/s. Around 18:00 GMT on 19 August 1991, Hurricane Bob had weakened to the category 2 and made landfall near Newport, Rhode Island. Shortly thereafter, it rapidly weakened to a tropical storm and moved across the Gulf of Maine (GoM) toward Maine and Canada, finally dissipating west of Portugal on 29 August 1991 after a long transit across the North Atlantic Ocean. The strong winds, high

storm surge, and heavy rains produced by Hurricane Bob caused extensive damage throughout New England with a total loss of $1.5 billion in economy, cleanup costs, uninsured losses, and flood claims (Mayfield 1992, Sun et al. 2013).

This study considers several processes such as tidal condition specification, model spin-up, storm data collection, and model validation (hindcasting). Simulated physical parameters, i.e. wind speed, water surface elevations, significant wave heights and peak wave periods in several NOAA CO-OPS (National Oceanic and Atmospheric Administration Center for Operational Oceanographic Products and Services) and NDBC (National Data Buoy Center) buoy stations are carefully compared with the recorded data. The model was validated by comparing hindcasting results with observed data.

HURRICANE TRACK

The category 2 Hurricane Bob developed in the central Bahamas on August 16. Then, steadily intensified and reached hurricane status on the evening of August 17. Bob continued to strengthen during the next 48 hours, as it began an acceleration north-northeastward, paralleling the East Coast. The eye of Hurricane Bob passed over Block Island, Rhode Island at approximately 1330 UTC, and made landfall over Newport, Rhode Island shortly before 1400 UTC (Vallee and Dion 1998).

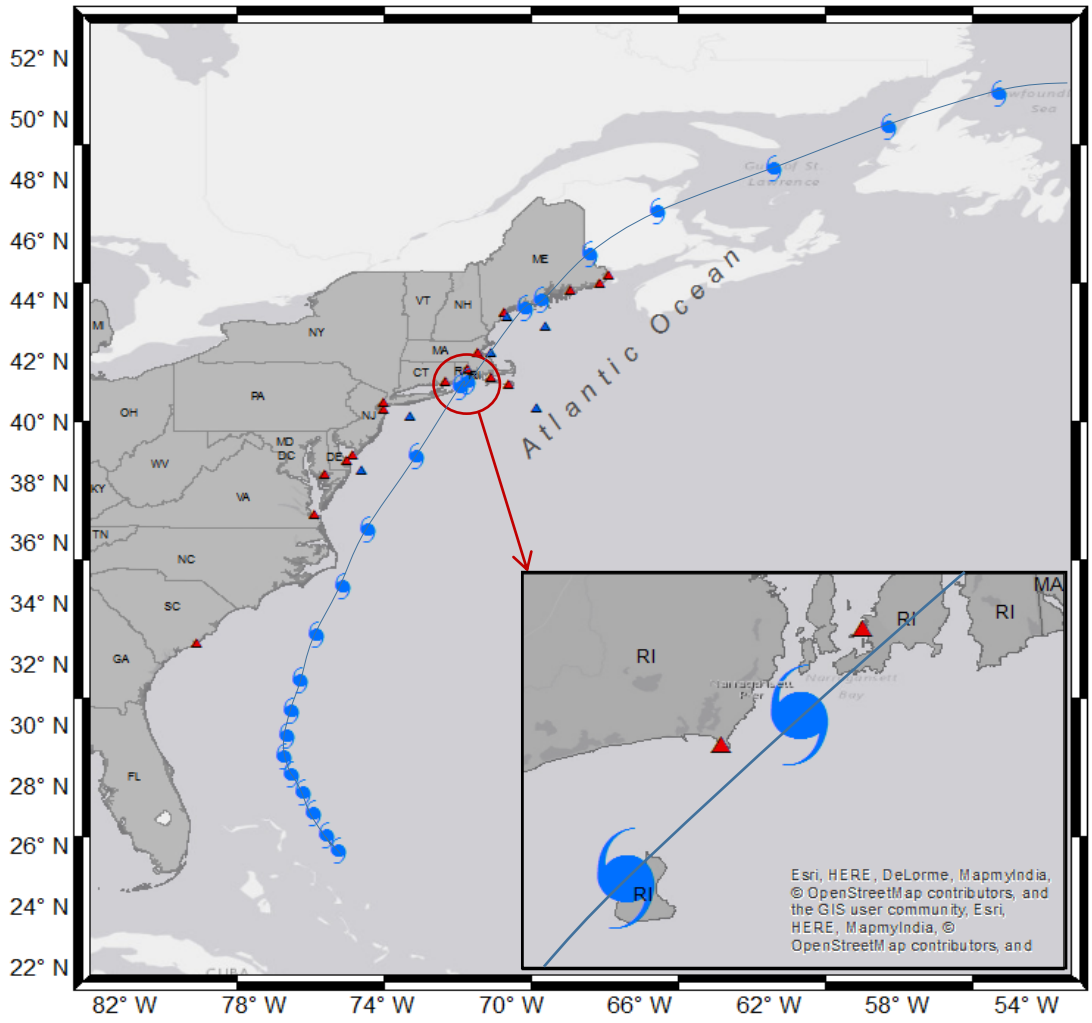

Figure 15. Hurricane Bob best Track. Hurricane Bob made landfall at Rhode Island.

The best track data of tropical storms, also known as HURricane DATabase (HURDAT), provided by NOAA as a report, contains the positional coordinates of the eye of the hurricane, hurricane central air pressure, and maximum sustained wind speed (Mayfield 1992). The variation of Hurricane Bob location is depicted in Figure 15.

NOAA GAUGE STATIONS AND BOUNDARY CONDITION

A number of NOAA CO-OPS and NDBC buoy stations were used as monitoring gauge stations. Observation was used to illustrate the discrepancies between recorded

Table 2. List of NOAA CO-OPS and NDBC BUOY stations.

No.	Station Name, State(or Location)	Station ID	Longitude	Latitude
1	Bar Harbor, ME	8413320	-68.21	44.39
2	Boston, MA	8443970	-71.05	42.35
3	Cape May, NJ	8536110	-74.96	38.97
4	Cutler Naval Base, ME	8411250	-67.30	44.64
5	Eastport, ME	8410140	-66.98	44.90
6	Lewes, DE	8557380	-75.12	38.78
7	Nantucket Island, MA	8449130	-70.10	41.29
8	Newport, RI	8452660	-71.33	41.51
9	Ocean City Finishing Pier, MD	8570280	-75.83	38.33
10	Point Judith, RI	8455083	-71.49	41.36
11	Portland, ME	8418150	-70.25	43.66
12	Providence, RI	8454000	-71.40	41.81
13	Sandy Hook, NJ	8531680	-74.01	40.47
14	The Battery, NY	8518750	-74.01	40.70
15	Woods Hole, MA	8447930	-70.67	41.52
16	New London, CT	8461490	-72.09	41.36
17	Charleston, SC	8665530	-79.81	32.74
18	Chesapeake Bay Bridge Tunnel, VA	8638863	-76.12	36.97
	NDBC Stations			
1	Portland, ME	44007	-70.16	43.54
2	Nantucket	44008	-69.25	40.51
3	Gulf of Maine, NH	44005	-68.95	43.21
4	Boston, MA	44013	-70.65	42.35
5	Long Island, NY	44025	-73.17	40.25
6	Delaware Bay, NJ	44009	-74.70	38.46
7	Ambrose Light, NY	ALSN6	-73.80	40.45
8	Matinicus Rock, ME	MISM1	-68.86	43.78
9	Buzzards Bay, MA	BUZM3	-71.03	41.40
10	Isle of Shoals, NH	IOSN3	-70.62	42.97
11	Mt Desert Rock, ME	MDRM1	-68.13	43.97

data and hydrodynamic and meteorological simulated variables. The list of monitoring station and location of observation points is illustrated in Table 2 and Figure 16, respectively. In this simulation, the water level elevation at Bermuda (2695540) is used as the tidal boundary condition.

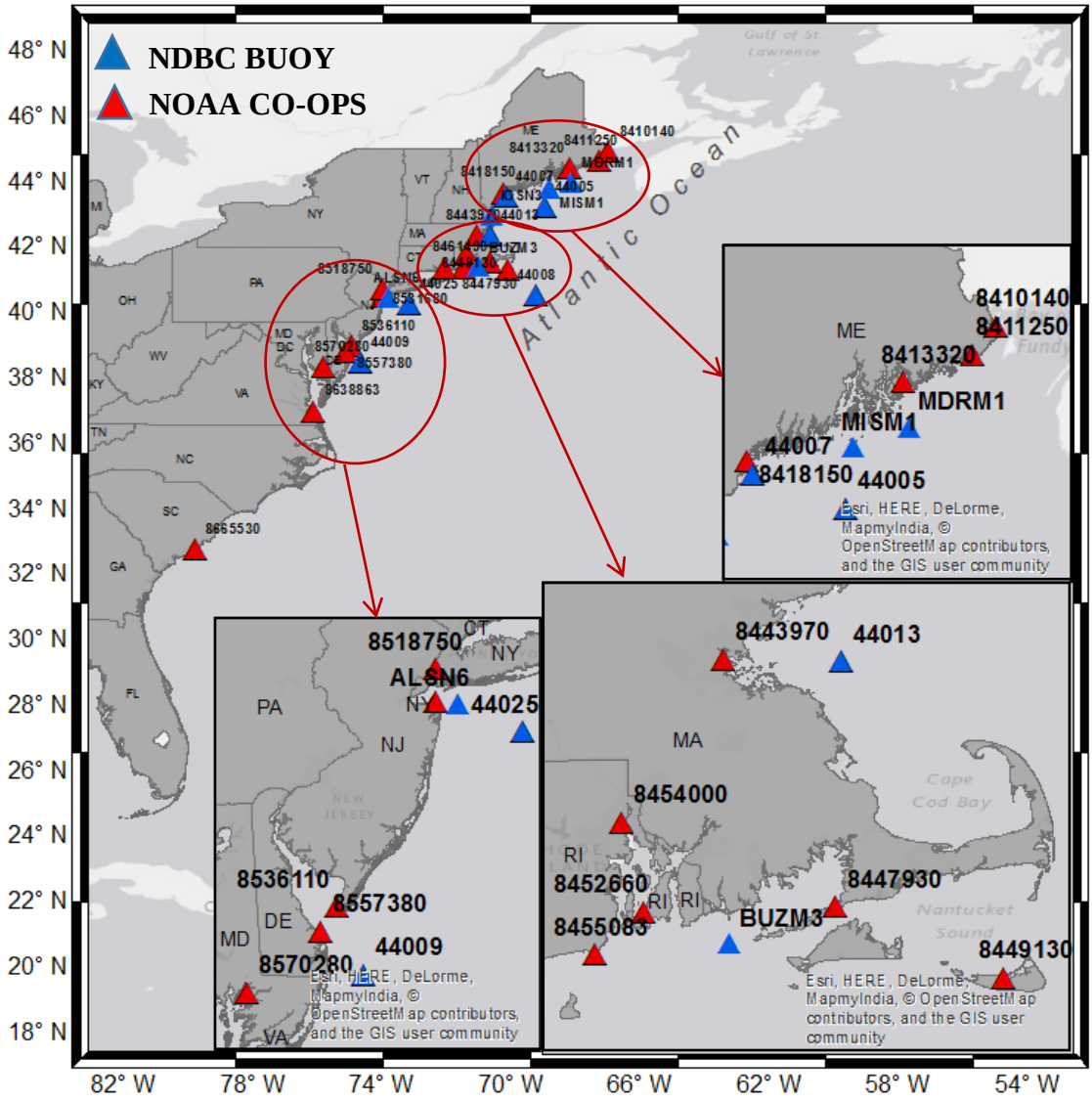

Figure 16. Gauging stations on North of East coast.

HURRICANE TRACK MODEL

A parametric cyclonic hurricane wind model proposed by Holland (1980) has been integrated in the CCHE2D-Coast model, which is to simulate variations of wind and atmospheric pressure along a given storm track. Provided that central pressure and maximum wind speed, Holland (1980) proposed a parametric wind model to reconstruct hurricane wind fields.

SIMULATION RESULT OF STORM SURGES AND WAVES

The simulation run of storm surges and waves started at 1200 UTC 08/17/1991 and ended on 1200 UTC 08/24/2012. The surface wind field of Hurricane Bob was reconstructed by using the symmetric parametric cyclone wind model, Holland model, which takes into account the decay effect of hurricane landfall (Ding et al. 2013b). Thus, after the cyclone made landfall in Rhode Island, the decay of landfall was automatically considered by modifying the maximum wind speed and the central air pressure based the nonlinear surface wind model developed by Ding et al. (2013).

As it was discussed in previous chapter, to avoid having the spurious fluctuation in simulated hydrodynamic variables, the model has to be initialized, or spun up. On the other hand, a well-developed sea state is created for flow dynamic simulations driven by the storm winds. This model was spun up by simulating the tidal flows over the US east coast for 10 days, i.e. from 1200 UTC 08/07/1991 to 1200 UTC 08/17/1991. The time-step size used was 120 seconds. During the spin-up period, the effect of surface wind was neglected.

In the simulation of surge tide, the wave-induced radiation stresses, surface wind stresses, and the bottom friction stresses were considered. The frequency of wave-current interaction was two hours, namely, the wave field driven by the cyclone wind was updated every 2 hours during the

storm surge simulation. In the computation of wave-action equation of the spectral wave energy, a total of 21 frequency bins and 25 wave directions were used to discretize the wave spectra for the computations of irregular wind-induced waves. In this simulation, the effect of wave breaking in shallow waters and the whitecapping in deep waters were included.

Wave set-up induced by storm winds can cause an additional increase in the water surface elevation and increases the extent of the inundation area. In the simulations of storm surge by coupling the wave model with the hydrodynamic model, the wave field was recomputed every two hours based on the latest flow results.

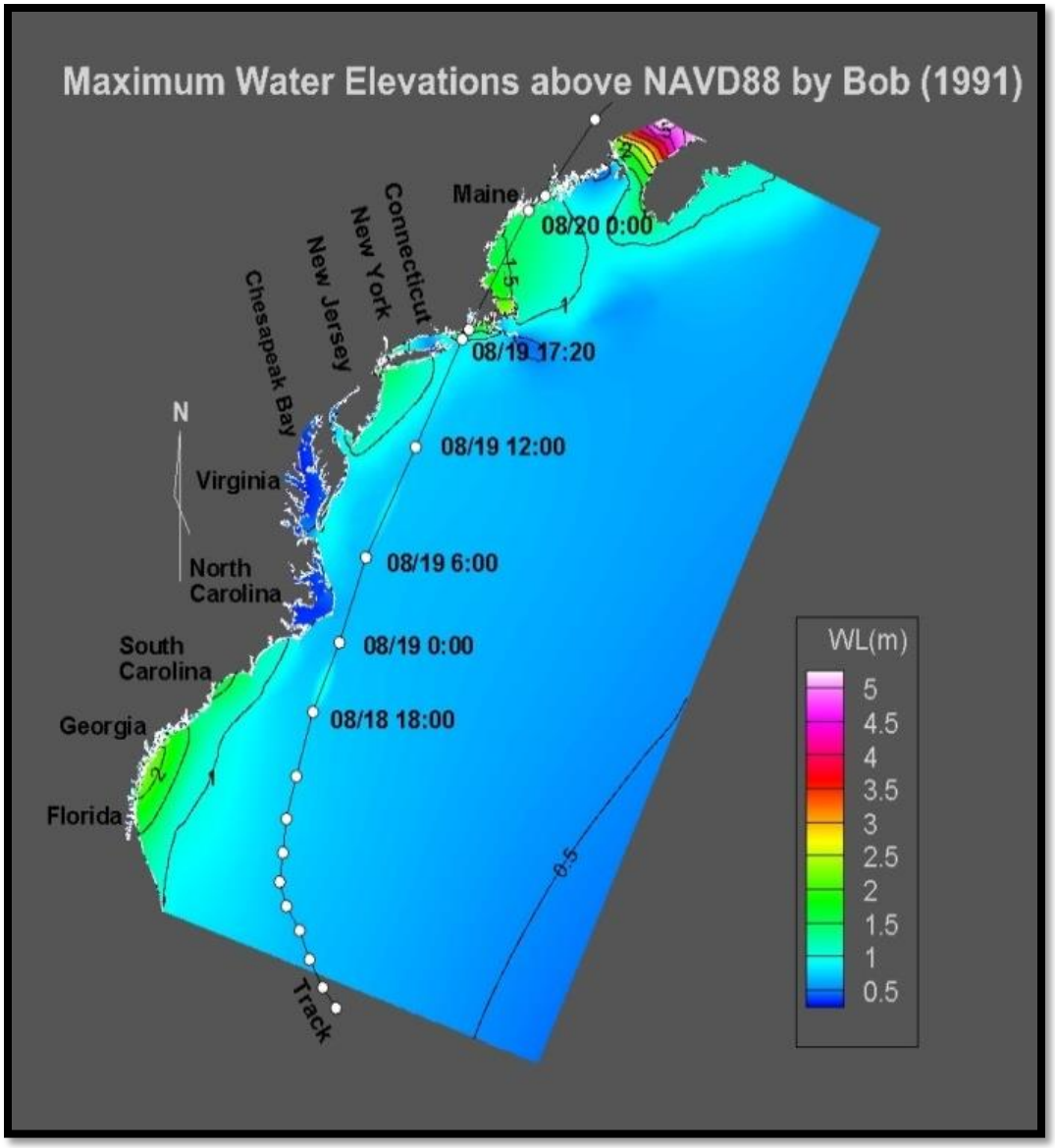

Figure 17. Maximum Water Elevation above NAVD88 by Bob (1991).

Figure 17 shows the computed maximum water surface elevations for Hurricane Bob across the East Coast of the United States. Maximum water level is observed at Bay Fundy where there is home of high tides on the East Coast. In Figure 18 and Figure 19, the predicted air pressure and

wind velocity are compared to the recorded data from gauge stations at the several points across the computational domain.

In stations, 44007, 44013, IOSN3, and BUZM3 the pressure drop match to the observed values while in ALSN6, MISM1, 44025, 44009, and 44005 the pressure model underestimated the pressure drop. The pressure model could not capture variation in pressure in far-field. This error is associated with parametric wind and pressure model that makes the wind and pressure field not very accurate in region far away from the hurricane's center.

Simulated wind velocity is in a good agreement with corresponding observed values in MDRM1, MISM1, BUZM3, IOSN3, 44008 BOUY stations at the moment when the hurricane passing is by them. In station 44008, the model performed well in capturing maximum wind speed, which matches to the observed value. However, the wind model's result showed some errors in reproducing simulated wind velocity in some stations such as 44005, 44013, ALSN6, and 44009. In station 44009 and ALSN6, the model was unable to capture intensification of wind velocity due to induced forces from Hurricane Bob. In 44013, 44007, and IOSN3 wind velocity variation had a sharp fall and rise at the peak zone while sudden intensification or reduction in observed wind was recorded.

In addition, the model performed well because there is not lag observed in simulated wind velocity and pressure drop. It commonly appears in simulation of hurricane wind field that the simulation has some delay in capturing the peaks. This error, if exists, can be attributed to the error within best track data from observations.

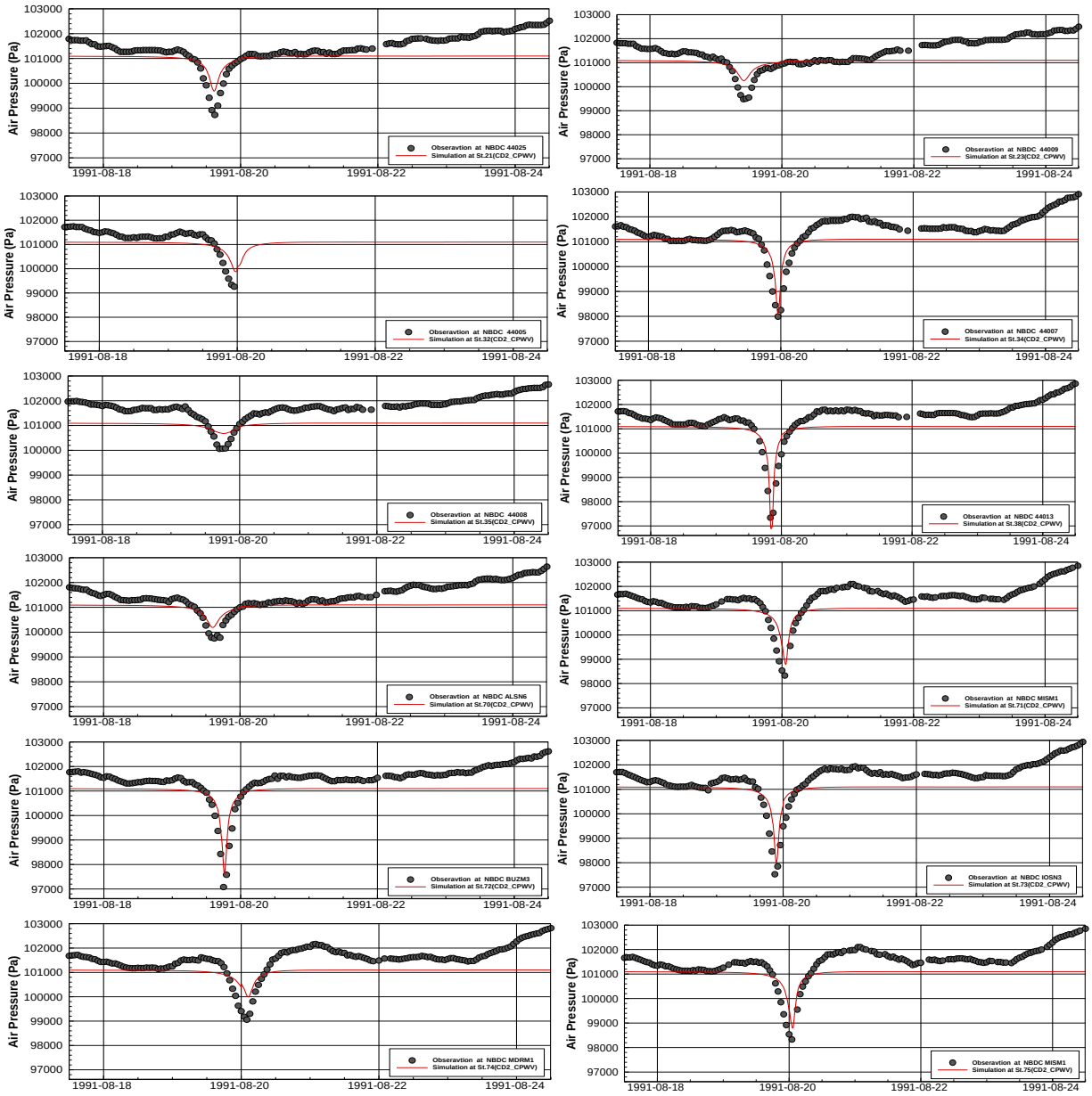

Figure 18. Comparisons of simulated pressure with observed data during Hurricane Bob.

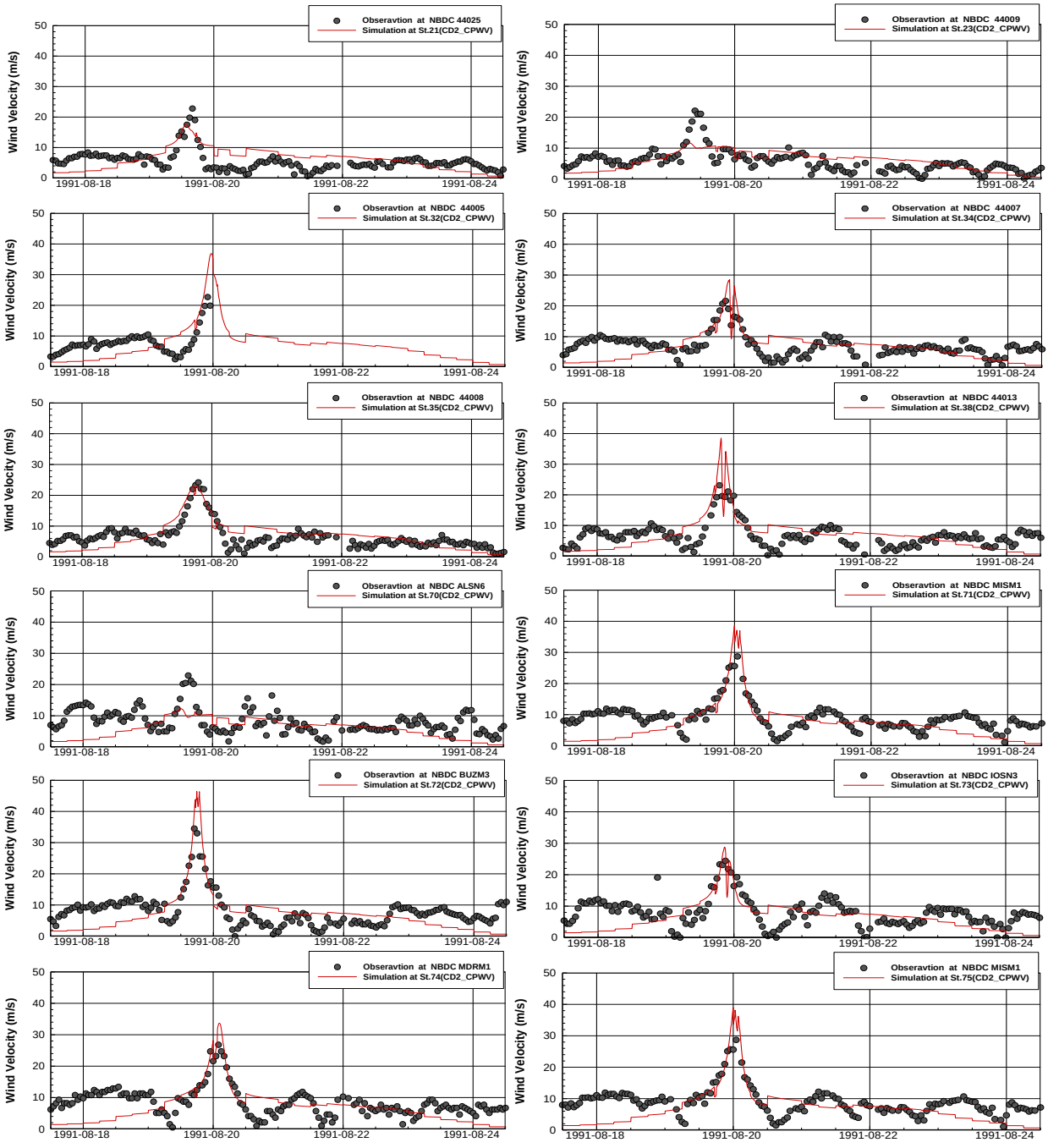

Figure 19. Comparisons of simulated wind speed with observed data during Hurricane Bob.

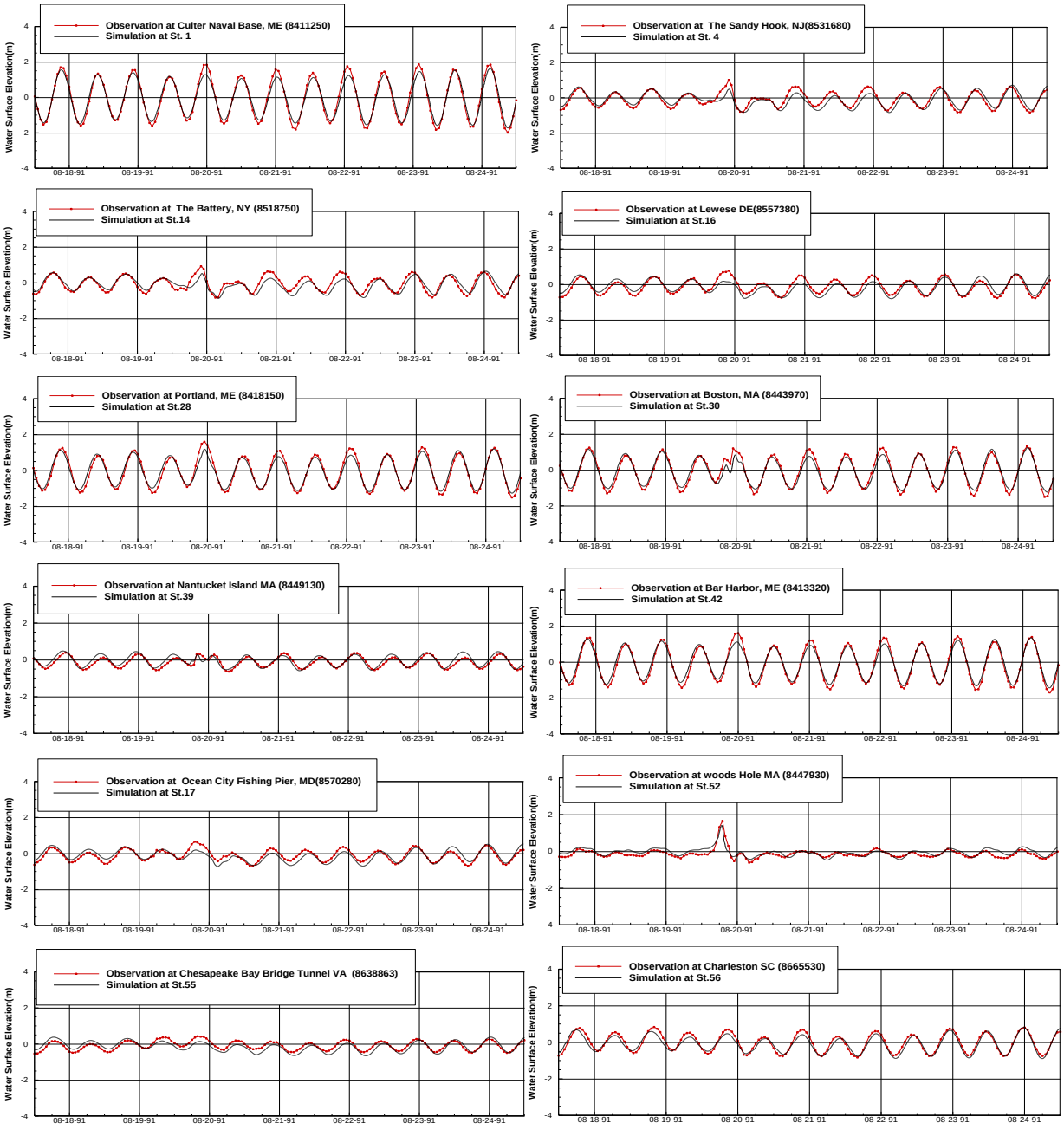

Figure 20. Comparisons of computed vs observation of water elevation at different stations.

Figure 20 and Figure 21 present the comparison between the computed and observed water surface level. Model's performance was quite well in hindcasting water level; the computed

amplitudes at Portland ME (8418150) and Boston MA (8447930) corresponded well with the observations values. In Woods Hole MA (8447930), Newport RI (8452660), Providence RI (8454000), Point Judith RI (8455083) the model captured the increase in water level due to hurricane driving forces while in Lewese DE (8557380) the model result underestimated the peak.

Comparison of the observed and computed significant wave heights and the peak periods for the three selected gauge stations are shown in Figure 22 and Figure 23. Offshore of the South Portland Coast, at the NDBC 44007 buoy, 44005, and 44013 the computed significant wave heights captured the variations of the observations, although there are some minor differences observed. Only the computed peak wave height is smaller than that observed value. There is a lag in the simulation of significant wave height. At the three other stations, i.e. NDBC 44009, 44008, and NDBC 44025 buoy, recorded peak is captured by the simulation result.

The computed peak wave periods are relatively close to the corresponding observed data. The model result showed large discrepancies between computed wave peak periods at stations 44013. In stations 44008 and 44007 the model was able to capture the variations in peak period.

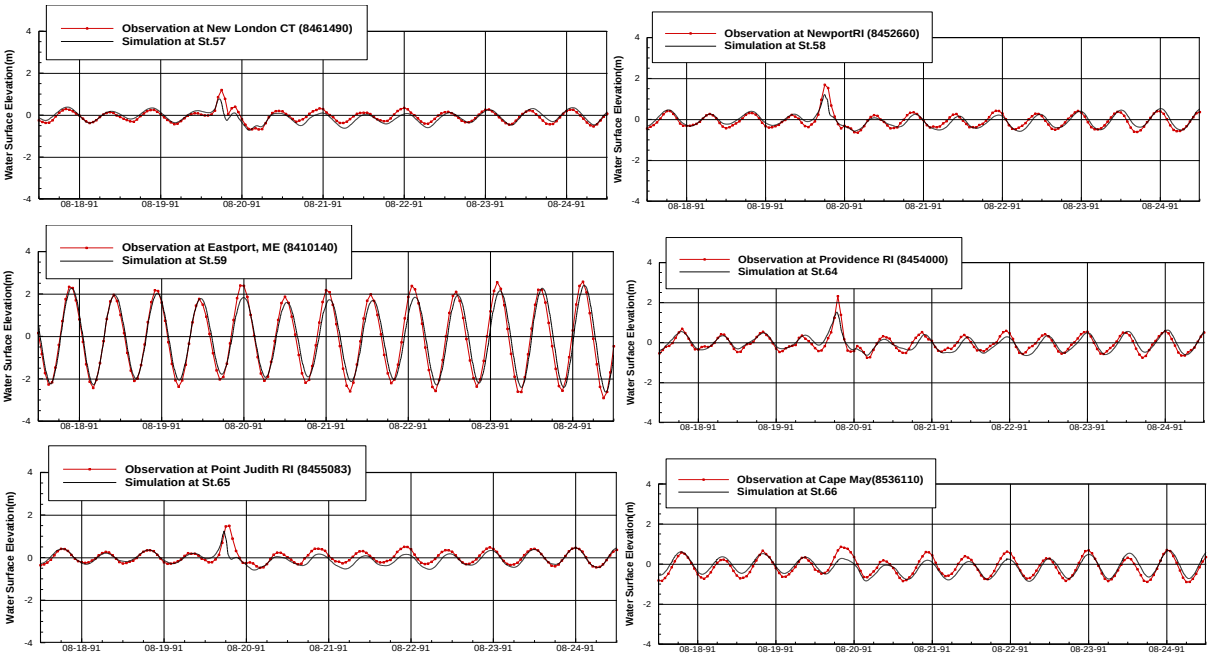

Figure 21. Comparisons of computed vs observation of water elevation at different stations.

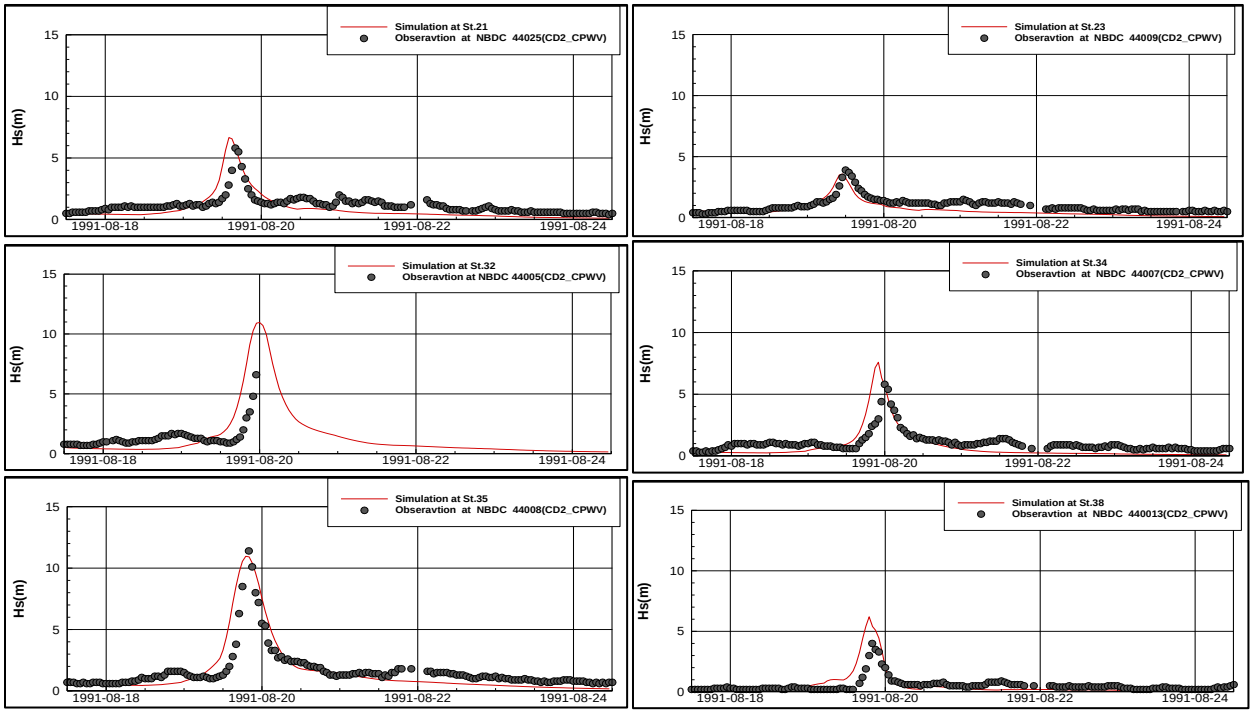

Figure 22. Comparison of wave properties at stations NDBC #44025, #44009, #44005, #44007, #44008, #44013.

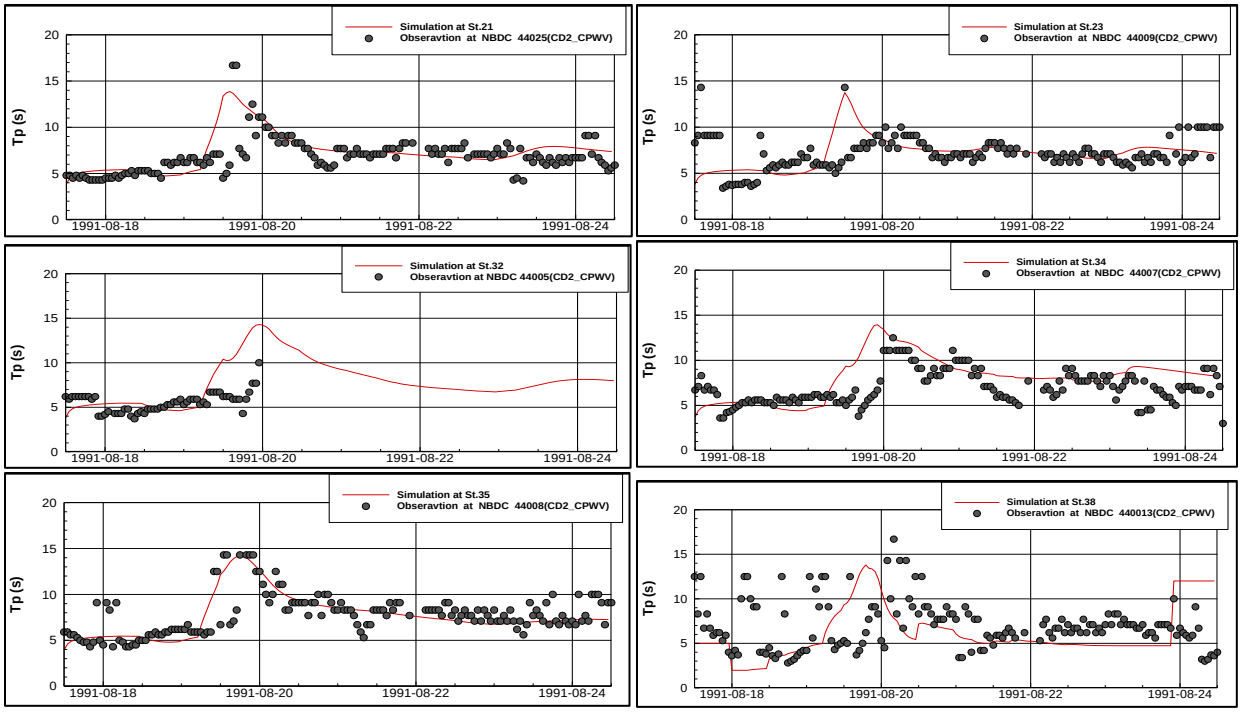

Figure 23. Comparison of wave properties at stations NDBC #44025, #44009, #44005, #44007, , #44008, , #44013.

CHAPTER IV:

DEVELOPMENT AND VALIDATION OF ASYMMETRIC PARAMETRIC HURRICANE WIND MODEL

In this chapter, an Asymmetric Gradient Wind Model (AGWM) is developed based on the modified synthetic Holland-type vortex model. AGWM is created to capture the azimuthal variation of hurricane's wind and pressure field. The curved fitted values of hurricane parameters are used to compute tangential velocity and pressure, at any azimuthal angle, around the storm center.

There are several physical processes and forces that must be taken into account in storm surge modeling such as tides, wind friction, pressure drop, and Coriolis forces. Among these factors, the atmospheric forces are the predominant force components, which include pressure gradient and especially wind forces. There are other forces such as temperature gradient or Ekman balance which are not taken into account in this study.

The hurricane's high winds are the primary force that generates storm surge and waves. Thus, a good prediction of wind intensity and building a more accurate hurricane's structure will improve the spatiotemporal extent of the hurricane storm surge simulation. Thus, it is critical to make use of any available data, usually provided by National Hurricane Center (NHC), to construct a more accurate wind body of a tropical storm. The real-time data of wind and surface pressure are insufficient to allow a direct analysis of the central region of most tropical cyclones and they cannot be used alone to generate the wind field needed for a storm surge model (Powell et al., 2010). For this reason several models have been developed to infer wind and pressure fields.

Over the past decades, several products, different numerical and statistical wind models, parametric and empirical formulas have been developed to help the improvement of the prediction and to enhance forecasting the spatial/temporal change of the hurricane wind field

during a storm event. Simple analytical and statistical models such as National Weather Service, NWS-23 (1979) contained specific official guidelines for the meteorological representation of a standard hurricane. The NWS-23 formulation was based on observational data that was recorded during hurricane reconnaissance flights in the North Atlantic from 1957 through 1969.

Other parametric models are Holland model 1980 (modified in 2010) Jelesnianski et al 1992, Houston et al 1999 formed a simple algebraic formulation of the radial gradient wind speed for storm surge analysis (SLOSH); Vickery 2000 developed a wind model by taking into account the effects of changing sea surface roughness and the air-sea temperature difference on the estimated surface-level wind speeds; Willoughby 1980, 2006 developed a wind profile as a statistical fit to the numerous observations; Emanuel et al 2004 formed a statistical/deterministic gradient wind model; Another approach is the steady-state dynamical model such as steady-state slab planetary boundary (PBL) model (Chow, 1970; Cardone et al., 1976,2009; Shapiro, 1983; Thompson, et al., 1996; Vickery et al., 2000).

The kinematical analysis winds such as National Oceanic and Atmospheric Administration (NOAA) National Hurricane Research Division H*Wind (Powell et al., 1996, 1998, 2010), mesoscale models such as interactive objective kinematic analysis (IOKA) (Cox et al., 1995), and Mesoscale numerical weather prediction model such as North American Mesoscale model known as NAM, Geophysical Fluid Dynamics Laboratory (GFDL), The MM5 (short for Fifth-Generation Penn State Mesoscale Model) is a regional mesoscale model used for creating weather forecasts and climate projections and is maintained by Pennsylvania State University and the National Center for Atmospheric Research, the mesoscale Weather Research and Forecasting (WRF) model.

Mesoscale dynamic models adopt the full governing equations which are taking into account the known physical processes and laws that govern the behavior of atmosphere. They can create a detailed picture of the dynamic state of atmosphere. However, in order to numerically simulate the complex structure of the atmosphere using mesoscale tools, a fine resolution mesh size is required. This requirement imposes numerical models to employ extensive resources to run heavy-duty computations. Nevertheless, the complexity of coupling atmosphere models to storm surge and wave models, limited run-time, and computer memory made the parametric wind models are widely uses in reproducing the hurricane wind fields and driving forces to the storm surge and wave models.

Parametrized wind models have zero computational cost and can be launched on personal computers. This is a big advantage over the mesoscale model which is basically using supercomputing machines to perform real-time hurricane's wind forecasting. Therefore, parametric models are a good alternative to tradeoff between the accuracy and cost.

To test the newly-developed model, Hurricane Gustav's (2008) best track data is used to test the asymmetric wind model performance. The values of maximum wind speed, radii of wind isotachs, and central pressure were used to capture the spatiotemporal variation of the hurricane induced wind. In this chapter, the theoretical background regarding the application of parametric wind models and determining its key parameters is explained. Different modules are tested and result's analysis presented for Gustav.

THEORETICAL BACKGROUND

Numerous numerical models employed analytical parametric gradient wind formulations. In this formulation, a few parameters exist; such as radius of maximum wind and maximum wind speed,

central pressure. In Figure 24, a schematic layout of hurricane's structure and the location of maximum wind speed, which is commonly named as the maximum radius (R_{max}), is illustrated. R_{max} is defined as the radial distance from the hurricane center at which the maximum wind speed is observed. The formulation can represent the radial profile of the pressure drops exponentially towards the center from the ambient pressure while wind profile has a sharp increase from the eye of the hurricane to the location of maximum wind and decreases towards the outer region of the storm (Figure 24).

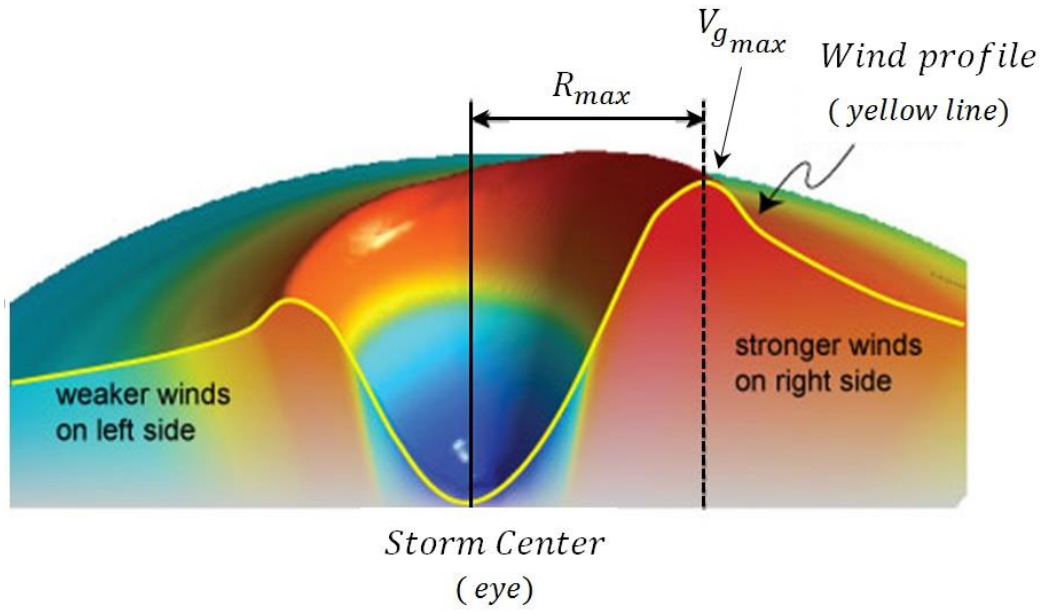

Figure 24.Schematic cross section of hurricane wind profile for north heading cyclones.

Simple parametric hurricane wind models generally consider the wind around the hurricane to be circularly symmetric (Figure 25). Therefore, at a given radius for all azimuthal angles, the same wind speed will be generated (by excluding the forward movement speed of the storm). A simple hurricane wind model would consist of a circular storm rotating counterclockwise (in the Northern Hemisphere) around a central axis without any storm motion and no inflow or outflow.

Holland's (Holland, 1980), popular parametric wind model, has been widely applied in tropical storm studies and has remained the most used method in forecasting hurricane wind field. This formula is basically a modified version of a Schlomer's (1954) formula which suggested that the pressure field can be approximated by:

$$p(r) = p_c + (p_n - p_c)e^{\left(-\frac{A}{r^B}\right)} \quad (1)$$

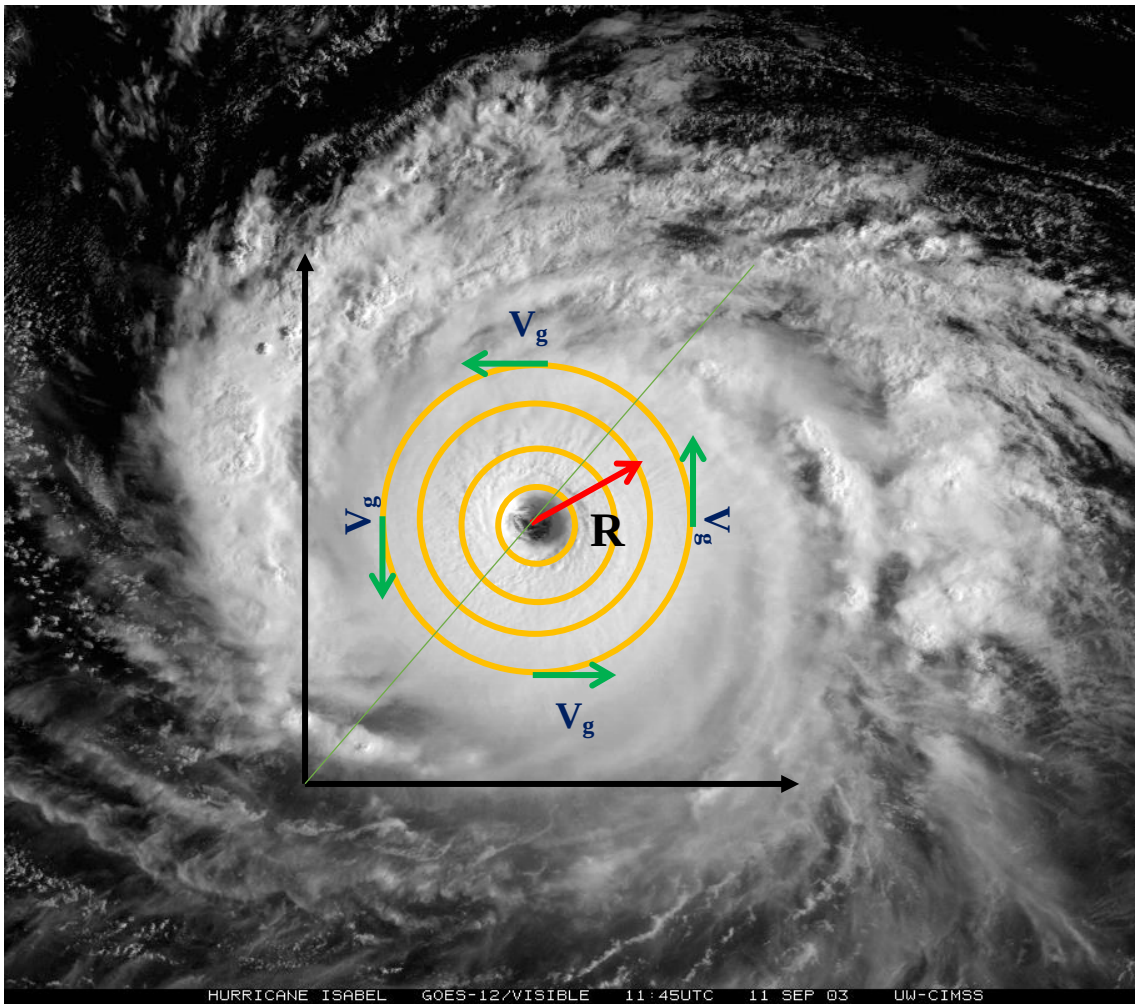

Figure 25. Schematic layout of symmetric hurricane wind field constructed based on Holland 1980 symmetric model.

Where $p(r)$ pressure at radial distance r, p_c is the pressure at the center of the hurricane, p_n the ambient pressure (theoretically at infinite radius) to specify pressure field that contains some parameters empirically estimated from the observations or determined climatologically (A and B are two parameters that can scale the wind profile). Hence, using the gradient wind equation which can be derived from the force balance between the Coriolis force, the centrifugal force, and the horizontal pressure gradient force:

$$\frac{V_g(r)}{r} + fV_g(r) = \frac{1}{\rho_{air}} \frac{\partial p(r)}{\partial r} \tag{2}$$

The wind profile becomes:

$$V_g(r) = \left[\frac{AB(p_n - p_c)e^{\left(-\frac{A}{r^B}\right)}}{\rho_{air} r^B} + \frac{r^2 f^2}{2} \right]^{\frac{1}{2}} - \frac{rf}{2} \tag{3}$$

Where $V_g(r)$ is the gradient wind at radius r, respectively. $f = 2\Omega \sin\phi$ is the Coriolis parameter, Ω rotation rate of the earth, ϕ is latitude, and ρ_{air} the air density (assumed constant). Holland (1980) postulates that at the region of maximum winds, the Coriolis effect is very small compared to the two other existing forces, which are the pressure gradient and centrifugal force, and the air is in the cyclostrophic balance. These tangential winds are given by:

$$V_g(r) = \left[\frac{AB(p_n - p_c)e^{\left(-\frac{A}{r^B}\right)}}{\rho_{air} r^B} \right]^{\frac{1}{2}} \tag{4}$$

$$A = {R_{max}}^B \tag{5}$$

And

$$B = {V_g}^2{}_{max} \rho_{air}\, e/(p_n - p_c) \tag{6}$$

Thus, the pressure field and tangential wind at radius r will be:

$$p(r) = p_c + (p_n - p_c)e^{\left(-\frac{R_{max}}{r}\right)^B} \quad (7)$$

$$V_g(r) = \sqrt{\left(\frac{B}{\rho_{air}}\right)\left(\frac{R_{max}}{r}\right)^B (p_n - p_c)e^{\left(-\frac{R_{max}}{r}\right)^B} + \frac{r^2 f^2}{2}} - \frac{rf}{2} \quad (8)$$

In the above formula, B is the key parameter that controls the shape of the wind profile (the steepness of the eyewall and the strength of the wind far from the cyclone's center). According to Holland (1980), B parameter remains constant. However, in Holland (2008), the parametrized method was modified in order to incorporate additional available observation of winds such as latitude, translational speed, and intensification rate ($\partial \mathrm{p_c}/\partial \mathrm{t}$). Some other method suggested different formula to compute Holland shape parameter B , as given for example in Harper and Holland (1999), Vickery et al. (2000), Jakobsen and Madsen (2004), Powell et al. (2005), Willoughby et al (2006), and Vickery and Wadhera (2008).

Due to existent friction and some other forces, the actual hurricane wind field is not symmetric (Figure 26). Since Holland's model is axisymmetric, some modifications must be implemented in order to consider the asymmetric structure of the real wind fields (Harper et al., 2001). Fortunately, in recent years, additional information has become available during tropical storms which can be used to enhance the accuracy of wind models.

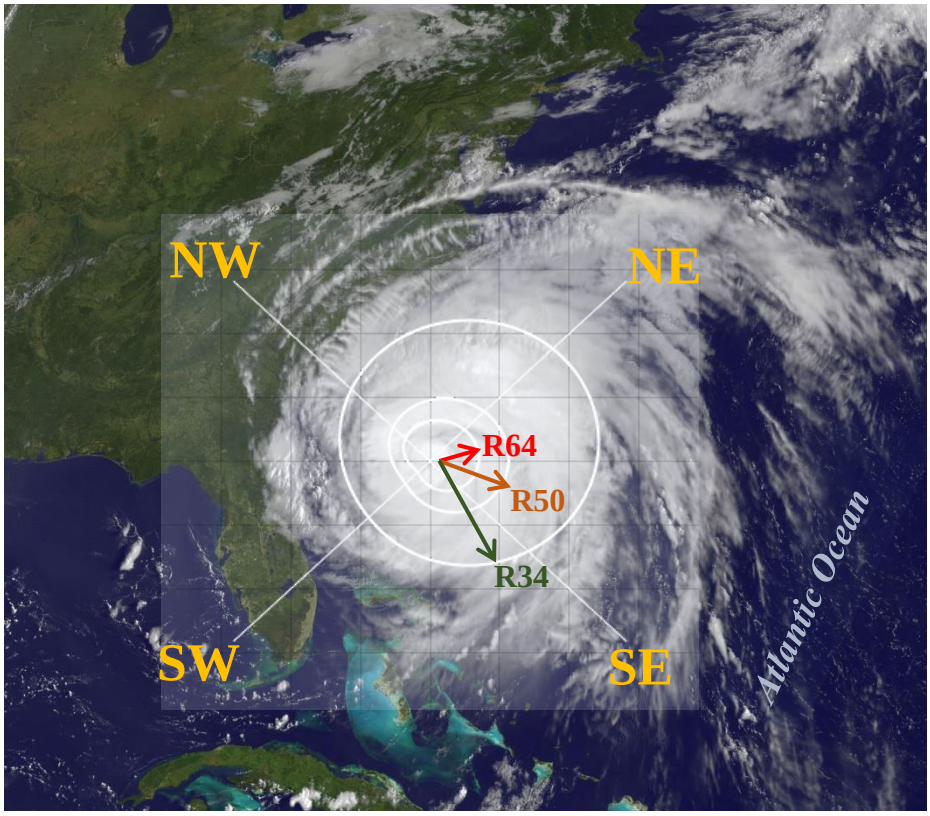

Figure 26. Asymmetric shape of a hurricane can be captured based on directionally variable parameters in Holland model.

In the past decade, more observational data from tropical storms has become available from NHC forecast advisories. Additionally, the ATCF has provided best track observation and forecast data of hurricane's spatiotemporal variation in position, wind field, and central pressure. Data from the best track data is composed of central pressure, maximum wind speed, and specified radius of the 1-min sustained surface wind isotachs 32.9, 25.7, and 17.5 ms^{-1} (64,50, and 34 kt) in four quadrants of storms which are Northeast, Southeast, Southwest, Northwest(NE, SE, SW, and NW). This additional data is used to calculate azimuthally variable parameters of asymmetric Holland model.

Most non-symmetric models used only the largest available specified wind velocity and its radius at each quadrant from best track data to compute the asymmetric wind model's parameter.

Due to the complexity of hurricanes, it is imperative to make use of all available data (all isotach). Using one set of specified data, radii and wind speed of one isotach, in parametric model can only represent the complete radial variation correctly along the wind profile. In Figure 27, it is illustrated that using information of one isotach can introduce large error in wind velocity either in far or near field; for instance, a wind profile (Figure 27-a) which was constructed based on the isotach 64kt data, underestimates the wind velocity at the far field.

The wind profile developed based on the Holland formula is not flexible; it rarely occurs that a wind profile, constructed based on Holland formula, can pass through three data points, available data, which are the radii and wind speed of three isotachs. A combination of $V_{g_{max}}$, R_{max} , B, ψ parameters is not always available that one profile can be built that can go through three data points: (R64,V64), (R50,V50), and (R34,V34). Therefore, using all the three (if available) isotachs data at each quadrant, and combining them correctly (Figure 27-d), can help to improve consistency of parametric model to the observation data.

Xie et al (2006) used the radial extent of hurricane's wind field data, provided by NOAA hurricane forecast guidance, to develop a non-symmetric wind model by incorporating an asymmetric effect into the Holland symmetric model. They employed the asymmetric wind model in the storm surge simulation to examine the asymmetric hurricane wind field forecast, as well. In their model, a single value of R_{max} for the wind field is replaced by a directionally varying $R_{max} = R_{max}(\theta)$ where θ is the azimuthal angle from the north to the angle of the quadrant of interest. With using the radii and wind speed from the best track data, R_{max} at four quadrants was calculated. To obtain the azimuthal variation of R_{max}, a curve fit procedure was utilized to interpolate data at each azimuthal angle. The issue with their fourth-order polynomial

curve fit was a numerical discontinuity at $\theta = 0$ and $\theta = 2\pi$ and using only the highest isotach's radii to build the wind profile.

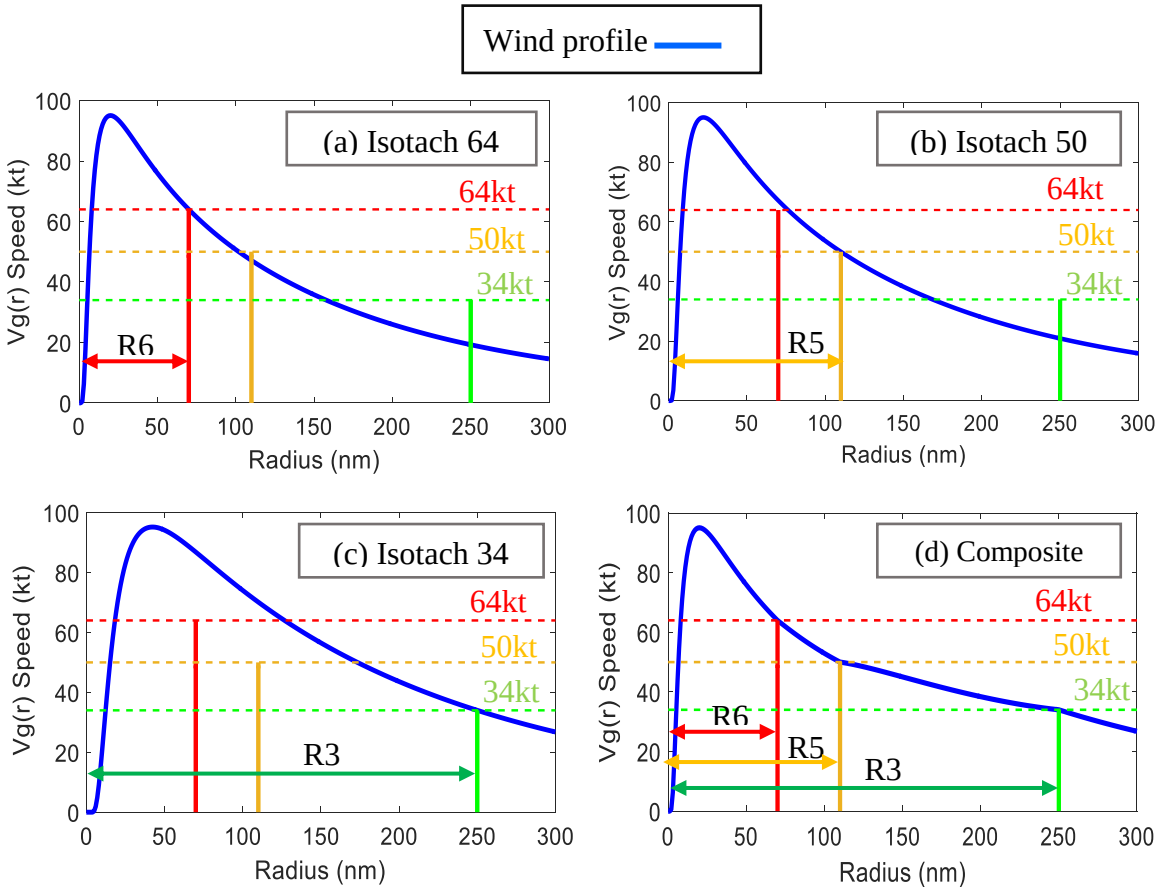

Figure 27. Wind profiles constructed under independent isotach data and composite profile using 3 isotachs data.

Mattocks et al (2008) used Xie's approach and developed their synthetic asymmetric vortex wind forcing and implemented it to examine several different features of storm surge and wave models. They used a cubic splines interpolation which meets the continuity of interpolated values between 0 and 2π angles. In the Forbes et al 2010 study, storm surge forecasts were forced using an asymmetric gradient wind model (similar to Mattocks et al, 2008), directly coupled to ADCIRC at every time step and at every grid node.

Xie et al (2011) investigated the influence of the asymmetric structure of hurricane wind field on storm surge using a three-dimensional storm surge model. Their results suggest that accurate wind forcing is a fundamental factor ensuring the accuracy of storm surge and inundation forecasts. Axis-symmetric parametric hurricane wind models are still often used to compute the wind forcing for storm surge and inundation forecasting. However, it is well known that the wind fields of actual hurricanes are rarely axis-symmetric. Thus, it is important to understand how the asymmetric structure of wind fields affects storm surge and inundation forecasts.

Hu et al (2012) developed a parametric hurricane wind model based on the asymmetric Holland-type vortex model. The model creates a two-dimensional surface wind field based on the National Hurricane Center forecast (or observed) hurricane wind and track data. In their study, some modification to the asymmetric wind model was made in order to retain consistency between the input parameters and the model output. It is pointed out that it is better to include the Coriolis effects in the determination of the shape parameter B

It is concluded that ignoring the Coriolis effects, in determining the scaling parameters of a synthetic wind model, can lead to an error greater than 20% in the maximum wind speed for weak but large tropical cyclones. In addition, a new method was introduced to develop a weighted composite wind field to make use of all wind parameters, not just the largest available specified wind speed and its 4-quadrant radii. It is pointed out that the improved parametric model performs well and has the ability to maintain the consistency of the input and output maximum wind speeds and wind structure.

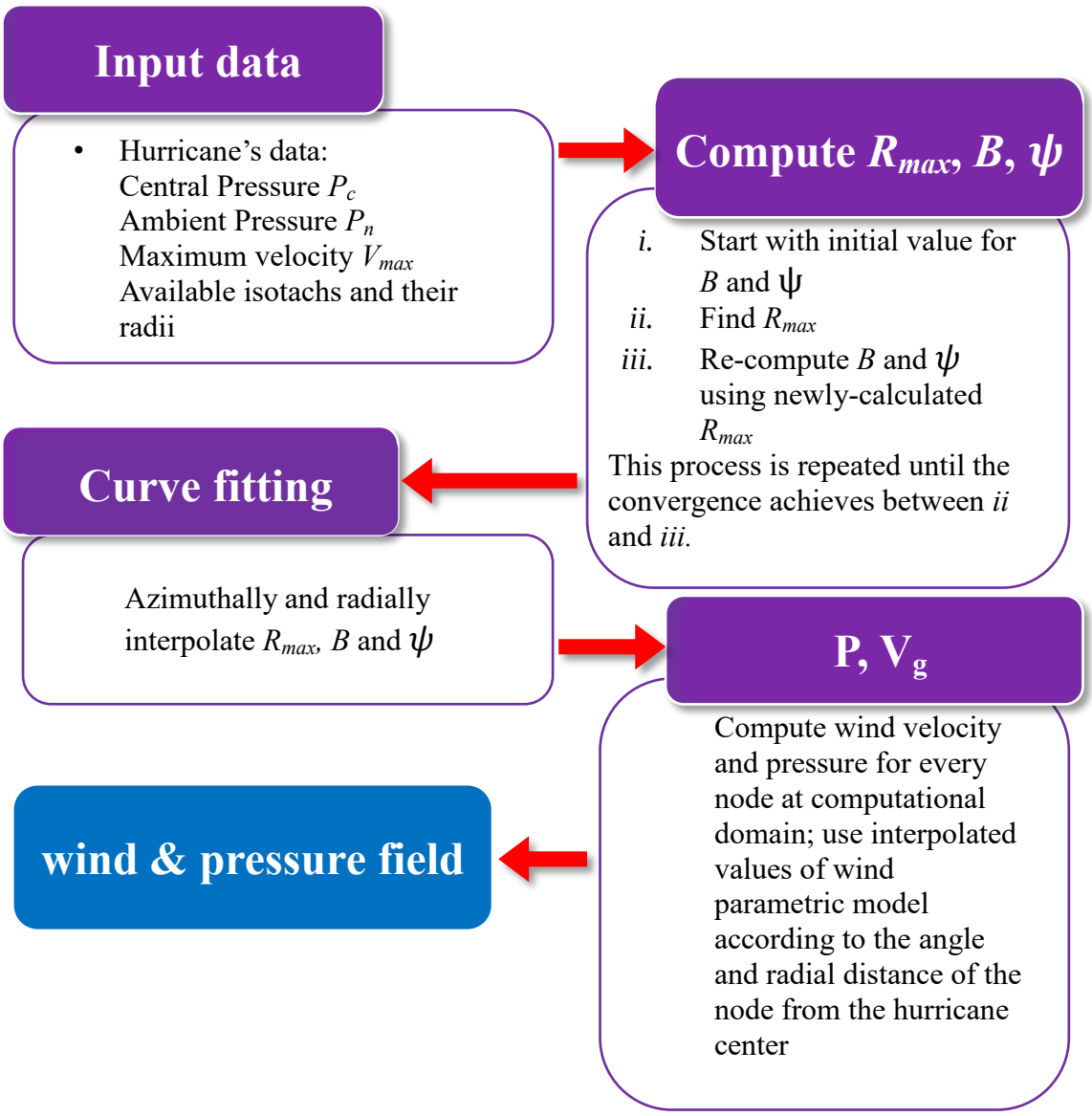

Figure 28. Flowchart of asymmetric wind model implementation.

METHOD DESCRIPTION

The new method to compute wind field around the storm center has been developed to make use of all available data, observed from inside of the hurricane structure, gathered either from the advisory or the best track data. Some modification was applied to Holland original model, which

is presented in following sections. In Figure 28, a flowchart that describes the implementation of asymmetric wind model is presented.

Scaling parameter B

As recommended by Hu et al (2012), neglecting Coriolis's parameter can create error in the computation of R_{max} and B. Therefore, rewriting the force balance, by keeping the Coriolis's effect term, between hurricane primary circulation forces i.e., radial pressure gradient, Coriolis, and centrifugal forces at radius of maximum wind and for maximum wind speed i.e. R_{max} and $V_{g_{max}}$, respectively and by considering $\psi = (A/Rmax^B)$:

$$B = \frac{\left(V_g{}^2{}_{max} + V_{g_{max}} R_{max} f\right) \rho_{air} e^{\psi}}{(p_n - p_c)\psi} \tag{9}$$

As in the formula of the shape parameter B, two parameters are available now, i.e., f and R_{max}. As Coriolis parameter varies spatially, and then values of B will no longer spatially and temporally remain constant. Parameter ψ is introduced first by ADCIRC group (Mattocks et al 2008) which indicates a relationship between B and ψ as following:

$$\psi = 1 + \frac{V_{g_{max}} R_{max} f}{B\left(V_g{}^2{}_{max} + V_{g_{max}} R_{max} f\right)} \tag{10}$$

Then, the tangential wind formula becomes in the form of:

$$V_g(r,\theta) = \sqrt{\left(V_g{}^2{}_{max} + V_{g_{max}} R_{max} f\right)\left(\frac{R_{max}}{r}\right)^B e^{\psi\left(1-\left(\frac{R_{max}}{r}\right)^B\right)} + \frac{r^2 f^2}{4}} - \frac{rf}{2} \tag{11}$$

If we know the value of $V_{g_{max}}$ and R_{max}, normally we can compute the value of B and ψ. However, the value of R_{max} frequently is not available. Therefore, it is practical to start with

initial value for B and ψ parameters and then once the value of R_{max} is computed, using a root finding procedure, we can re-compute values of B and ψ. We will discuss this step in our procedures, in further detail, in the next section. Additionally, the translational speed motion of hurricane vortex is computed based on the location and time interval specified for the simulation run. The total wind speed at each point in the computational domain is calculated based on the combination of the tangential and translational speed of the vortex:

$$\overrightarrow{W} = \overrightarrow{V_g} + \overrightarrow{V_t} \quad (12)$$

Where $\overrightarrow{W}$ denotes as total wind speed, $\overrightarrow{V_g}$ is gradient (tangential), and $\overrightarrow{V_t}$ is translation speed (ms^{-1}).

Compute Rmax

As shown in equation (11), the tangential wind formula can be solved to determine the value of R_{max} where the value of $V_g(r)$ tangential wind and its r radii are given. A popular root finding procedure, Brent's method is used to calculate the Rmax for each set of isotach data at each quadrant (Mattocks et al 2008).

Curve Fitting

In the Asymmetric Gradient Wind Model, the added feature is considered to maintain the consistency between the parametric hurricane wind model and observation from the real wind field. Since hurricanes are not symmetric, the radius of wind isotach varies by quadrant (azimuthally). Therefore, to take into account the azimuthal variation of the hurricane's parameters, a periodic cubic spline curve fitting procedure is employed.

This method is a good alternative to the polynomial interpolation (used by Xie et al 2006) because it can resolve the discontinuity issue between interpolated data, especially at 0 and 2π azimuthal angles which occurs as a result of accumulation of error at the end points.

The advantage of the adopted method is that the first and second derivatives are continuous. As a result, the hurricane parameters are defined as a function of azimuthal angles around the hurricane. In addition, as the parameters, which need to be interpolated radially according to their location, will also vary. Then, they are a function of the distance from the center of the hurricane i.e. $B(r,\theta)$, $\psi(r,\theta)$, $R_{max}(r,\theta)$.

Composite wind

As explained above, one simple vortex wind profile cannot represent the asymmetric geometry of the hurricane. Therefore, a combining method is used to build a weighted composite wind field in order to combine different wind profiles; For each set of isotach data, wind speed and their radii (inputs), one wind profile can be developed. Obviously, near the position(radius) of one tangential wind profile in four quadrants, the wind field based on the same wind speed would be much more accurate than the other wind fields (other isotach's data) and should be given the highest weight in the combined wind field, while simultaneously, the weighting coefficient for other wind field(s) should approach zero.

If the radii of three specified wind speeds, i.e., 34, 50, and 64 knots (17.5, 25.5, and 33 m/s, respectively), are provided in the NHC/ATCF forecast advisories, three modeled wind profiles (in ms^{-1}), W64, W50 and W34 can be developed, respectively (Hu et al 2012).Then, a weighted composite wind field can be established by:

$$W= \begin{cases} \overrightarrow{W}_{64} & I \quad W_{64} \geq 64 \\ \dfrac{f_{50}^{-1}(1-f_{64})\overrightarrow{W}_{50} + f_{64}(1-f_{50}^{-1})\overrightarrow{W}_{64}}{f_{50}^{-1}(1-f_{64}) + f_{64}(1-f_{50}^{-1})} & II \quad 50 \leq W_{50} \,\&\, W_{64} < 64 \\ \dfrac{f_{34}^{-1}(1-f_{50})\overrightarrow{W}_{34} + f_{50}(1-f_{34}^{-1})\overrightarrow{W}_{50}}{f_{34}^{-1}(1-f_{50}) + f_{50}(1-f_{34}^{-1})} & III \quad 34 \leq W_{34} \,\&\, W_{50} < 50 \\ \overrightarrow{W}_{34} & IV \quad W_{34} < 34 \end{cases} \tag{13}$$

Where $f_{64} = (W_{64}/64)$, $f_{50} = (W_{50}/50)$, $f_{34} = (W_{34}/34)$. The performance of this methodis presented in the next section for two instances of Hurricane Irene and for fully simulated Hurricane Gustav (2008) wind field.

VALIDATION RESULT AND ANALYSIS

A hurricane wind field based on the modified Holland's(1980) wind vortex, which takes into account asymmetric features, is set up to assess the asymmetric wind model's performance. By using the asymmetric gradient wind model and considering the azimuthal and radial variation, a tangential wind field is created based on the real advisory data from NHC for Hurricane Irene (2011).

The model is tested against two instances of advisories; high and low intensity wind speeds, maximum wind speed, and their radii that were collected in four quadrants (NE, SE, SW, and NW), as shown in Table 3.

Table 3. Parameters for asymmetric wind model test (high & low intensity wind)

Wind with High Intensity		**Wind with Low Intensity**	
Parameter	**Value**	**Parameter**	**Value**
Latitude	28.3° N	Latitude	41.4° N
Longitude	77.1° W	Longitude	73.7° W
Central Pressure	94200	Central Pressure	96600
R64 (NE)	70 nmi (130 km)	R64 (NE)	0 nmi (0 km)
R64 (SE)	60 nmi (111 km)	R64 (SE)	0 nmi (0 km)
R64 (SW)	25 nmi (46 km)	R64 (SW)	0 nmi (0 km)
R64 (NW)	50 nmi (93 km)	R64 (NW)	0 nmi (0 km)
R50 (NE)	110 nmi (204 km)	R50 (NE)	150 nmi (278 km)
R50 (SE)	100 nmi (185 km)	R50 (SE)	150 nmi (278 km)
R50 (SW)	50 nmi (93 km)	R50 (SW)	80 nmi (148 km)
R50 (NW)	75 nmi (139 km)	R50 (NW)	30 nmi (56 km)
R34 (NE)	250 nmi (463 km)	R34 (NE)	230 nmi (426 km)
R34 (SE)	200 nmi (370 km)	R34 (SE)	280 nmi (519 km)
R34 (SW)	125 nmi (232 km)	R34 (SW)	130 nmi (241 km)
R34 (NW)	160 nmi (296 km)	R34 (NW)	50 nmi (93 km)

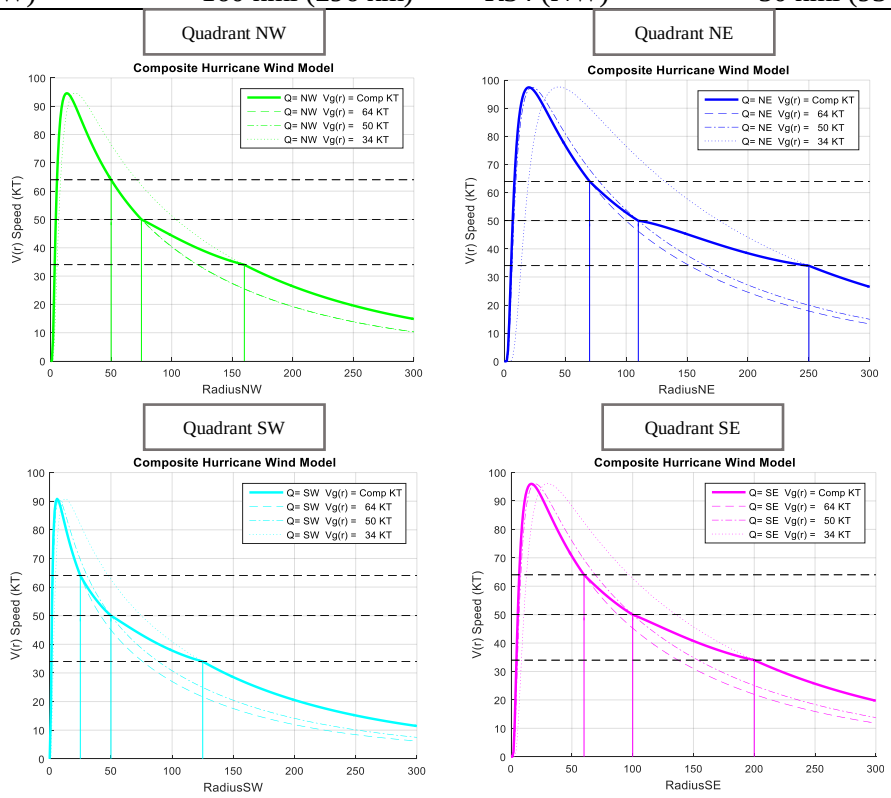

Figure 29. Implementation of weighted composite method for high intensity wind.

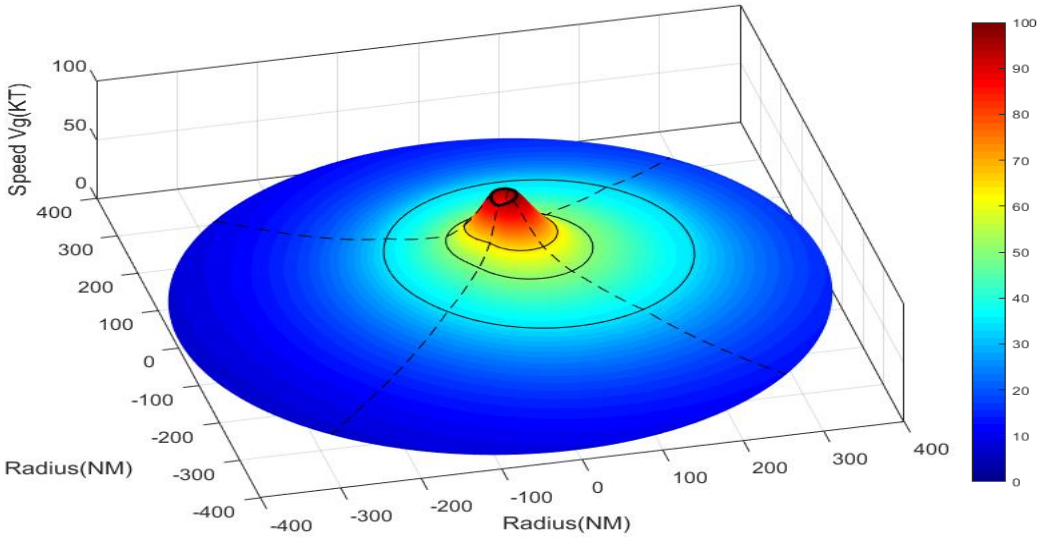

Figure 30. Wind field contour for high intensity wind.

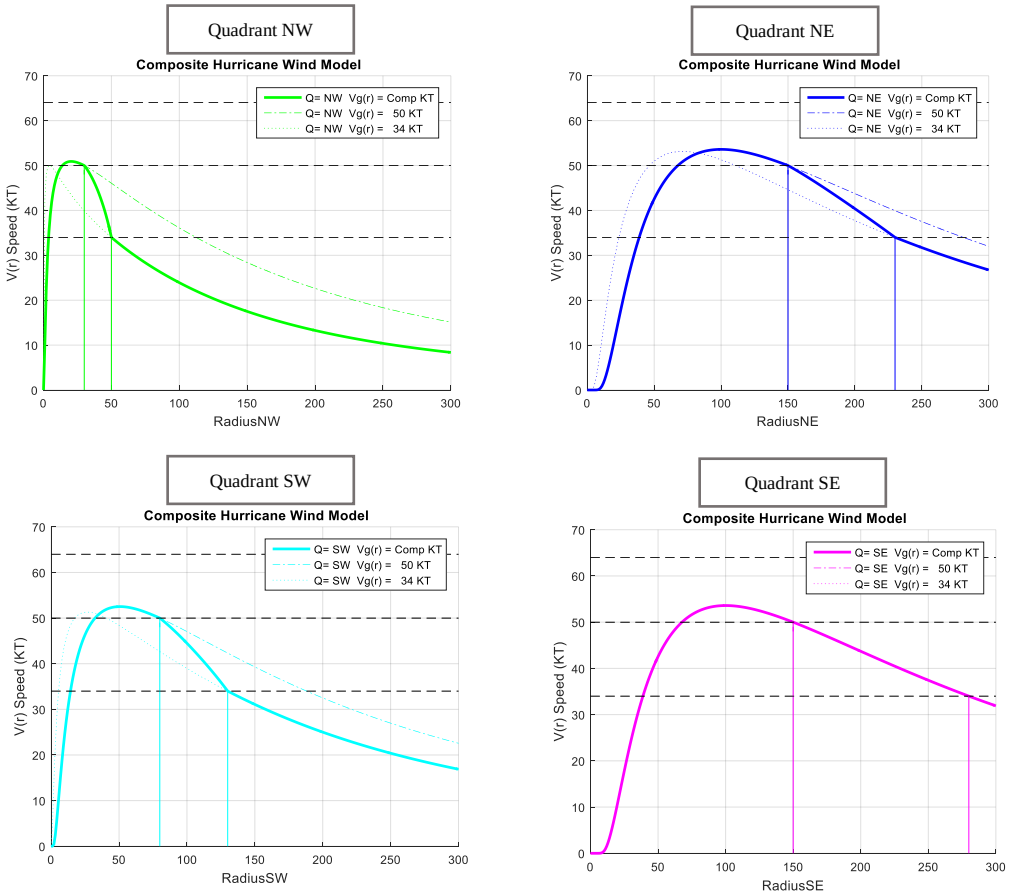

Figure 31. Implementation of weighted composite method for low intensity wind.

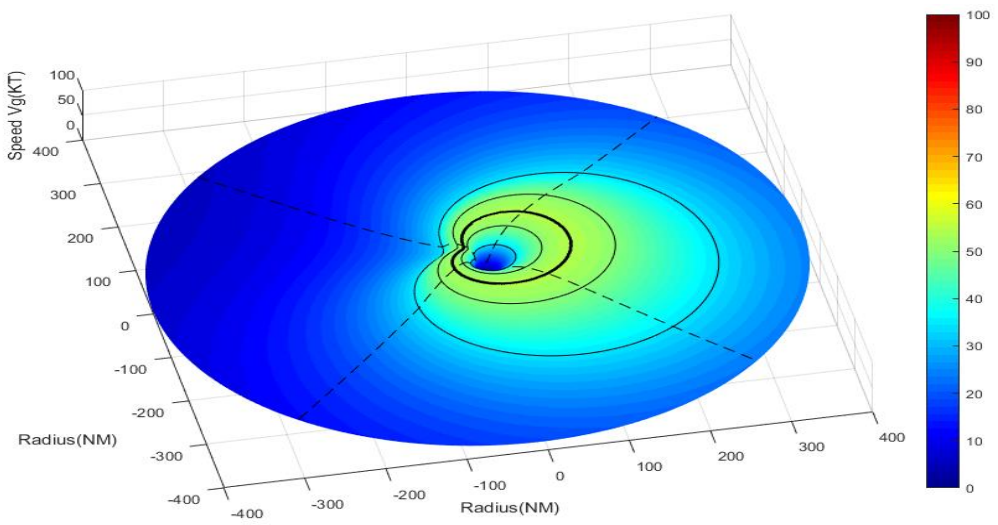

Figure 32. Wind field contour for low intensity wind.

The model result for the composite wind profile with high and low maximum wind is shown in Figure 29, and Figure 31. The contour plot of hurricane's wind field is illustrated in Figure 30, and Figure 32. The figures suggest that the composite method could successfully combine the three wind's profile at each quadrant for the wind with high and low intensities (3 and 2 isotach's radii data are available for high and low intensity, respectively).

Gustav (2008)

By ensuring that different parts of the asymmetric wind model, from the root finding (Rmax) to the weighted composite wind procedure, worked correctly, the model's performance was further evaluated for time-varying actual hurricane data; an asymmetric wind model was developed based on the input parameters from the best track data:

- Time of the storm's advisories(every 6 hours) : yyyy-mm-dd hh
- Longitude and Latitude of hurricane center (deg) : Long, Lat
- Surface Pressure at the center of hurricane (Pa): Pc

- Ambient undistributed synoptic background surface pressure (Pa): Pn
- Longitude and Latitude of hurricane center (deg) : Long, Lat
- Maximum 1-min sustained wind speed of hurricane (kt) : Vmax
- Wind radii in four quadrants (NE, SE, SW, NW) of hurricane at either 64kt, 50kt, 34kt (n.m): A set of radiuses (1:12)

Gustav began as a tropical storm in the Lesser Antilles and rapidly intensified to form a hurricane. It was the most intense storm to hit Cuba in five decades. Hurricane Gustav decreased its strength in the Gulf of Mexico due to increased wind shear and intrusions of dry air. When Gustav made landfall at 1500 UTC on September 1, 2008 near Cocodrie, LA, USA, it was a category 2 storm on the Saffir–Simpson scale and subsequently weakened to a tropical storm. Its forward motion slowed down as it crossed southern and western Louisiana on September 1. By September 2, its status was down- graded to a tropical depression over northwestern Louisiana.

Table 4. List of NOAA CO-OPS and NDBC observation station.

Station No.	Operator	Station ID	Location	Latitude	Longitude
32	NOAA CO-OPS	8762482	West Bank 1, Bayou Gauche, LA	29.8	-90.4
35	NOAA CO-OPS	8761927	New Canal Station, LA	30.0	-90.1
38	NOAA CO-OPS	8760922	Pilots Station East, Sw Pass, LA	28.9	-89.4
40	NOAA CO-OPS	8761724	Grand Isle, LA	29.3	-90.0
49	NOAA CO-OPS	8736897	Coast Guard Sector Mobile, AL	30.6	-88.1
55	NOAA CO-OPS	8764227	Lawma, Amerada Pass, LA	29.4	-91.3
79	NOAA-NDBC BUOY	DPIA1	Dauphin Island, AL	30.2	-88.1
82 & 42	NOAA CO-OPS	8747437	Bay Waveland Yacht Club, MS	30.3	-89.3

The simulation of wind field starts from 00:00 UTC on August 25, 2008 when the hurricane initiated. The simulation ran to the end of the last available best track data which was issued on12:00 UTC on September 05, 2008. In order to evaluate the accuracy of the model, a number of monitoring stations were selected in the Gulf of Mexico. The model results were compared to the actual observation at a number of the stations such as South of Louisiana, Mississippi, and Alabama, as well as to the symmetric wind model of CCHE2D-Coast. A map and the list of observation gauge stations are illustrated in Figure 33 and Table 4, respectively.

In Figure 34, Figure 35,Figure 36, Figure 37,Figure 38,and Figure 39 the wind velocity and the pressure compared to the observed data and symmetric model's output at West Bank 1 Bayou Gauche LA (8762482), New Canal Station, LA (8761927), Pilots Station East Sw Pass, LA (8760922) Grand Isle LA (8761724), Bay Waveland Yacht Club MS (8747437), Coast Guard Sector Mobile AL (8736897) Lawma Amerada Pass LA (8764227), Dauphin Island AL (DPIA1), Bay Waveland Yacht Club MS (8747437) monitoring stations.

In Bayou Gauche LA (8762482), New Canal Station LA (8761927), Waveland Yacht Club MS (8747437), the asymmetric model's results are in a close agreement with the observed data. The asymmetric model captured a 25 (ms^{-1}) wind velocity in Lawma Amerada Pass LA (8764227) station where the symmetric model failed to correctly reproduce the wind velocity at the peak; The symmetric model has a sharp rise and fall in wind velocity values at the peak while there is indication exist from the recorded data that wind model had a sharp and sudden variation around the peak.

In the either asymmetric or symmetric model, the effect of background wind field does not exist. Much of the inconsistency between observed data and wind field, when the hurricane is at a far

distance from the monitoring station, is due to lack of background wind. In order to improve the two wind models, background wind should be included in the computation of total wind field.

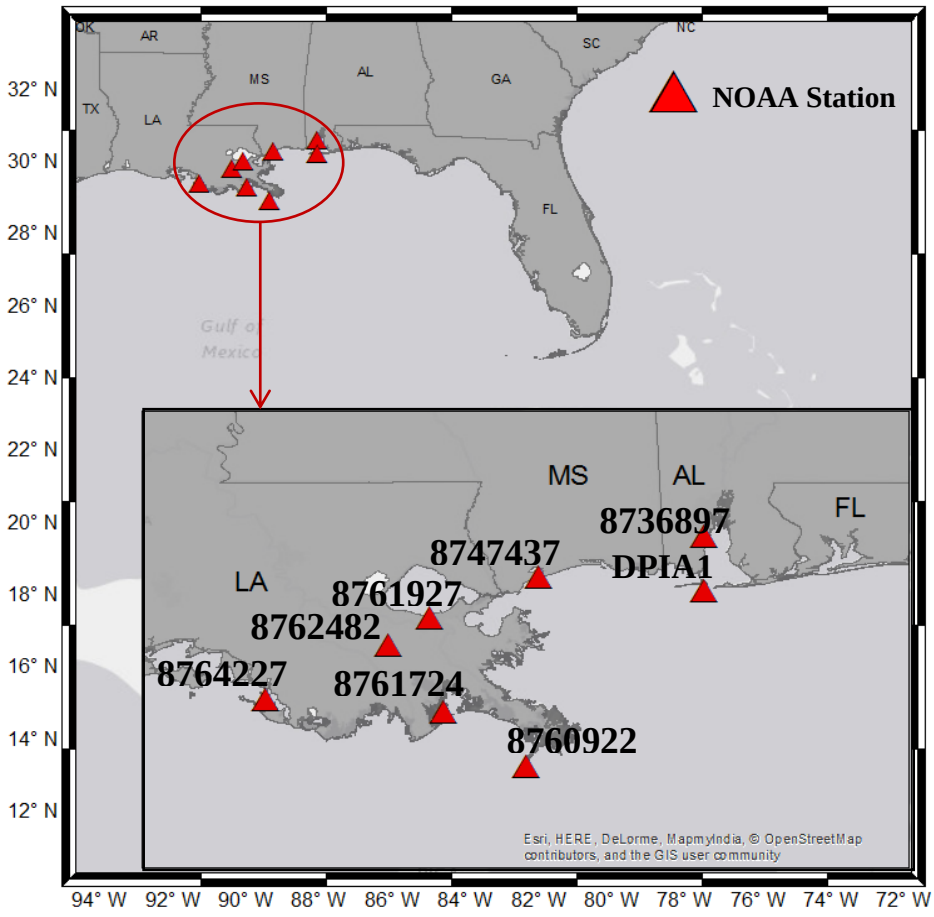

Figure 33. Map of observational measuring gauges operates by NOAA.

The pressure result is shown in Figure 37, Figure 38, Figure 39 showed a close agreement between symmetric and asymmetric model. This agreement occurs because the pressure field in both models (asymmetric and asymmetric) is computed in a similar way. However, there are small differences exist in computation of the pressure field. It is worth noting that the symmetric model takes into account the effect of the landfall while asymmetric model does not have any

adjustment to the key parameters wind field upon the landfall. The asymmetric model showed an improvement in pressure profile in the far field.

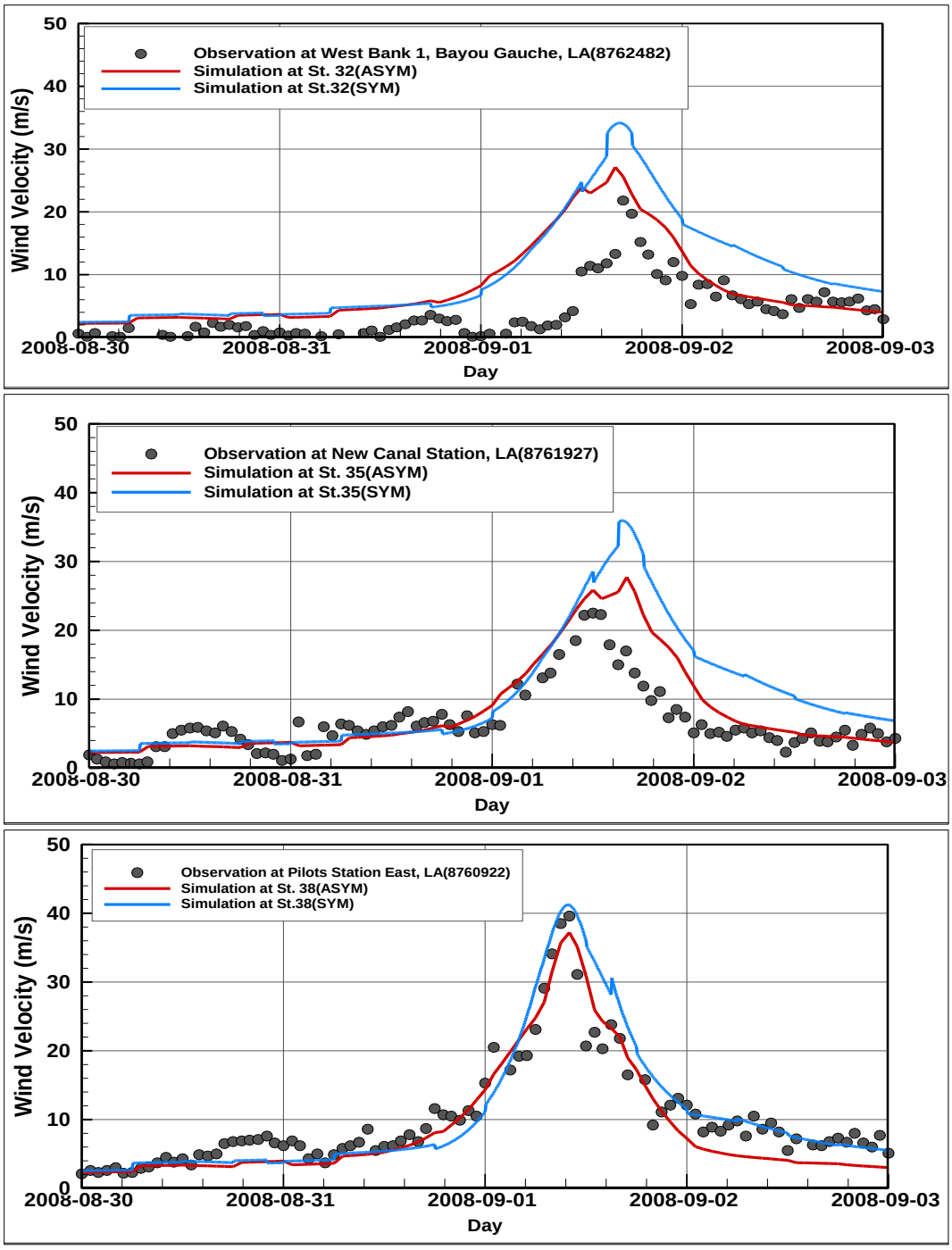

Figure 34. Comparisons of the wind velocity produced by the Asymmetric model (Red line) and Symmetric model result (Blue line) and observed data (Black circle) , all valid for Hurricane Gustav at West Bank 1 Bayou Gauche (LA), New Canal Station (LA), Pilots Station East Sw Pass (LA).

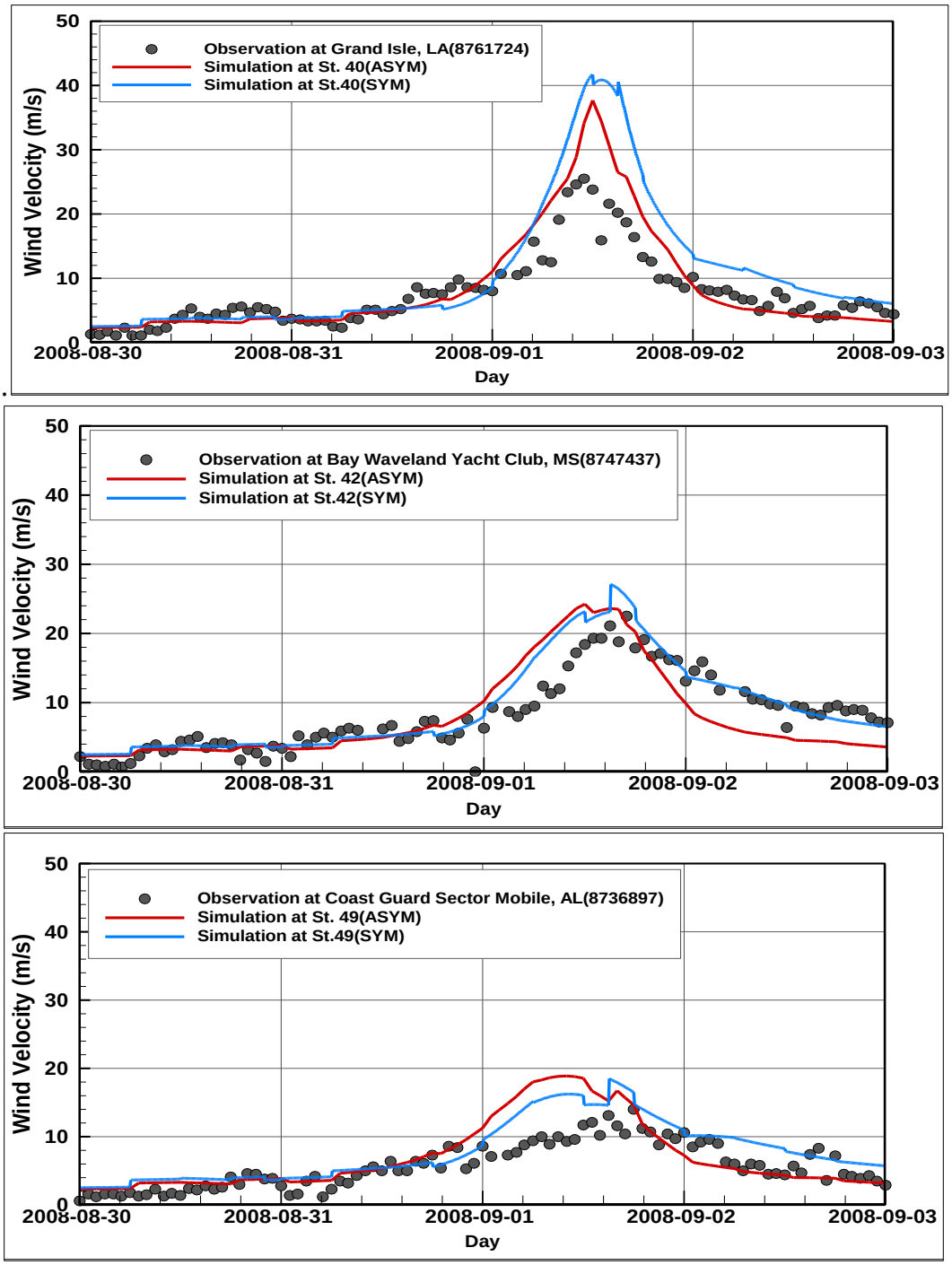

Figure 35. Comparisons of the wind velocity produced by the Asymmetric model (Red line) and Symmetric model result (Blue line) and observed data (Black circle), all valid for Hurricane Gustav at Grand Isle LA (8761724), Bay Waveland Yacht Club MS (8747437), and Coast Guard Sector Mobile AL (8736897).

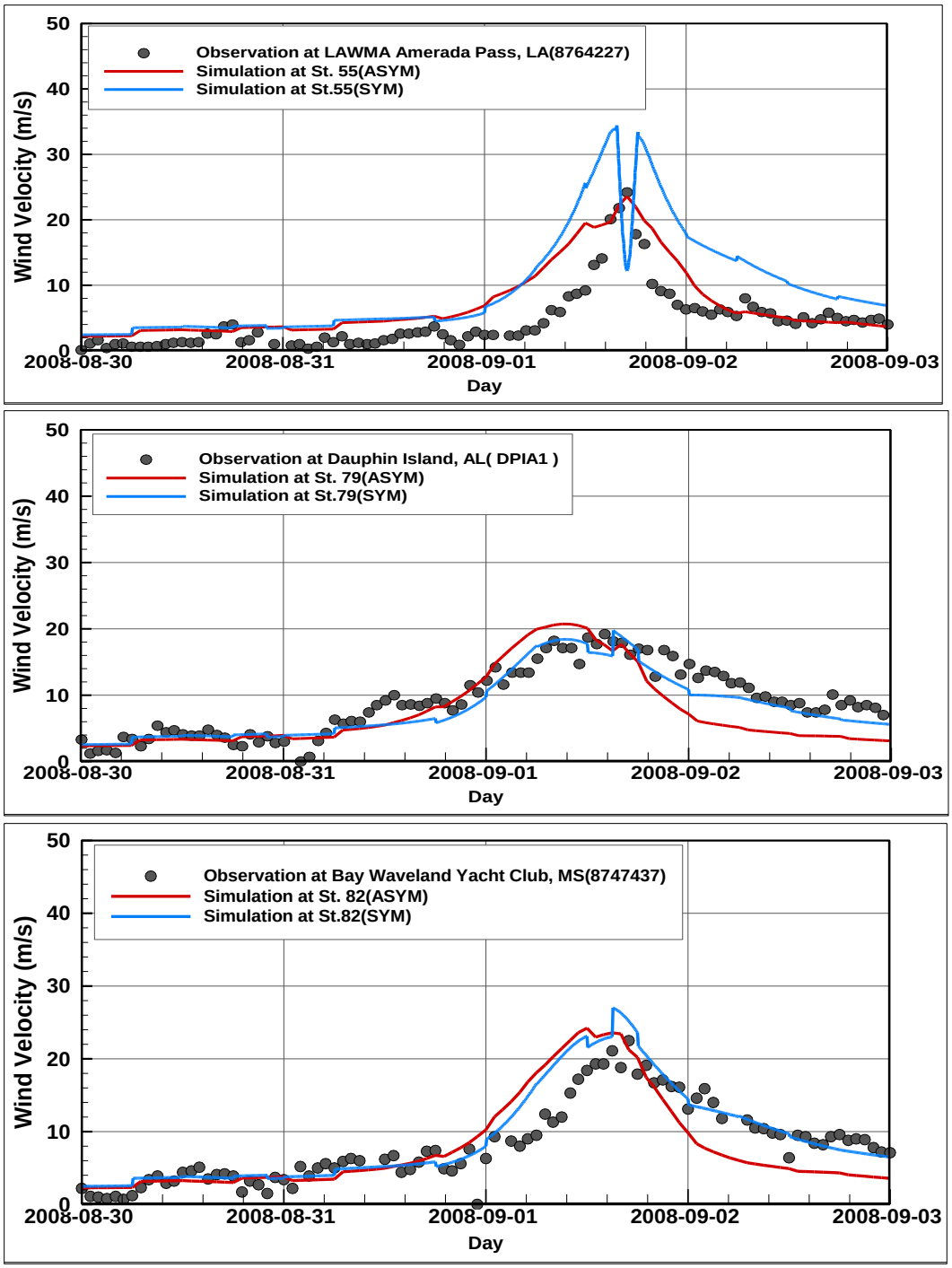

Figure 36. Comparisons of the wind velocity produced by the Asymmetric model (Red line) and Symmetric model result (Blue line) and observed data (Black circle), all valid for Hurricane Gustav at Lawma Amerada Pass LA (8764227), Dauphin Island AL (DPIA1), and Bay Waveland Yacht Club MS (8747437).

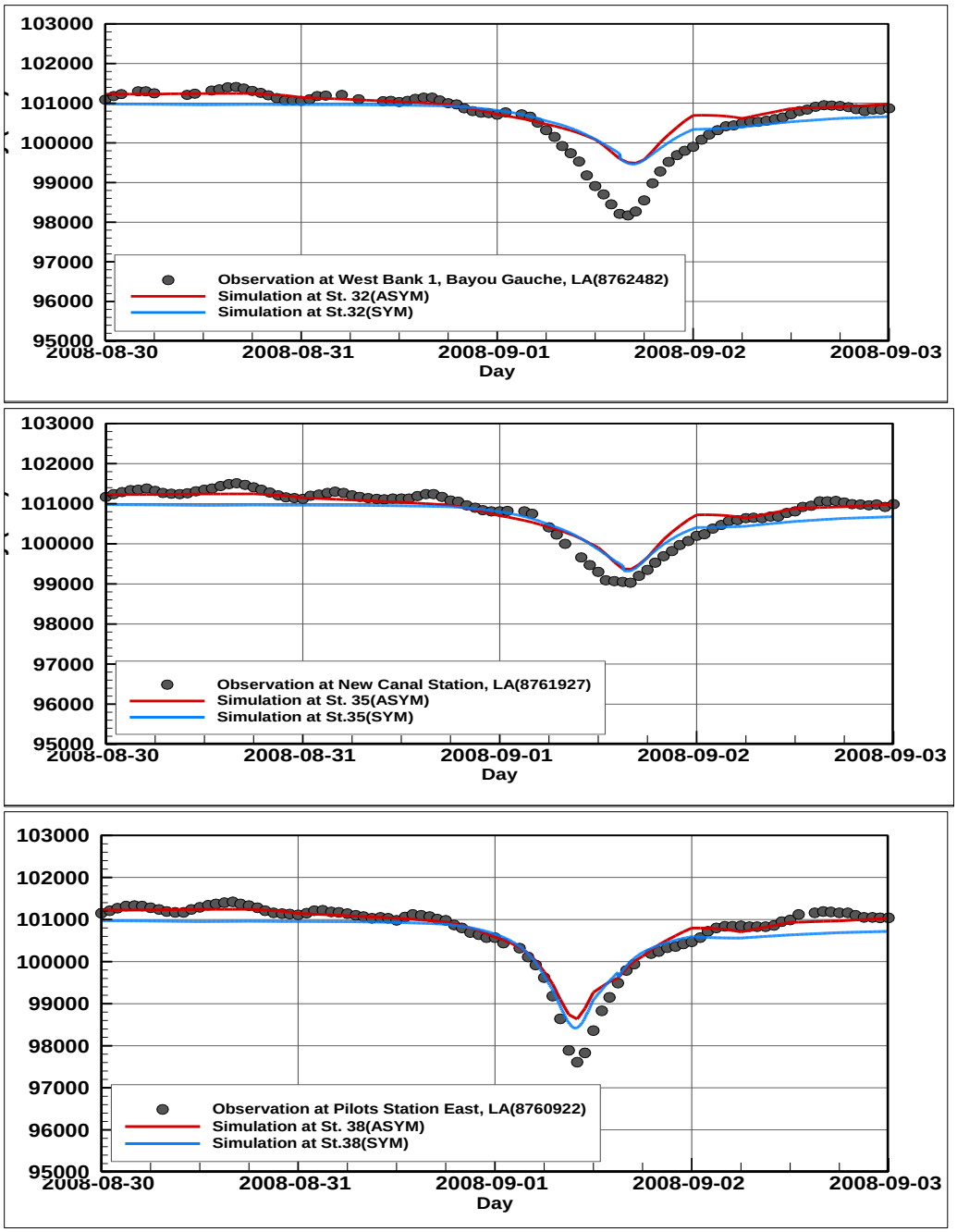

Figure 37. Comparisons of the air pressure produced by the Asymmetric model (Red line) and Symmetric model result (Blue line) and observed data (Black circle) , all valid for Hurricane Gustav at West Bank 1 Bayou Gauche LA (8762482), New Canal Station, LA (8761927), and Pilots Station East Sw Pass, LA (8760922).

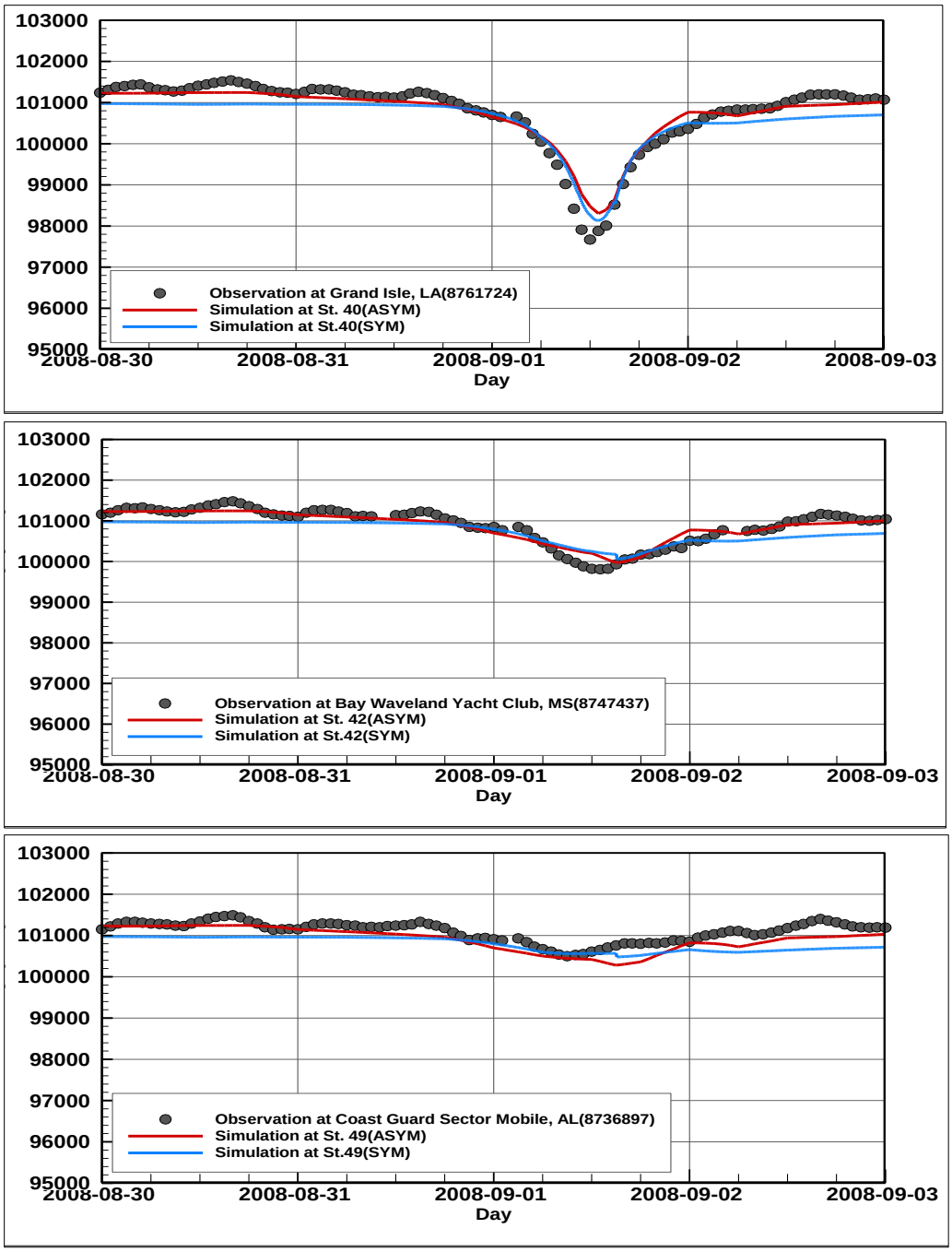

Figure 38. Comparisons of the air pressure produced by the Asymmetric model (Red line) and Symmetric model result (Blue line) and observed data (Black circle) , all valid for Hurricane Gustav at Gustav Grand Isle LA (8761724), Bay Waveland Yacht Club MS (8747437), and Coast Guard Sector Mobile AL (8736897).

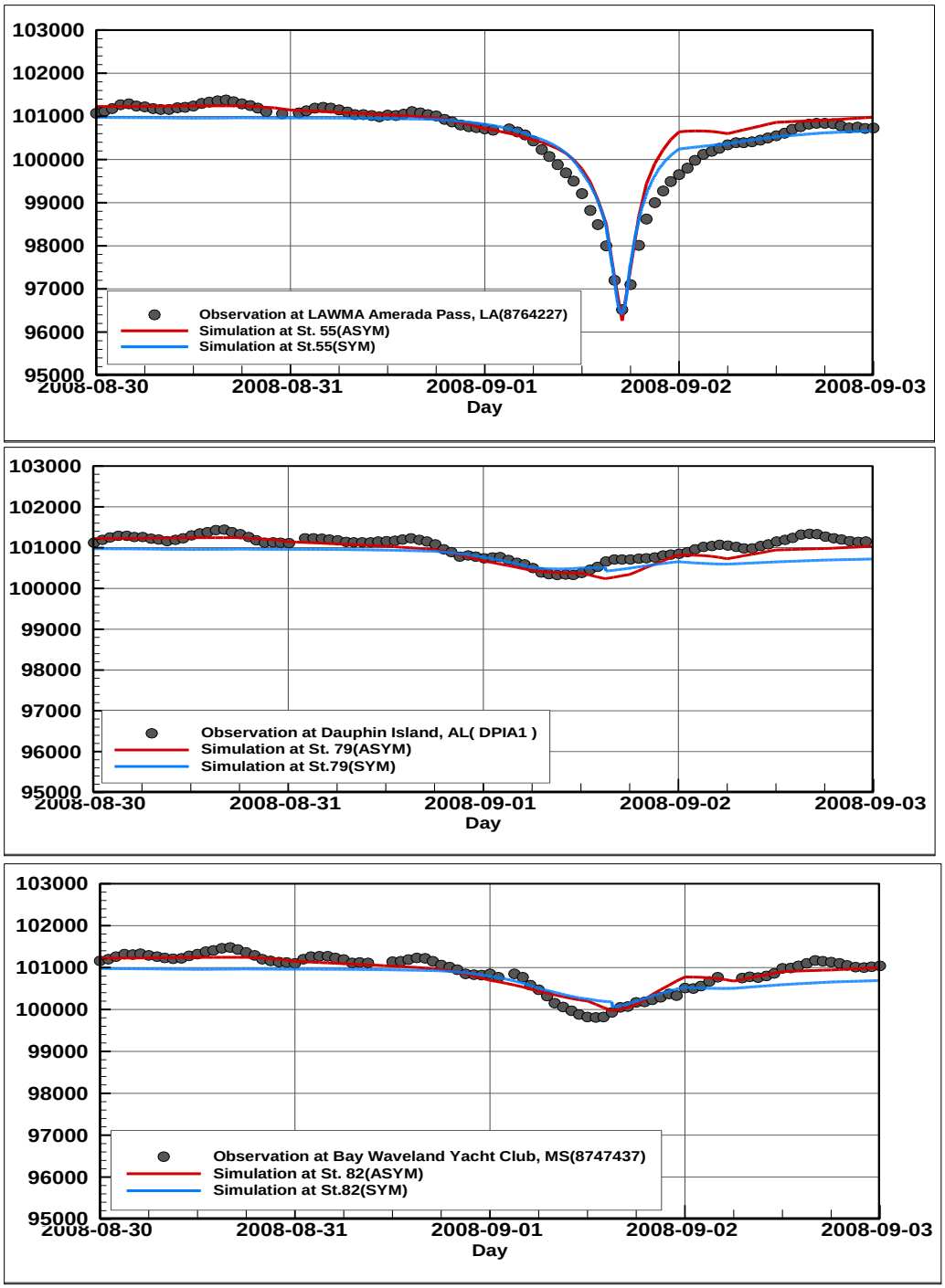

Figure 39. Comparisons of the air pressure produced by the Asymmetric model (Red line) and Symmetric model result (Blue line) and observed data (Black circle) , all valid for Hurricane Gustav at Lawma Amerada Pass LA (8764227), Dauphin Island AL (DPIA1), and Bay Waveland Yacht Club MS (8747437).

CHAPTER V:

CONCLUSION AND REMARKS

In the presented study, an integrated modeling system, CCHE2D-Coast, was applied to simulate flow dynamics across the U.S. Northeast and Mid-Atlantic coast. The results demonstrated that the model, driven by astronomical tide-only generating forces, was able to capture Coast-Ocean flow dynamics across the U.S. East Coast where complex geometry exists. To further enhance the model skill in simulation of tide currents and improve the accuracy of the integrated model in hindcasting storm surges and waves induced by the wind, a finer resolution must be taken in shallow water regions.

In the first phase of this study, the model was validated under astronomical tides-only simulation. Then, the validated model was used to simulate the storm surges and wind driven by Hurricane Bob (1991). In order to improve the accuracy of the integrated model, an asymmetric parametric model based on the Holland-type vortex model developed and evaluated against the actual hurricane best track data.

The model accuracy in reproducing flow circulation was tested through two simulations runs within different time spans. In the first simulation, model performance was evaluated in reproducing water level and the simulation result was compared against the observed data at several NOAA monitoring stations. To further assess the model's performance, the modeled time series was employed to perform the harmonic analysis in order to identify harmonic constituents. Then, identified parameters were compared with the known values provided by NOAA at each observation gauge.

A number of conventional skill assessments metrics were used to assess the model performance and quantifying the misfit between modeled and "a priory" known data. In this study, a suite of metrics comprised of Normalized Root-Mean Square Deviation, Coefficient of Determination,

Scatter Index, and Averaged Bias, for two sets of modeled time series, long and short simulation run, was utilized.

The comparisons between the two cases showed that each metric has about equal value. Overall, the extent to which most metrics were obtained suggests that there is good agreement between modeled time series and observed data in the majority of monitoring points. This assured us that quality of simulation run is good enough to perform the harmonic analysis.

A newly-developed parameter identification approach was used to identify harmonic constituents. As a phase shift that commonly exists in simulation results of water level time series, a direct use of modeled results in quantifying error between simulated and observed value, may introduce incorrect comparisons between them. Therefore, calculation of statistical index through identified parameters, harmonic constituents, can eliminate some sources of errors stemming from phase-lag between observation and simulation result.

The identified components, amplitudes and phases, were used to compute the employed criterion with respect to known values. The result of statistical analysis suggests that the accuracy in identified amplitudes is greater than identified phases.

In the second phase of model's validation, the storm surges and wind driven by Hurricane Bob (1991) were computed with good correspondence to the observed data. The collected data from NOAA CO-OPS and NDBC BUOY monitoring stations were used to compare with the simulated wind, water elevation and wave. The agreement between simulation results and observation data showed that model was able to reproduce well the storm surge tide and waves at the East Coast of the US during hurricane Bob.

Moreover, the model result from the asymmetric model showed that wind field could more accurately be reproduced if asymmetric structure of hurricanes is implemented. The asymmetric model was developed to make use of all available observed data broadcasted by NOAA. The historical Hurricane Gustave's best track data was used to test the asymmetric wind model against the observed data as well as symmetric model.

Based on the model's simulation result, the quality of the pressure model remained unchanged using the newly-asymmetric wind model. However, different wind fields were produced using asymmetric model in comparison with the symmetric one. The presented asymmetric model, similar to symmetric model, has no computational cost. Although, some other models such as H*wind model have shown better representation of actual wind model, the operational advantages of parametric model is, forecast data from each advisory, can be used to build and forecast wind field in a real-time hurricane simulation and create predictions for 6, 12, 24, 48 and up to 120 hours.

There are a number of adjustments that can be implemented to enhance the asymmetric wind model, such as a more realistic damping factor for translational speed, some changes in curve fitting procedure, removing the effect of translational speed and considering boundary layer approximation in computing Rmax. In addition, implementation of parallel computing can reduce the total simulation run time for either asymmetric or symmetric model. In addition, the asymmetric model's capability in creating more accurate storm surge and wind driven waves need to be tested.

BIBLIOGRAPHY

Arbic, B. K., S. T. Garner, R. W. Hallberg, and H. L. Simmons (2004). The accuracy of surface elevations in forward global barotropic and baroclinic tide models,Deep Sea Res., Part II 51, 3069–3101, doi:10.1016/j.dsr2.2004.09.014.

Barron, C.N., Kara, A.B., Martin, P.J, Rhodes, R.C., Smedstad, L.F., (2005). Formulation, implementation and examination of vertical coordinate choices in the Global Navy Coastal Ocean Model (NCOM). Ocean Modeling 11, 2006, pp. 347-375.

Blumberg, A. F., Mellor,G.L., (1987). A description of a three-dimensional coastal ocean circulation model, In Three-Dimensional Coastal Ocean Models, N. S. Heaps (Ed.), 1-16, American Geophysical Union, Washington, DC, 1987.

Blumberg, A., Khan, L., and St. John, J. (1999). "Three-Dimensional Hydrodynamic Model of New York Harbor Region." J. Hydraul. Eng., 10.1061/(ASCE)0733-9429(1999)125:8(799), 799-816.

Brown C.D., and H.T. Davis. (2006). Receiver operating characteristics curves and related decision measures: a tutorial. Chemometrics and Intelligent Laboratory Systems 80: 24–38.

Cardone, V., Pierson, W., and Ward, E. (1976). Hindcasting the directional spectrum of hurricane generated. 28, 385-394

Cardone, V. J., and Cox, A. T. (2009). Tropical Cyclone Wind Field Forcing for Surge Models: Critical Issues and Sensitivities. Nat. Haz, 51, 29-47.

Carrere, L., and F. Lyard (2003). Modeling the barotropic response of the global ocean to atmospheric wind and pressure forcing-Comparisons with observations, Geophys. Res. Lett.30, 1275, doi:10.1029/2002GL016473.

Chen, C., Liu, H., Beardsley, R. C., (2003). An unstructured grid, finite-volume, three-dimensional, primitive equations ocean model: Applications to coastal ocean and estuaries. J. Atmos. Ocean. Tech. 20, 159-186.

Cheng, Y., and O. B. Andersen (2011). Multimission empirical ocean tide modeling for shallow waters and polar seas, J. Geophys. Res., 116, ,C11001, doi:10.1029/2011JC007172

Chow, S. H. (1970). A study of the wind field in the planetary boundary layer of a moving tropical cyclone. MS Thesis. New York University, School of Engineering and Science, New York, NY.

Connor, J., and Wang, J. (1973). “Finite element modeling of hydrodynamic circulation.” Proceedings of the International Conference on Numerical Methods in Fluid Dynamics, Southampton, England.

Cox, A., Greenwood, J., Cardone, V., and Swail, V. (1995). An interactive objective kinematic analysis system. 4th international workshop on wave hindcasting and forecasting (pp. 109–118). Banff, Alberta: 16–20 October 1995.

Dee D P. (1995). A pragmatic approach to model validation. In: Lynch DR and Davies AM (eds), Quantitative skill assessment of coastal ocean models, AGU, Washington. p1–13.

Ding, Y., Jia Y., and Wang, S. S. Y. (2004). Identification of the Manning's roughness coefficients in shallow water flows, Journal of Hydraulic Engineering, ASCE, Vol. 130, No.6, pp.501-510, June, 2004.

Ding, Y. and Wang, S., (2005). Tests of capability and reliability of a model simulating coastal processes. World Water Congress, pp. 15-19.

Ding, Y., Wang, S. S. Y., and Jia, Y., (2006). Development and validation of a quasi-three-dimensional coastal area morphological model, J. Waterway, Port, Coastal, and Ocean Engineering, ASCE, Vol.132, No.6, pp. 462-476.

Ding, Y. and Wang, S., (2008). Development and Application of a Coastal and Estuarine Morphological Process Modeling System. Journal of Coastal research, pp. 127-140.

Ding, Y., Rusdin, A., Kuiry, S.N., Zhang, Y.-X., Jia, Y., Altinakar, M.S (2012). Validation of an integrated coastal processes model by simulating storm-surge and wave in Mississippi/Louisiana Gulf Coast. In Proceeding of the 3rd International Symposium on Shallow Flows. IowaCity, USA,.

Ding, Y., Kuiry, S., Elgohry, M., Jia, Y., Altinakar, M., and Yeh, K.-C. (2013a). Impact assessment of sea-level rise and hazardous storms on coasts. Ocean Engineering, 71, 74-95.

Ding, Y., Ding, T. and Altinakar, M., (2013b). Prediction of Wind, Wave, and Storm due to Hurricane ISAAC in the northern Gulf Coast, In: Proceedings of ASCE-EWRI Congress May 2013 Showcasing the Future. Cincinnati, OH,., pp. 1793-1807.

Ding, Y., Zhang, Y.-X., and Jia, Y. (2013c). Graphical User Interface for CCHE2DCoast − Quick Start Guide, August, 2013.

Ding, Y., Rusdin, A., Kuiry, S.N., Zhang, Y.-X., Jia, Y., Altinakar, M.S (2012). Validation of an integrated coastal processes model by simulating storm-surge and wave in Mississippi/Louisiana Gulf Coast. In Proceeding of the 3rd International Symposium on Shallow Flows. IowaCity, USA,.

Ding, Yan., Hossain, A. K. M. Azad., Zhang,Yaoxin., Jia, Yafei., and Altinakar, Mustafa S. (2014). Simulation of Wind, Storm Surge, and Wave in Hurricane Sandy, Presented in the ASCE-EWRI Congress 2014, Portland, Oregon, June 1-5, 2014, 10

Dingman JS and Bedford KW. (1986). Skill tests and parametric statistics for model evaluation. Journal of Hydraulic Engineering, 112 (2), 124–141.

Egbert,G.D.,A.F.Bennett, and M.G.G.Foreman(1994).TOPEX/ POSEIDON tides estimated using a global inverse model,J. Geophys.Res. 99 (C12), 24,821–24,852, doi:10.1029/94JC01894.

Egbert, G. D., R. D. Ray, and B. G. Bills (2004). Numerical modeling of the global semidiurnal tide in the present day and in the last glacial maximum,J. Geophys. Res.109, C03003, doi:10.1029/2003JC001973.

Emanuel, K. (2004). Tropical cyclone energetics and structure, in Atmospheric Turbulence and Mesoscale Meteorology, edited by E. Fedorovich, R. Rotunno, and B. Stevens, pp. 165–192, Cambridge Univ. Press, Cambridge, U. K.,

Fitzpatrick J.J. (2009). Assessing skill of estuarine and coastal eutrophication models for water quality managers. Journal of Marine System 76: 195–211.

Forbes C, Luettich RA Jr, Mattocks CA, Westerink JJ (2010). A retrospective evaluation of the storm surge produced by Hurricane Gustav (2008): forecast and hindcast results. Weather Forecast 25:1577–1602

Ganju, N.K., M.J. Brush, B. Rashleigh, A.L. Aretxabaleta, P. del Barrio, J.S. Grear, L.A. Harris, S.J. Lake, G. McCardell, J. O'Donnell, D.K. Ralston, R.P. Signell, J.M. Testa, J.M.P. Vaudrey. (2015). Progress and challenges in coupled hydrodynamic-ecological estuarine modeling. Estuaries and Coasts. DOI: 10.1007/s12237-015-0011-y.

Gary D. Egbert and Svetlana Y. Erofeeva, (2002). Efficient Inverse Modeling of Barotropic Ocean Tides. J. Atmos. Oceanic Technol., 19, 183–204.

Green, J. A. M. (2010). Ocean tides and resonance, Ocean Dyn., 60, 1243–1253, doi:10.1007/s10236-010-0331-1.

Griffiths, S. D., and W. R. Peltier (2008). Megatides in the Arctic Ocean under glacial conditions, Geophys. Res. Lett., 35, L08605, doi:10.1029/ 2008GL033263.

Griffiths, S. D., and W. R. Peltier (2009). Modeling of polar ocean tides at the Last Glacial Maximum: implification, sensitivity, and climatological implications, J. Clim., 22, 2905–2924, doi:10.1175/2008JCLI2540.1.

Haefner J.W. (2005). Modeling biological systems: principles and applications. New York: Springer.

Halliwell, Jr., G. R., Bleck, R., Chassignet, E., (1998). Atlantic Ocean simulations performed using a new hybrid-coordinate ocean model (HYCOM). EOS, Trans. AGU, Fall 1998 AGU Meeting.

Harper, B., Hardy, T., Mason, L., Bode, L., Young, I., and Nielsen, P. (2001). Queensland climate change and community vulnerability to tropical cyclones, ocean hazards assessment. Stage 1 report. Department of Natural Resources and Mines, Queensland, Brisbane, Australia.

Harper, B.A., Holland, G.J., (1999). An updated parametric model of the tropical cyclone. In: Preprint, 23rd Conference on Hurricanes and Tropical Meteorology, American Meteorological Society

Hendershott, M. C., (1972). The effects of solid earth deformation on global ocean tides. Geophys. J. Roy. Astron. Soc, 29, 389–402.

Herbich, J. B. (1999). Handbook of coastal engineering, McGraw-Hill.

Hess, K. W, (1976). A Three-dimensional Numerical Model of the Estuary Circulation and Salinity, Narragansett Bay. Estuarine and Coastal Marine Science, 4, 325-338.

Holland, G., (1980). Ananalytic model of the wind and pressure profiles in hurricanes.. J.Appl.Meteorol, Volume 108, p. 1212–1218.

Holland G (2008). A revised hurricane pressure-wind model. Mon Weather Rev 136:3432–3445

Holland, G. J., J. I. Belanger, and A. Fritz (2010). A revised model for radial profiles of hurricane winds, Mon. weather Rev., 138, 4393–4401

Houston, S. H., W. A. Shaffer, M. D. Powell, and J. Chen, (1999). Comparisons of HRD and SLOSH surface wind fields in hurricanes: Implications for storm surge modeling. Wea. Forecasting, 14, 671–686.

Hu, K., Chen, Q., & Kimball, S. K. (2012). Consistency in hurricane surface wind fore-casting: an improved parametric model. Nature Hazards, 61, 1029-1050.

Jayne, S. R., and L. C. St. Laurent (2001). Parameterizing tidal dissipation over rough topography, Geophys. Res. Lett.28, 811–814.

Jelesnianski, C. P., Chen, J., and Shaffer, W. A. (1992). SLOSH: Sea, Lake, and Overland Surges from Hurricanes. Silver Spring, MD: National Weather Service.

Jia, Y., Wang, S. and Xu, Y., (2002). Validation and Application of a 2D model to Channel with Complex Geometry.. Int.J.Comput,Engineering Science, pp. 3(1), 57-71.

Jolliff J.K., J.C. Kindle, I. Shulman, B. Penta, M.A.M. Friedrichs, R. Helber, and R.A. Arnone. (2009). Summary diagrams for coupled hydrodynamic-ecosystem model skill assessment. Journal of Marine Systems 76(1-2): 64–82.

Kawahara, M., Yoshimura, N., Nakagawa, K., and Ohsaka, H. (1976). “Steady and unsteady finite element analysis of incompressible viscous fluid.” International Journal for Numerical Methods in Engineering, 10, 437–456.

King, M. A., and L. Padman, (2005). Accuracy assessment of ocean tide models around Antarctica. Geophysical Research Letters 32:L23608. doi: 10.1029/2005GL023901

Large, . W. and Pond, S., (1981). Open ocean momentum fluxes in moderate to strong winds. J.Phys.Oceanogr., Volume 11, p. 324–336.

Leendertse, J. J. (1967). “Aspects of a computational model for long-period water wave propagation.” Memorandum RM5294-PR, Rand Corporation, Santa Monica, California.

Leendertse, J. J. (1970). “A water-quality simulation model for well-mixed estuaries and coastal seas, I: Principles of computation.” Memorandum RM6230-RC, Rand Corporation, Santa Monica, California.

Leendertse, J. J., and Gritton, E. C. (1971). “A water-quality simulation model for well-mixed estuaries and coastal seas, II: Computational procedures.” Memorandum R-708-NYC, Rand Corporation, Santa Monica, California.

Le Provost, C., F. Lyard, J. M. Molines, M. L. Genco, and F. Rabilloud (1998). A hydrodynamic ocean tide model improved by assimilating a satellite altimeter-derived data set, J. Geophys. Res. 103(C3), 5513–5529.

Liu, D. C., and Nocedal, J. (1989). ‘‘On the limited memory method for large scale optimization.’’ Math. Program, 45~3!, 503–528.

Luettich, R., Westerink, J. J., Scheffner, N. W. (1992). ADCIRC: an advanced three-dimensional circulation model for shelves coasts and estuaries, report 1: theory and methodology of ADCIRC-2DDI and ADCIRC-3DL. Dredging Research Program Technical Report DRP-92-6, U.S. Army Engineers Waterways Experiment Station, Vicksburg, MS, page 137.

Lyard, F., F. Lefevre, T. Letellier, and O. Francis (2006). Modelling the global ocean tides: Modern insights from FES2004, Ocean Dyn.,56, 394–415, doi:10.1007/s10236-006-0086-x.

Lynch D. , D. McGillicuddy, F. Werner (2009). Skill Assessment for Coupled Physical-Biological Models of Marine Systems, special issue of J. Marine Systems, 250pp.

Lynch, D. R. (1983). “Progress in hydrodynamic modeling, review of U.S. contributions, 1979-1982.” Reviews of Geophysics and Space Physics, 21(3), 741–754.

Mason S.J., and N.E. Graham. (1999). Conditional probabilities, relative operating characteristics, and relative operating levels. Weather and Forecasting 14: 713–725.

Mattocks C, Forbes C (2008). A real-time, event-triggered storm surge forecasting system for the state of North Carolina. Ocean Model 25:95–119.

Mayfield, M., (1992). Hurricane Bob Prelimenary Report, Miami, FL.: National Hurricane Center.

More´, J. J., and Wright, S. J. (1993). Optimization software guide, SIAM, Philadelphia.

Mukai, A.Y., Westerink, J. J., and Luettich, R. A.. (2001). “Guidelines for using Eastcoast 2001 database of tidal constituents within Western North Atlantic Ocean, Gulf of Mexico and Caribbean,” Coastal and Hydraulics Engineering Technical Note CHETN-IV-40, U.S. Army Engineer Research and Development Center, Vicksburg, MS. http://chl.wes.army.mil/library/publications/chetn/

Navon, I. M. (1988). “A review of finite-element methods for solving the shallow-water equations.” Proceedings of the International Conference on Computer Modeling in Ocean Engineering, Venice, Italy, 273–278.

Nocedal, J., and Wright, S. J. (1999). Numerical optimization, Springer Verlag Series in Operation Research, P. Glynn and S. M. Robinson, eds., Springer, New York.

NWS-23, (1979). Meteorological criteria for standard project hurricane and proBaBle maximum hurricane windfields, gulf and east coasts of the united states. noaa technical report, coastal services center.

Pain. C, Piggott. M, Goddard. A, F. Fang, G. Gorman, D. Marshall, M. Eaton, P. Power, C. de Oliveira (2005). Three-dimensional unstructured mesh ocean modelling, Ocean Modell, 10, pp. 5–33.

Parrish R.S., and C.N. Smith. (1990). A method for testing whether model predictions fall within a prescribed factor of true values, with an application to pesticide leaching. Ecological Modelling 51: 59–72.

Partridge, P. W., and Brebbia, C. A. (1976). “Quadratic finite elements in shallow water problems.” Journal of Hydraulic Engineering, 102(HY9), 1299–1313.

Pearson, C. E., and Winter, D. F. (1977). “On the calculation of tidal currents in homogeneous estuaries.” Journal of Physical Oceanography, 7, 520–531.

Piggott, M. D., Pain, C. C., Gorman, G. J., Marshall, D. P., Killworth, P. D., (2008). Unstructured adaptive meshes for ocean modeling. In: Ocean modeling in an eddying regime, Ed. M. W. Hecht and H. Hasumi, Geophysical Monograph 177, AGU, 383-408.

Powell, M. D., and Houston, S. H. (1996). Hurricane Andrew’s landfall in South Florida.Part II: surface wind fields and potential real-time applications. Weather Forecast, 11, 329–349.

Powell, M. D., and S. H. Houston (1998). Surface wind fields of 1995 Hurricanes Erin, Opal, Luis, Marilyn, and Roxanne at landfall. Mon. Wea. Rev., 126, 1259–1273.

Powell M.D., G. Soukup, S. Cocke, S. Gulati, N. Morisseau-Leroy, S. Hamid, N. Dorst, L. Axe (2005). State of Florida hurricane loss prediction model: atmospheric science component J. Wind Eng. Ind. Aerodyn., 93, pp. 651–674.

Powell, M. D., Murillo, S., Dodge, P., Uhlhorn, E., Gamache, J., Cardone, V., et al. (2010). Reconstruction of Hurricane Katrina's wind fields for storm surge and wave hindcasting. Ocean Engineering, 37, 26-36.

Ray, R. D., and G. T. Mitchum (1996). Surface manifestation of internal tides generated near

Hawaii, Geophys. Res. Lett., 23, 2101–2104.

Ray, R. D., and G. T. Mitchum (1997). Surface manifestation of internal tides in the deep ocean: Observations from altimetry and tide gauges, Prog. Oceanogr.40, 135–162.

Ray, R., S. B. Luthcke, and J.-P. Boy, (2009). Qualitative comparisons of global ocean tide models by analysis of intersatellite ranging data. Journal of Geophysical Research 114:C09017. doi: 10.1029/2009JC005362.

Reckhow K.H., and S.C. Chapra. (1983). Engineering approaches for lake management, volume 1: data analysis and empirical modeling. Boston: Butterworth Publishers.

Reckhow K.H., J.T. Clements, and R.C. Dodd. (1990). Statistical evaluation ofmechanisticwater-quality models.Journal ofEnvironmental Engineering 116(2): 250–268.

Reid, R. O., and Bodine, B. R. (1968). “Numerical model for storm surges in Galveston Bay.” Journal of the Waterways and Harbors Division, 94(WW1), 33–57.

Robinson AR, Lermusiaux PFJ, Haley Jr PJ and Leslie WG. (2002). Predictive skill, predictive capability and predictability in ocean forecasting. Proc. Oceans 2002 IEEE/MITS Conf, 787–794.

Schloemer, R. W., (1954). Analysis and synthesis of hurricane wind patterns over Lake Okeechobee. NOAA Hydromet Rep. 31, 49 pp

Schwiderski, E. W. (1980). “On charting global ocean tides.” Reviews of Geophysics and Space Physics, 18(1), 243–268.

Shapiro, L. J. (1983). The asymmetric boundary layerflow under a translating hurricane. J. Atmos. Sci., 40, 1984-1998.

Sheng, Y. P., (1986). A three-dimensional numerical model of coastal and estuarine circulation and transport in generalized curvilinear grids. Technical Report No. 587.

Sheng P and Kim T. (2009). Skill assessment of an integrated modeling system for shallow coastal and estuarine ecosystems. Journal of Marine Systems, 76, 212–243.

Shum, C. K., P. L. Woodworth, O. B. Andersen, G. D. Egbert, O. Francis, C. King, S. M.Klosko, C. Le Provost, X. Li, J-M. Molines, M. E. Parke, R. D. Ray, M. G. Schlax,
D. Stammer, C. C. Tierney, P. Vincent, and C. I. Wunsch, (1997). Accuracy assessment of recent ocean tide models. Journal of eophysical Research 102(C11):25173–25194. doi: 10.1029/97JC00445.

Stammer. D, et al. (2014). Accuracy assessment of global barotropic ocean tide models. Rev. Geophys., 52 , pp. 243–282.

Stow, C.A., Joliff, J., McGillicuddy, D.J., Doney, S.C., Allen, J.I., Friedrichs, M.A.M., Rose, K.A., Wallhead, P., (2009). Skill assessment for coupled biological/physical models of marine systems. Journal of Marine Systems 76 (1e2), 4e15.

Stumpf RP, Tomlinson MC, Calkins JA, Kirkpatrick B, Fisher K, Nierenberg K, Currier R and Wynne TT. (2009). Skill assessment for an operational algal bloom forecast system. Journal of Marine Systems, 76, 151–161.

Sun, Yunfang, Chen, Changsheng ,Beardsley, Robert C. ,Xu, Qichun, Qi, Jianhua, Lin, Huichan (2013). Impact of current-wave interaction on storm surge simulation: A case study for Hurricane Bob. Journal of Geophysical Research: Oceans, 118(5), pp. 2685-2701.

Thomann R.V. (1982). Verification of water quality models. Journal of Environmental Engineering 108((EE5)): 923–940.

Thompson, E. F., and Cardone, V. J. (1996). Practical modeling of hurricane surface wind fields. J. Wtrwy., Port, Coast., and Oc. Engrg., 122(4), 195-205.

Timko, P. G., B. K. Arbic, J. G. Richman, R. B. Scott, E. J. Metzger, and A. J. Wallcraft (2012). Skill tests of three-dimensional tidal currents in a global ocean model: A look at the North Atlantic, J. Geophys. Res., 117, C08014, doi:10.1029/2011JC007617.

Uehara, K., J. D. Scourse, K. J. Horsburgh, K. Lambeck, and A. P. Purcell (2006). Tidal evolution of the northwest European shelf seas from the Last Glacial Maximum to the present, J. Geophys. Res.,111, C09025, doi:10.1029/2006JC003531.

Vallee, D. R. and Dion, M. R., (1998). Southern New England Tropical Storms and Hurricanes, A Ninety-eight Year Summary 1909-1997, Taunton, MA.: National Weather Service.

Vested HJ, Nielson JW, Jensen HR and Kristensen KB. (1995). Skill assessment of an operational hydrodynamic forecast system for the North Sea and Danish Belts. In:
Lynch DR and Davies AM (1995). Quantitative Skill Assessment of Coastal Ocean Models, AGU, Washington. p373–396.

Vickery, P. J., Skerlj, P. F., Steckley, A. C., and Twisdale, L. A. (2000). Hurricane Wind Field Model for Use in Hurricane Simulations. Journal of Structural Engineering, 126, 1203-1221.

Vickery P.J., D. Wadhera (2008). Statistical models of Holland pressure profile parameter and radius to maximum winds of hurricanes from flight level pressure and H*Wind data J. Appl. Meteorol. Climatol., 46 pp. 2497–2517.

Wallhead PJ, Martin AP, Srokosz MA and Franks PJS. (2009). Skill assessment via cross-validation and Monte Carlo simulation: An application to Georges Bank. Journal of Marine Systems, 76, 134–150.

Warner JC, Geyer WR and Lerczak JA. (2005). Numerical modeling of an estuary: A omprehensive skill assessment. Journal of Geophysical Research, 110(5), C05001.

Westerink, J. J., and Gray, W. G. (1991). “Progress in surface water modeling.” Reviews in Geophysics, 29, 210–217.

Wilkin, J. L., and E. J. Hunter (.). An assessment of the skill of real-time models of Mid-Atlantic Bight continental shelf circulation, J. Geophys. Res. Oceans, 118, doi:10.1002/jgrc.20223.

Williams RG, Bethem TD and Frey HR. (1989). Tampa Bay current prediction quality assurance miniproject.NOAA Technical Memorandum NOS OMA 50, National Ocean Service, Office of Oceanography and Marine Assessment, Rockville, Maryland, 11p.

Willoughby H.E.M.E. Rahn (1980). Parametric representation of the primary hurricane vortex. Part I: observations and evaluation of the Holland (1980) Model.

Willoughby, h. e., r. w. r. darling and m. e. rahn, (2006). parametric representation of the primary hurricane vortex. part ii: a new family of sectionnally continuous profiles. mon. wea. rev., 134, 1102-1120.

Wilmott CJ. (1981). On the validation of models. Physical Geography, 2, 184–194.

Wilmott CJ, Ackleson SG, Davis RT, Feddema JJ, Klink KM, Legates DR, O'Donnell J and Rowe CM. (1985). Statistics for evaluation and comparison of models. Journal of Geophysical Research, 90, C5, 8995–9005.

Xie L, Liu H, Liu B, Bao S (2011). A numerical study of the effect of hurricane wind asymmetry on storm surge and inundation. Ocean Model 36:71–7.

Xie L, Bao S, Pietrafesa LJ, Foley K, Fuents M (2006). A real-time hurricane surface wind forecasting model: formulation and verification. Mon Weather Rev 134:1355–1370.

Young, I., (1988). a parametric hurricane wave prediction model.. Journal of Waterways. Port Coastal Ocean Engineering.,ASCE, Volume 114, pp. 637-652.

Zhang A., K.H. Hess, E. Wei, and E.P. Myers,(2006): Implementation of Model Skill Assessment Software for Water Level and Currents. NOAA Technical Report NOS CS 24, 61 pp.

Zhang, Y.L., Baptista, A.M. and Myers, E.P., (2004). A cross-scale model for 3D baroclinic circulation in estuary-plume-shelf systems: I. Formulation and skill assessment. Cont. Shelf Res. 24: 2187-2214.

Zhang, Y., Baptista, A. M., (2008). SELFE: A semi-implicit Eulerian- Lagrangian finite-element model for cross-scale ocean circulation. Ocean Modelling 21, 71-96.

Zhang. A, K W Hess & F Aikman III (2010). User-based skill assessment techniques for operational hydrodynamic forecast systems, Journal of Operational Oceanography, 3:2, 11-24, DOI: 10.1080/1755876X.2010.11020114.

Zhang, Y.-X. and Jia, Y.-F, (2009). CCHE-MESH: 2D structured mesh generator user's manual – Verion 3.X, Technical Report No. NCCHE-TR-2009-01,: National Center for Computational Hydroscience and Engineering, The University of Mississippi, University, U.S.A.

VITA

AFSHIN GAZERZADEH

335 Brevard Hall, UM • Oxford, MS 38655 • (662) 915-8935 • agazerza@go.olemiss.edu

EDUCATION

M.Sc., Engineering, University of Mississippi, Oxford, MS August 2016

Concentrations: Computational Hydro-Sciences and Engineering
Thesis: Validation of Integrated Coast-Ocean Model CCHE2D-Coast and Development of wind model

M.Sc., Engineering, Shahidchamran University, Ahvaz, Iran August 2010

Concentrations: Hydraulics, Hydraulic Structures

Thesis: Estimation of Manning Roughness Coefficient in Rivers Using Nonlinear Optimization

B.Sc., Engineering, Shahidchamran University, Ahvaz, Iran May 2006

Concentrations: Civil Engineering

AWARDS

Research Award from Graduate School of University of Mississippi, 2015

PUBLICATIONS and PRESENTATIONS

"Skill Assessment of Coastal Ocean Circulation Model in the U.S. East Coast", EWRI Congress, West Palm Beach, FL, 2016

"Hindcasting Storm Surge and Waves in Hurricane Bob in the Gulf of Maine Using CCHE2D-Coast", EWRI Congress, Austin, TX, 2015

"Simulation and Prediction of Storm Surges and Waves Driven by Hurricanes and Assessment of Coastal Flooding and Inundation", 11th Int. Conf. on Hydro science and Engineering (ICHE), Hamburg, Germany, 2014

"A Simplified Procedure to Assess the Dynamic Pressures on Lock Gates", ICTWS Conference, Busan, South Korea, 2014

"Estimation of Manning Roughness Coefficient in Rivers Using Nonlinear Optimization", Mid-South Annual Engineering and Sciences Conference (MAESC), Oxford, MS, 2013